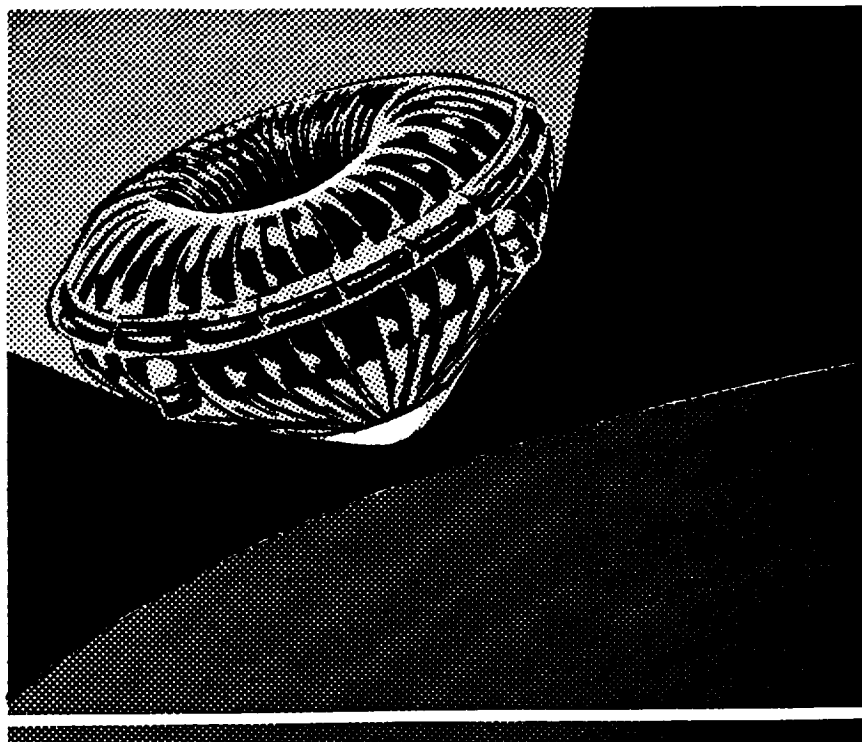
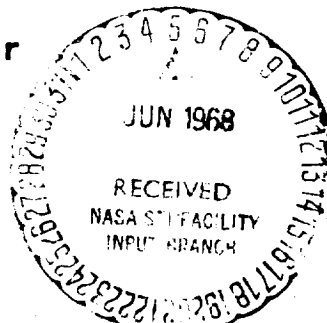


Development of ATTACHED INFLATABLE DECELERATORS for Supersonic Application

68-25487
(ACCESSION NUMBER)
148
(PAGES)
NASA-CR-66613
(NASA CR OR TXR OR AD NUMBER)
(THRU)
(CODED)
(CATEGORY)
FACILITY FORM 602



Prepared under Contract No. NAS1-7359 for
NATIONAL AERONAUTICS AND SPACE ADMINISTRATION
Langley Research Center Hampton, Virginia



GOODYEAR AEROSPACE CORPORATION
Akron Ohio



DEVELOPMENT OF ATTACHED
INFLATABLE DECELERATORS FOR
SUPERSONIC APPLICATION

by
R. Reed Barton

Distribution of this report is provided in the interest of
information exchange. Responsibility for the contents
resides in the author or organizations that prepared it.

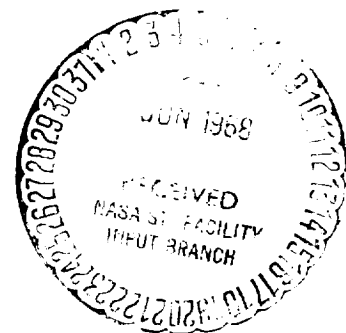
Prepared under Contract No. NAS1-7359 by

GOODYEAR AEROSPACE CORPORATION

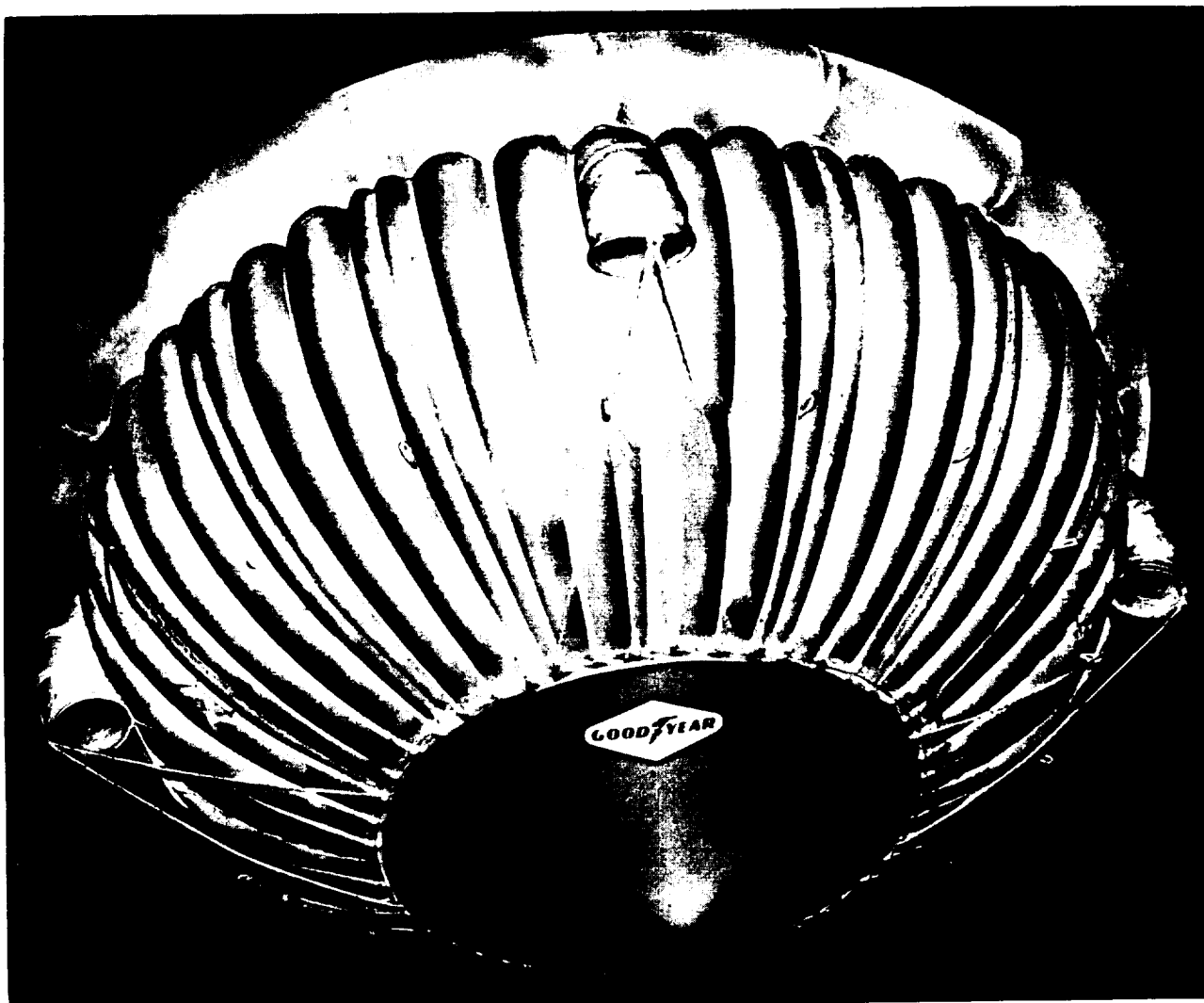
Akron, Ohio

for

NATIONAL AERONAUTICS AND SPACE ADMINISTRATION



PRECEDING PAGE BLANK NOT FILMED.



Attached Inflatable Decelerator



FOREWORD

This report was prepared by Goodyear Aerospace Corporation (GAC), Akron, Ohio, for the National Aeronautics and Space Administration, Langley Research Center (NASA-LRC), Hampton, Virginia, under Contract No. NAS1-7359. The purpose of the report is to summarize the design, analysis, fabrication, and test performed by Goodyear Aerospace in this initial program for developing attached inflatable supersonic decelerators.

The program was a group effort headed by Mr. F. R. Nebiker, manager of the Recovery Systems Engineering Department, assisted by Mr. A. C. Aebischer, section head; Mr. R. R. Barton, project engineer; Mr. W. A. Barr, configuration analysis; Mr. R. E. Nissel, materials and fabrication techniques; Mr. J. E. Houmard, structural analysis; Mr. I. M. Jaremenko, aerodynamics analysis; Mr. W. W. Sowa, inflation analysis; Mr. B. E. Sahli, tests and instrumentation; Mr. D. L. Mansfield, packaging techniques; and Mr. W. P. Stricker, mass properties.

Mr. H. L. Bohon and Mr. M. M. Mikulas, Jr. of the Structures Research Division of NASA-LRC served as contract monitors. Goodyear Aerospace acknowledges the cooperation and support by NASA personnel.

The contractor's report number is GER-13680. The manuscript was submitted in February 1968 for approval as a NASA contractor report.

TABLE OF CONTENTS

	<u>Page</u>
FOREWORD	v
LIST OF ILLUSTRATIONS	ix
LIST OF TABLES	xiii
LIST OF SYMBOLS	xv
<hr/> Title <hr/>	
SUMMARY	1
INTRODUCTION	1
DESIGN CONDITIONS	2
DESIGN REQUIREMENTS	3
Aerodynamic Considerations	3
Configuration Selection	6
Decelerator Stress Analysis	21
Hard Structure Stress Analysis	26
DESIGN DOCUMENTATION	26
General	26
Control of Attachment Points	33
MATERIALS SELECTION	35
Hard Structure	35
Decelerator	35
DEVELOPMENT TESTS	36
Reservoir Acceptance Pressure Test	36
Tensile Tests of Nomex Fabrications	37
Fabric Permeability Test	39
Decelerator Packaging Demonstration	40
Inflated Shape Inspection	41
Deployment and Inflation Tests	43

Title		Page
CONCLUSIONS AND RECOMMENDATIONS		55
Introduction		55
Conclusions		55
Recommendations		55
<u>Appendix</u>		
A	DECELERATOR PARAMETERS AS FUNCTIONS OF THE OUTER ATTACHMENT ANGLE	57
B	SHAPE DEVELOPMENT	61
C	INFLATION ANALYSIS	71
D	DRAWINGS	77
LIST OF REFERENCES		115

LIST OF ILLUSTRATIONS

		<u>Page</u>
FRONTISPIECE		iii
<u>Figure</u>	<u>Title</u>	
1	Aerodynamic Configuration for Attached Inflatable Decelerator	2
2	Flow Field About Aeroshell	4
3	Shape and Pressure Profiles ($\phi = 22.6$ Deg).	9
4	Shape and Pressure Profiles ($\phi = 19.5$ Deg).	10
5	Nominal Lobing Dimensions at Burble Fence	10
6	Geometric Section Properties	12
7	Surface of Revolution with Meridians	16
8	Surface Element with Lobing	17
9	Lobe Cross Section and Fabric Element.	18
10	Hard Structure	28
11	Dimensional Control of Attachments	29
12	Aeroshell Cone and Outer Clamp	30
13	Support Sleeve and Installed Cabling	30
14	Decelerator Afterbody, Cone, and Clamp	31
15	Sensors and Operating Components	31
16	Basic Envelope Folds	41
17	Daisy Chain Hoop	42
18	Front Contour Profile.	44
19	AID Inspection Fixture, Front Contour	45
20	AID Contour Inspection	45
21	Rear Contour Profile and Variances	46

<u>Figure</u>	<u>Title</u>	<u>Page</u>
22	Pressure and Temperature at AID Deployments .	48
23	Pressure and Temperature at AID Deployment (Test No. 4)	49
24	Regular Deployment Setup	50
25	Test No. 2 Deployment	51
26	Structural Additions	52
27	Guided-Shape Deployment Setup	52
28	Test No. 4 Guided Deployment	53
29	Fluid Weight versus Inflation Pressure	54
30	Decelerator Weight Parameter and Drag Coeffi- cient versus Attachment Angle	57
31	Bias Thread Angle and Number of Lobes versus Attachment Angle	58
32	Shape Profile for 30-Deg Attachment Angle . . .	59
33	Loading Diagram	62
34	Wind-Tunnel Setup	71
35	Vapor Pressure Data	73
36	Model Assembly with 60-In. D_P (Drawing 610A000- 001, Sheet 1)	79
37	Model Assembly with 60-In. D_P (Sheet 2)	81
38	Model Assembly with 60-In. D_P (Sheet 3)	83
39	Model Assembly with 60-In. D_P (Sheet 4)	85
40	Decelerator Assembly with 60-In. D_P (Drawing 610A000-002, Sheet 1)	87
41	Decelerator Assembly with 60-In. D_P (Sheet 2) .	89
42	Decelerator Assembly with 60-In. D_P (Sheet 3) .	91
43	Decelerator Assembly with 60-In. D_P (Sheet 4) .	93
44	Decelerator Assembly with 60-In. D_P (Sheet 5) .	95

<u>Figure</u>	<u>Title</u>	<u>Page</u>
45	Decelerator Assembly with 60-In. D_P (Sheet 6) . .	97
46	Aeroshell (Drawing 610A000-101)	99
47	Support Assembly (Drawing 610A000-102)	101
48	Model Details (Drawing 610A000-103)	103
49	Clamp Assembly (Drawing 610A000-104)	105
50	Inlet Assembly, 4-In. Diameter (Drawing 610A000-105).	107
51	Inlet Sleeve, 4-In. Diameter (Drawing 610A000-106)	109
52	Inlet Base (Drawing 610A000-107)	111
53	BALLUTE Inlet Ring (Drawing 530A005-110). . . .	113

PRECEDING PAGE BLANK NOT FILMED.

LIST OF TABLES

<u>Table</u>	<u>Title</u>	<u>Page</u>
I	AEDC (PWT) 16S Test Schedule	3
II	Geometrical Relationships	7
III	Isotenoid Profile Parameters	8
IV	Lobe Geometry, Radial Growth, and Fabric Stresses	20
V	Margins of Safety and Design Factors	21
VI	Composite Design Factors	25
VII	Safety Factors for Hard Structure	27
VIII	Actual Weight and Center of Gravity, AID No. 1 . .	32
IX	Actual Weight and Center of Gravity, AID No. 2 .	33
X	Possible Variance from Established Relationship of Attachments	34
XI	Physical Characteristics of Goodyear Aerospace-Coated Fabric	36
XII	Reservoir Weight Data	36
XIII	Isotenoid Coordinates, 344 Points ($\phi = 23.6$ Deg)	67
XIV	Liquid Vaporization Characteristics	75

LIST OF SYMBOLS

A	total surface area (sq ft)
A	projected area of flight body (sq ft)
A	canopy or burble fence section area (sq in. or sq ft)
A_b	surface area of burble fence (sq in.)
A_s	canopy surface area of revolution
C	specific heat of vaporizing fluid (Btu/lb-deg F)
C_f	specific heat of Nomex fabric (Btu/lb-deg F)
C_ℓ	ℓ_m/R , coefficient for meridian length
C_A	A_s/R^2 , coefficient for surface area of revolution
C_D	system drag coefficient
C_{D_e}	aeroshell drag coefficient at entry
$(C_D A)_d$	deployed drag area (sq ft)
$(C_D A)_e$	undeployed drag area at entry (sq ft)
C_p	pressure coefficient
C_{p_i}	internal pressure coefficient
d_g	depth of lobing (in.)
D_b	burble fence aerodynamic drag (lb)
D_P	projected diameter of flight body (ft)
D	system aerodynamic drag (lb)
f	revolved surface element (fabric) stress (lb/in.)

f_{ϕ}	fabric stress in meridional direction (lb/in.)
f_b	fabric stress in bias direction (lb/in.)
F	axial fabric component plus meridian loads, rear (lb)
F	circumferential membrane stress coefficient
F_f	circumferential membrane stress coefficient, front surface
F_r	circumferential membrane stress coefficient, rear surface
F_b	bias membrane stress coefficient
F_t	tensile strength (lb/in.)
h_a	original aeroshell height (in.)
h_b	burble fence height (in.)
h_c	support cylinder height (in.)
h_v	heat of vaporization (Btu/lb)
I	section moment of inertia (cu in.)
k	meridian tension coefficient
k_f	meridian tension coefficient, front surface
k_r	meridian tension coefficient, rear surface
l_b	burble fence arc length (in.)
l_m	meridian length (in.)
M	Mach number
M_{∞}	free-stream Mach number
M_y	pitching moment (ft-lb)
n	number of lobes or meridians

N	normal force (lb)
N_{ϕ}	meridional revolved surface element (fabric) stress (lb/in.)
N_{θ}	circumferential revolved surface element (fabric) stress (lb/in.)
p	static pressure (psi)
p_B	base pressure (psi)
p_i	internal pressure (psi)
p_L	local pressure (psi)
p_o	stagnation pressure behind the shock (psi)
p_{∞}	ambient free-stream pressure (psi)
$(p_i - p_{\infty})$	envelope differential pressure (psi)
q	dynamic pressure (psi)
Q	heat available (Btu)
Q_s	sensible heat realized from fluid (Btu)
Q_v	heat required for vaporization (Btu)
r	radius (in. or ft)
r_b	true base radius of aeroshell (12 in.)
r_b'	original base radius of aeroshell (10.5 in.)
r_g	lobe radius (in.)
R	vapor gas constant (ft-lb/lb-deg R)
R	decelerator profile radius at equator (27.3 in.)
R_P	projected radius of flight body (30 in.)
S_x, S_y	separation distances between attachment points (in.)

S	section perimeter (in.)
S_g	half-arc length of lobe (in.)
t	thickness (in.)
T, T_m	meridian tension (lb)
T	maximum design temperature (F)
T_a	initial temperature (F)
T_b	resulting temperature (F)
T_t	stagnation temperature (F)
T_1, T_2	thermocouple measurements of temperature (F)
T_i	internal equilibrium temperature (R)
V	total enclosed volume (cu ft)
V_a	aeroshell net volume (cu ft)
V_b	burble fence volume (cu ft)
V_B	canopy volume (cu ft)
W	weight of vaporizing fluid (lb)
W_f	weight of decelerator fabrics (lb)
W/C_D	ballistic coefficient (lb)
x	profile radii of revolution
x'	deformed profile radii of revolution
$x/R, y/R$	decelerator coordinate shaping factors
\bar{x}, \bar{y}	centroids of canopy and fence section lines
$\bar{\bar{x}}, \bar{\bar{y}}$	centroids of canopy and fence section areas
w_f	strength-to-weight ratio of fabric (in.)

w_m	strength-to-weight ratio of meridians (in.)
α	angle of attack (deg)
α	$\sqrt{\rho} = x/R$ at $(y/R)_{\max}$
α	meridian design factor for flight-test times π
β	central half-lobe angle (deg)
β	fabric design factor for flight test
ϵ	strain due to thread racking (in./in.)
γ	bias thread set angle (deg)
θ	surface angle from straight flow (deg)
ϕ	original outer attachment angle (deg)
ϕ'	true outer attachment angle (deg)

Subscripts

A	section area
b	burble fence
b	aeroshell base
B	base
d	deployed
e	entry
e	equator
f	fabric
f	front surface
i	inner attachment location
i	internal
l	length
L	section line



L	local
m	meridian
o	outer attachment location
o	stagnation
r	rear surface
t	tensile
t	total or stagnation
u	ultimate
x', y', z'	axes at line centroid
θ	circumferential direction of surface element
ϕ	meridional direction of surface element
∞	free stream

DEVELOPMENT OF ATTACHED INFLATABLE DECELERATORS FOR SUPERSONIC APPLICATION

By R. Reed Barton
Goodyear Aerospace Corporation

SUMMARY

An attached inflatable decelerator is considered for augmenting needed drag of a capsule during Mars entry. The inflatable afterbody, configured as a variation from a tucked-back BALLUTE,* is packaged within a 120-deg conical aeroshell for deployment at Mach 3.0 and at a dynamic pressure of 125 psf. Outer attachment of the expandable afterbody is made to the hard-body aeroshell profile, and inner attachment is made to a tubular support for wind-tunnel mounting.

The model was designed, fabricated, and development tested and is recommended for wind-tunnel testing to prove workability of the concept.

This report discusses design conditions, requirements, documentation, materials selection, development tests, and conclusions.

INTRODUCTION

Size constraint of the Saturn V booster and weight-restricting low density atmosphere at Mars entry pointed to the need for deploying additional drag area. An Attached Inflatable Decelerator (AID) system was designed, fabricated, and static tested in preparation for wind-tunnel testing an expandable lightweight concept to demonstrate its workability.

The design of the afterbody decelerator is based on meeting the contractual design conditions for operation and is intended to be optimum within the limitations of the state of the art. The aeroshell and support hardware is designed to meet the contractual stress requirements specified for operation in the wind tunnel of the Arnold Engineering Development Center (AEDC).

The described requirements for meeting the design of AID are the configuration selection together with aerodynamic considerations and structural analyses. Configuration analysis and materials selection for design and the results of developmental tests for static qualification also are presented.

* TM, Goodyear Aerospace Corporation, Akron, Ohio

DESIGN CONDITIONS

Recognized conditions for designing the AID system were those applicable to the optimally designed afterbody decelerator and those applicable to a boilerplate-designed hard structure consisting of the aeroshell and mounting support (see Figure 1).

The system design includes a 120-deg aeroshell with an attached inflatable envelope fashioned after the tucked-back BALLUTE to provide the least-weight practical decelerator for the performance specified. The aerodynamic and structural requirements to meet free-flight loading conditions were as follows:

1. Maximum diameter projected (including fence),
 $D_P = 2R_P$, 5 ft.
2. Deployed frontal area ratio, $\frac{(C_{DA})_d}{(C_{DA})_e} = \frac{(C_{DR_P^2})_d}{(C_{Dr_b^2})_e}$, 4.5
3. Dynamic pressure (q), 125 psf
4. Deployment Mach number (M), 3.0
5. Maximum temperature (T), 350 deg F

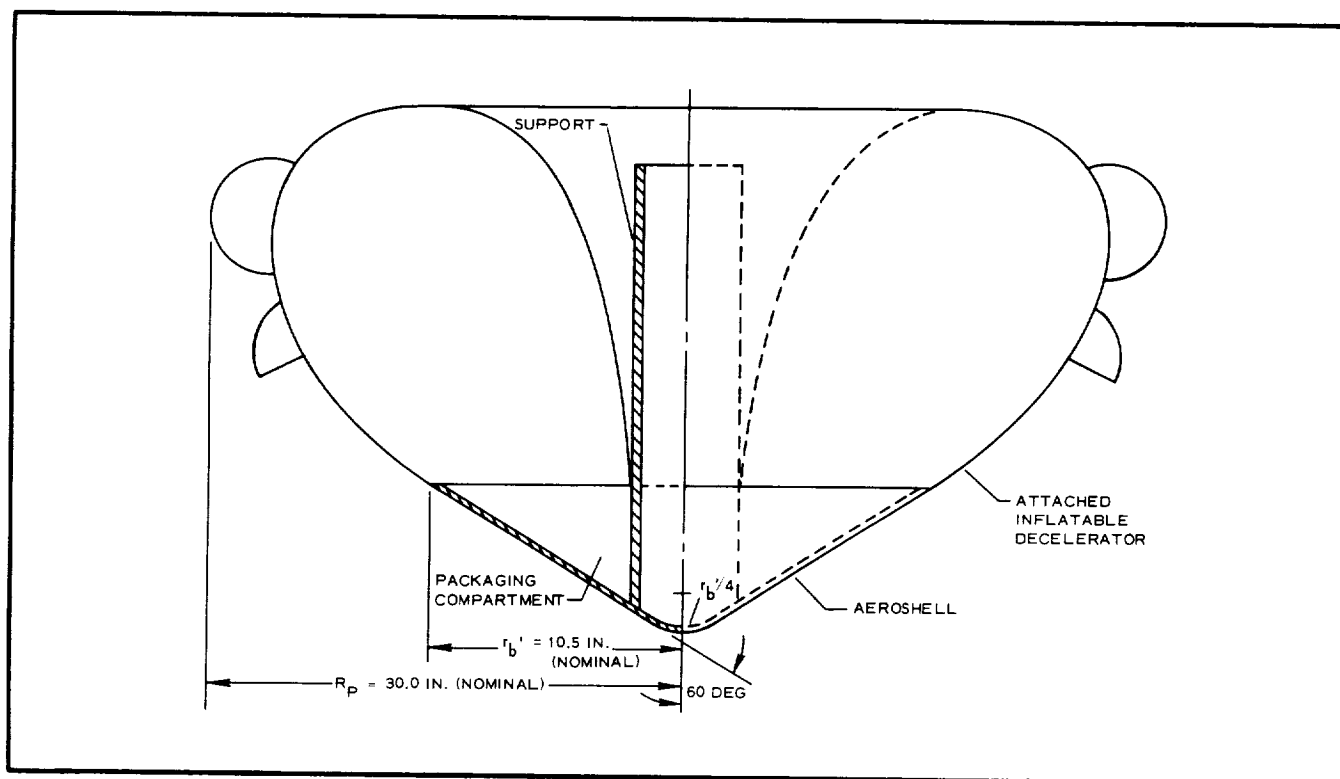


Figure 1 - Aerodynamic Configuration for Attached Inflatable Decelerator

The aeroshell and support were not optimized structurally and were to have a lenient safety factor to meet AEDC wind-tunnel design and strength requirements specified in AEDC Document QCP-000-21, dated March 1967. Basis for designing the hard structure also included the wind-tunnel test schedule and conditions established at the AEDC pretest conference, 7 July 1967. Table I lists the conditions of operation by changed angle of attack, Mach number, and dynamic pressure.

TABLE I - AEDC (PWT) 16S TEST SCHEDULE

Event ^a	Conditions ^b				Data ^b
	q (psf)	M	T _t (F)	α (deg)	
1. Startup, undeployed	120	3.0	180	0	p _i , (p _i - p _∞), P _B , D, T ₁ , T ₂ , camera
2. Angle of attack	120	3.0	180	2, 5, 10	Same as 1 and M _y , N
3. Deployment	120	3.0	180	0	Same as 1
4. Angle of attack	120	3.0	180	2, 5, 10	Same as 2
5. Mach number reduction	120	2.5	180	0	Same as 1
6. Angle of attack	120	2.5	180	2, 5, 10	Same as 2
7. Integrity test	380	2.5	Minimum	0	Same as 1
8. Shutdown	0	0	. . .	0	Same as 1

^a24 pps (color), all events covered; 200 pps (color), events 1, 2, 4, 5, 6, and 8 covered; and 400 pps (color), events 3 and 7 covered.

^bp_i, envelope internal pressure; T_t, stagnation temperature; T₁, T₂, internal temperatures; α, angle of attack; (p_i - p_∞), pressure envelope differential; P_B, base pressure; D, drag; M_y, pitching moment; and N, normal force.

DESIGN REQUIREMENTS

Aerodynamic Considerations

Introduction. - The decelerater design requires aerodynamic inputs to determine the shape and loading for the structural analysis and to contribute to the overall design of the AID system. The following aerodynamic investigation is based on the listed design conditions together with the specified general configuration.

are compromised by configuration, flow structure, and weight and package-ability. Based on these factors and experience, the height of the burble fence was established as five percent of the profile diameter extending beyond the projection of a half profile. Under compressible flow loading, it assumes the shape shown in Appendix D.

Reduction from an interim consideration of a conventional 10-percent fence was prompted by weight and package volume saving. To provide comparable aerodynamic drag efficiency anticipated from the 10-percent fence, the leading edge of the five-percent fence was moved forward until the fence quarter point corresponded with the decelerator equator to induce an earlier flow separation.

Pressure distribution. - The pressure distribution over the aeroshell decelerator was determined for several afterbody profiles using the modified Newtonian impact theory. The theory is used to obtain the stagnation point pressure on the aeroshell and the pressure distribution on the afterbody up to a point preceding the burble fence at which separation is estimated to occur. The modified Newtonian pressure distribution then was corrected as affected by flow separation at the burble fence. Experimental results indicate that the pressure increases in the vicinity of the burble fence and reaches a local maximum at the top of the fence. This local maximum may be up to three times the magnitude of the local minimum pressure preceding the fence.

The equation used to compute a pressure distribution is given by modified Newtonian theory as:

$$C_p = C_{p_{\max}} \sin^2 \theta$$

where

$$C_p = \frac{p_L - p_\infty}{q_\infty} \left(p_\infty = \frac{q_\infty}{0.7 M_\infty^2} = 19.84 \text{ psf} \right)$$

$$C_{p_{\max}} = \frac{p_o - p_\infty}{q_\infty}$$

θ = local surface angle measured from straight flow

or

$$\frac{p_L}{p_\infty} = 1 + \left(\frac{p_o}{p_\infty} - 1 \right) \sin^2 \theta$$

Pressure distributions were prepared accordingly for shapes in the several steps of iteration to isotenoid. The iterated shapes and corresponding

pressure distributions are compared by studying Figures 3 and 4 under the shape summary.

Inflation considerations. - The purpose of this design for wind-tunnel testing was to show that the AID concept was deployable and could serve as an efficient decelerator. Hence, full and fast deployment to the basic shape was desired and could be provided by the liquid vaporization method. The decelerator was outfitted with four conventional ram-air inlets located at $y/R = 0.293$ to maintain the inside pressure level necessary for shape retention. This location ahead of the burble fence places the inlets in the flow with minimum interference facilitating the continuing pressure by ram air.

The magnitude of the internal pressure coefficient generated by the inlets is not a function of their size, within large limits, assuming a nonporous fabric. Accordingly, the inlet configuration qualified in the Gemini BALLUTE application was chosen to pressurize the decelerator. By using this qualified inlet, one imponderable of the wind-tunnel test was eliminated.

A C_{p_i} of two is expected to be produced by a Gemini-type inlet located immediately forward of the burble fence, as it was in the PRIME and Gemini configurations considered without a separated forebody (see Figure 49 of Reference 2).

Configuration Selection

System geometry. - The support, located in the central volume of the aeroshell, is the counterpart of an entry payload. Its general configuration is arbitrary and solely depends on a design that properly supports the model on the AEDC 16S wind-tunnel sting.

The inflatable afterbody decelerator is designed for least weight in the shape analysis by applying the concept of isotenoid design as given in Reference 3. A complete profile less the burble fence is defined by joining two isotenoid curves (a front and back half curve) having common boundary conditions at their juncture, which is the maximum diameter. Because of the shape and the design pressure distribution, the fabric and meridian stresses are constant.

For the specified design conditions, the drag coefficient for an isotenoid profile resulting from the application of a reasonable pressure distribution (modified Newtonian) was $C_D = 1.2$, which was considerably higher than that assumed by using a nominal size decelerator and aeroshell (60- and 21-in. diameters) for the desired frontal area relationship. By adopting a 24-in. aeroshell, the desired frontal area ratio of 4.5 was closely approximated:

$$\frac{(C_D A)_d}{(C_D A)_e} = \frac{(C_D R_P^2)_d}{(C_D r_b^2)_e} = \frac{1.2 (30)^2}{1.6 (12)^2} = 4.7$$

where

R_P projected radius of decelerator deployed

r_b base radius of aeroshell or projected radius at undeployed entry

Shape summary. - Corresponding fixed coordinates and coordinate relationships were established as ground rule bases for pursuing a parametric analysis of applicable and refined isotenoid shapes (Reference 3) to satisfy the configurational restraints. A limited analysis, intended to aid in selecting the model shape, roughly compared W/C_D with the outer attachment angle (ϕ), a shape-affecting parameter (see Appendix A). Table II gives established geometrical relationships.

Refinement was attained by a step-by-step iteration of the isotenoid shape for $C_{p_i} = 2.0$ and for the estimated pressure distribution for that shape. Each successive profile was developed by computer and programmed in FORTRAN from the applicable equations (see Appendix B).

TABLE II - GEOMETRICAL RELATIONSHIPS

Term	Definition	Dimension (in.)	Coordinates	
			x/R	y/R
R_P	Total radius of decelerator (with 5 percent fence)	30.0	1.10	. . .
R	Radius of decelerator profile at equator $R = \frac{1}{2} \left(\frac{2 R_P}{1 + 0.05 + 0.05} \right) = \frac{R_P}{1.1}$	27.3	1.00	. . .
h_b	Height of burble fence (five percent) $h_b = R_P - R = 0.05 (2R)$	2.7
d_g	Depth of lobe at fence	1.0
r_b	Base radius of the aeroshell to outer attachment	12.0	0.44	. . .
Subscript o	Outer attachment location (ϕ')	. . .	0.44	(y/R) _o
Subscript i	Inner attachment location	. . .	0.13	(y/R) _o + 0.11
Subscript e	Equator of profile	. . .	1.00	(y/R) _e
	Center of burble fence	. . .	1.00	(y/R) _e + 0.05
	Original attachment location (ϕ) at $r_b' = 10.5$ in.	. . .	0.38	0

Pressure distribution was estimated successively for each step-computed shape by developing a faired profile and incorporating values determined from the modified Newtonian equations given under aerodynamic considerations.

The result was a good geometrical and structural decelerator configuration that had an outer attachment angle (ϕ) of 23.6 deg (cosecant $\phi = 2.5$), whereas a very marginal result was achieved from $\phi = 19.5$ deg (cosecant $\phi = 3$). Depending upon small changes in the estimation of pressure distribution, plots of the 19.5-deg profile passing through the established attachment points had negative or minute circumferential membrane forces that were not compatible with maintaining a stable shape.

Figures 3 and 4 show the profiles of shape and pressure distribution for the two angles. Although the plot in Figure 4 does not pass directly through the inner attachment point, it misses by only an inch and is representative for comparing characteristics given in Table III. This table shows that, for $\phi = 19.5$ deg, an impractical number (n) of nearby semicircular lobes are required to be compatible with the circumferential membrane stress coefficient (F_r). A related discussion is given in Appendix A.

TABLE III - ISOTENSOID PROFILE PARAMETERS

ϕ' (deg)	ϕ (deg)	k_f	k_r	$(y/R)_e$	y/R (max)	α^2 or ρ	C_D	$\frac{(C_D A)_d}{(C_D A)_e}$	F_r	n
. . .	19.5	0.55	0.485	0.55	0.81	0.512	1.19	4.65	0.004	90
26.2	23.6	0.52	0.440	0.65	0.94	0.470	1.14	4.45	0.089	48

Figure 5 shows the lobing geometry for the profile resulting from $\phi = 23.6$ deg. The 1.0-in. depth of required lobing (d_g) reduces the burble fence effectiveness to approximately four percent.

Shape and pressure distribution profiles for $\phi = 30$ deg also were examined but were rejected because of general shape; the value of $(x/R)_{\min}$ was only 0.059 for the plot passing through the inner attachment point, $(x/R)_i = 0.13$.

The true outer attachment angle, for $r_b = 12$ in., is $\phi' = 26.2$ deg.

General shape analysis. - In applying the isotensoid concept to the AID, a computer program was written for the IBM 360 that determines the isotensoid profile shape along with the associated stress parameters, drag coefficient, meridian length, and surface area of revolution. Appendix B describes the governing equations and the computer program.

Three values of ϕ (19.5, 23.6, and 30.0 deg at the edge of the 21-in. diameter aeroshell) were considered in selecting the configuration shown in

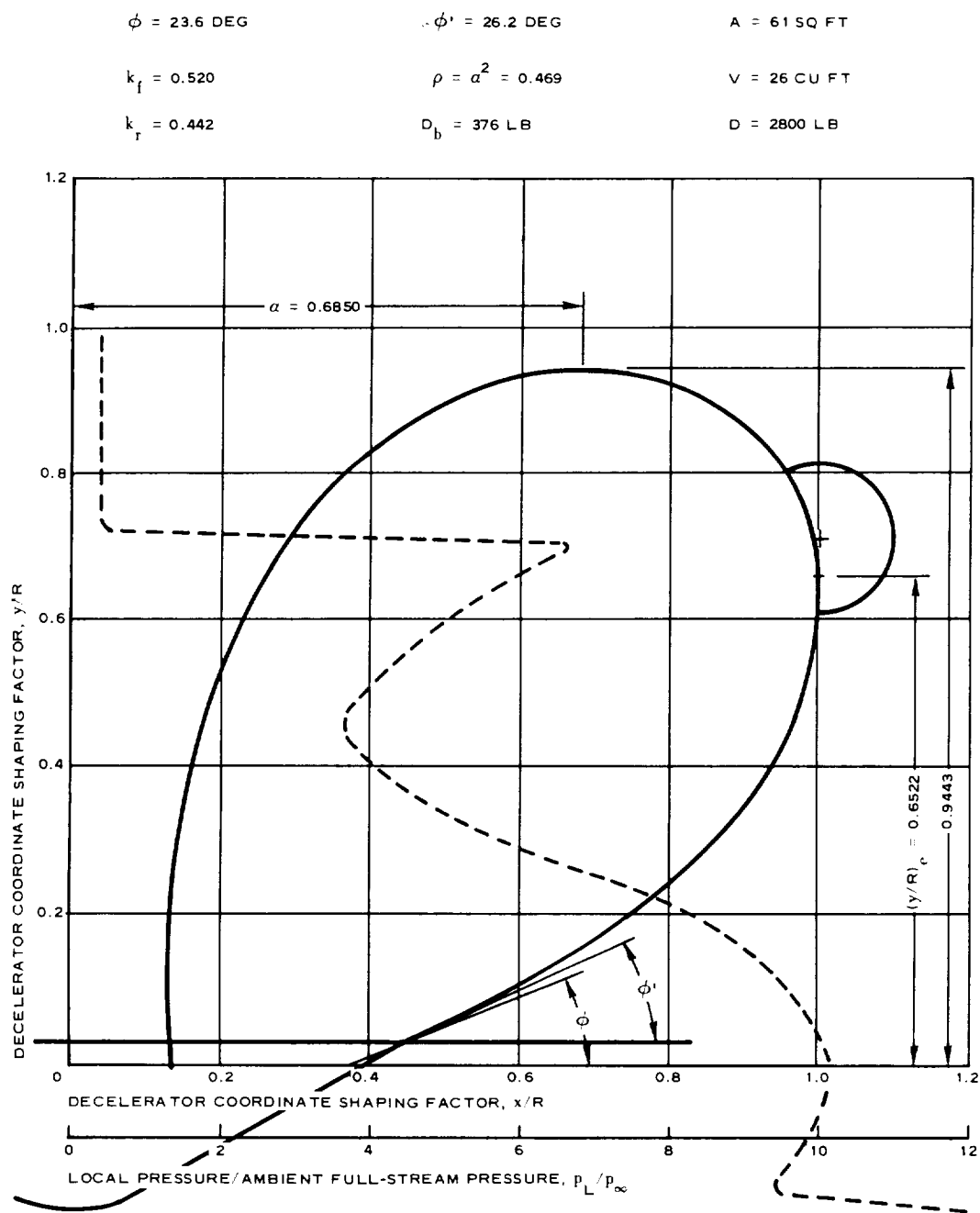


Figure 3 - Shape and Pressure Profiles ($\phi = 22.6 \text{ Deg}$)

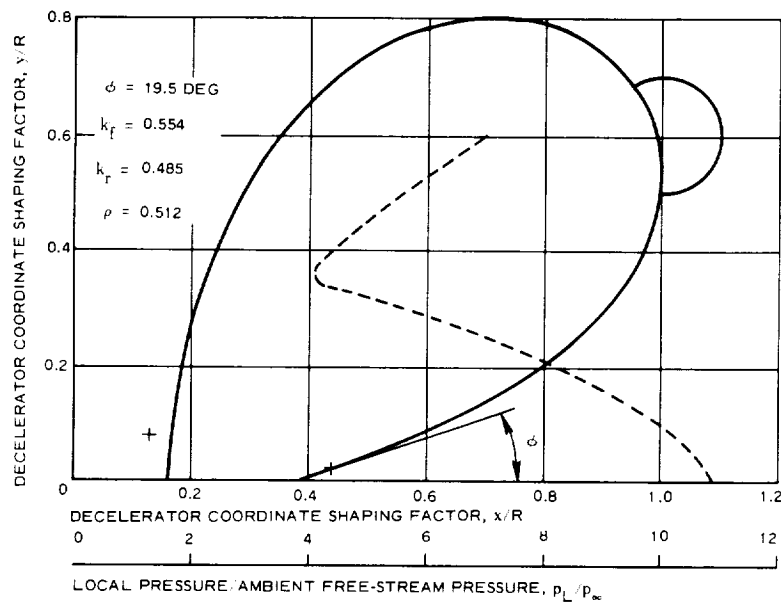


Figure 4 - Shape and Pressure Profiles ($\phi = 19.5 \text{ Deg}$)

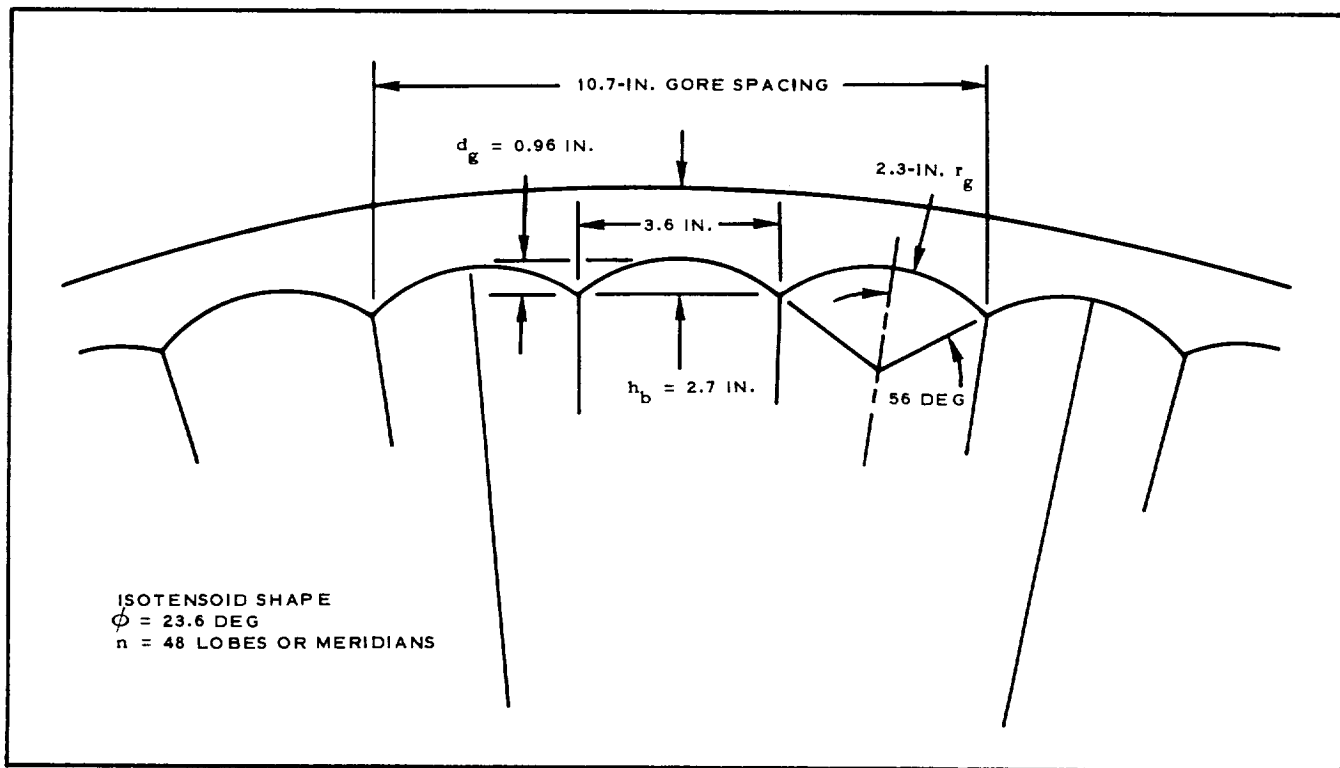


Figure 5 - Nominal Lobing Dimensions at Burble Fence

Figure 3. The profile cross section was plotted by the off-line Calcomp plotter using the cartesian coordinates at 344 points (see Appendix B).

Development of the shape profile for each attachment angle (ϕ) resulted from an iteration of shape and pressure distribution. The shape resulting from an assumed pressure distribution was evaluated for a new estimate of pressure distribution. The estimated profile of pressure distribution shown as the dashed curve in Figure 3 resulted from the shape profile in Figure 3. Using this distribution as a computer input resulted in a shape profile that agreed closely with the shape shown. The small differences were considered well within the accuracy of the aerodynamic theory used to estimate pressure input.

The calculated drag coefficient, based on the frontal area that includes the nominal five percent burble fence and the conical aeroshell, is

$$C_D = 1.14 \quad (1)$$

This value was obtained by the computer numerical integration of the pressure distribution of Figure 3 as applied to the shape of Figure 3. The value of $p_L/p_\infty = 5.15$ that occurs at the forward burble fence attachment was taken as occurring immediately in front of the equator $(x/R)_e = 1.00$, and the constant pressure of $p_L/p_\infty = 0.4$ was taken rear of the equator. Since the indicated pressure distribution over the front of the burble fence is approximately linear, the drag on the fence was determined by taking an average value over the frontal projected annular area (from Figure 3) and by subtracting the constant $p_L/p_\infty = 0.4$ pressure over the rear projected annular area. The burble fence drag, therefore, is given by

$$\begin{aligned} D_b &= \left(\frac{5.15 + 6.75}{2} - 0.4 \right) \left[(1.1)^2 - (1.0)^2 \right] p_\infty \pi R^2 \\ &= 1.166 p_\infty \pi R^2 \end{aligned} \quad (2)$$

This burble fence drag was applied as a concentrated line load at the equator and then was used in conjunction with the integrated drag over the body of the decelerator along with the drag on the aeroshell to obtain the drag coefficient of Equation (1). The drag coefficient of the aeroshell was taken as $C_{D_e} = 1.6$; a corresponding constant pressure of $p_L/p_\infty = 10.1$ (from Figure 3) was used.

The cartesian coordinates were used as inputs into a second computer program that determined the area of the decelerator cross section and the centroid of the area to determine the enclosed volume. Figure 6 gives this area and cross section by

$$\begin{aligned} V_B/R^3 &= 2\pi(\bar{x}/R)_A \left(\frac{A}{R^2} \right) \\ &= 2\pi(0.55)(0.584) = 2.018 \end{aligned} \quad (3)$$

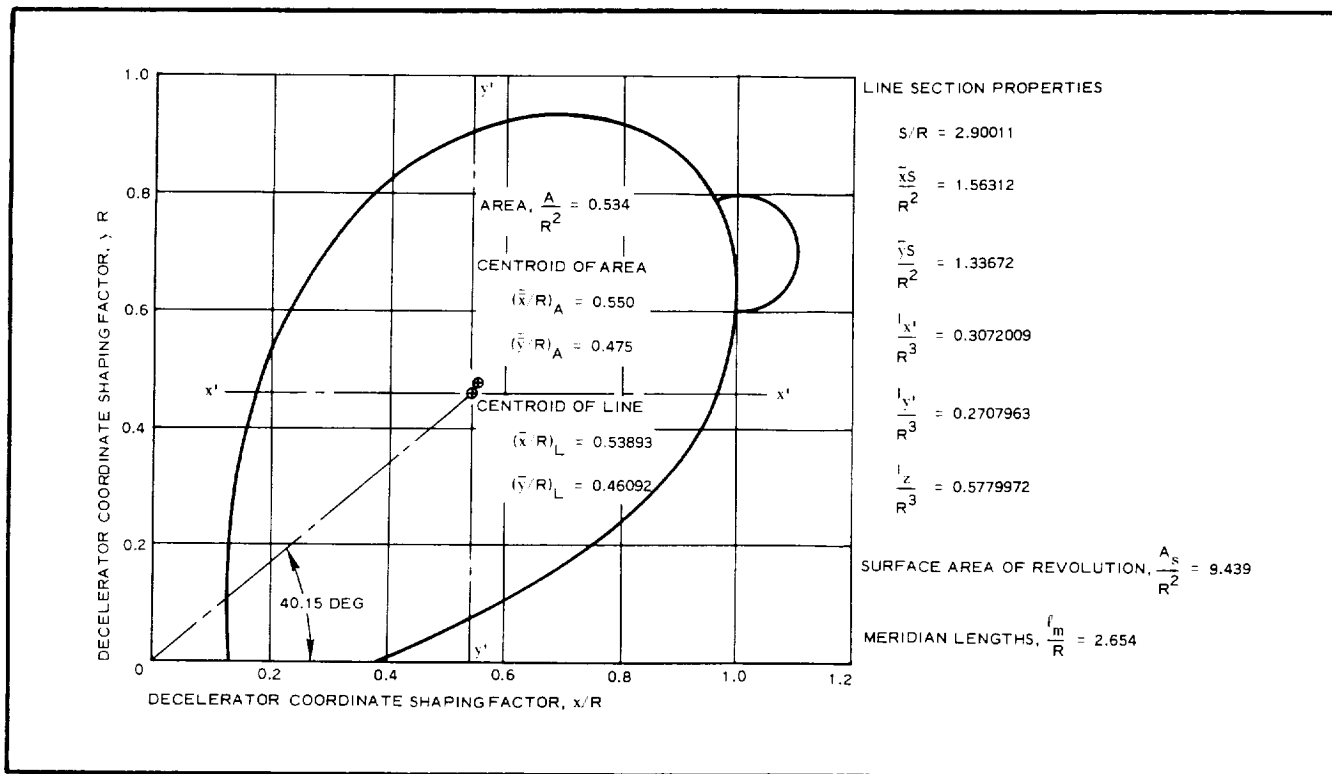


Figure 6 - Geometric Section Properties

This second program also calculated the properties of the line that encloses the cross section. These line section properties (see Figure 6) were required for the buckling analysis.

All these geometric properties must be qualified as follows:

1. The burble fence is not included.
2. The profile shape corresponds to the meridians so that the membrane spanning the meridians will lobe outside this profile.
3. All computer results are based on the total shape of Figures 3 and 6 above the plane $y/R = 0$, originally established for outer attachment at the base of the nominal 21-in. diameter aeroshell ($x/R = 0.380$), where $\phi = 23.6$ deg.

Based on aerodynamic and mechanical design considerations, these boundary conditions were changed to those indicated in Figure 3 so that (1) for the inner attachment, $(x/R)_i = 0.126$ and $(y/R)_i = 0.137$ and (2) for the outer attachment, $(x/R)_o = 0.440$ and $(y/R)_o = 0.027$.

The new angle (ϕ') at the outer attachment is slightly greater than 23.6 deg. By numerical differentiation based on the coordinates, the new angle is approximately

$$\begin{aligned}\phi' &= \tan^{-1} \left(\frac{0.27776 - 0.024929}{0.44200 - 0.4358} \right) \\ &= \tan^{-1} (0.49140) \\ &= 26.2 \text{ deg}\end{aligned}$$

The following values are used along with the preceding drag coefficients and nondimensional geometric properties to obtain the values tabulated in Figure 3.

1. $R = 27.3 \text{ in.}$ (shape summary)
2. $q = 125 \text{ psf}$ (design conditions)
3. $p_{\infty} = 19.84 \text{ psf} = 0.1378 \text{ psi}$ (aerodynamic considerations)

Then:

$$\begin{aligned}\text{Total drag, } D &= q C_D A \\ &= (125)(1.14) \left(\frac{\pi}{4} \right) (5)^2 \\ &= 2800 \text{ lb}\end{aligned}$$

$$\begin{aligned}\text{Burbles fence drag, } D_b &= 1.166 p_{\infty} \pi R^2 \\ &= (1.166)(0.1378)\pi(27.3)^2 \\ &= 376 \text{ lb}\end{aligned}$$

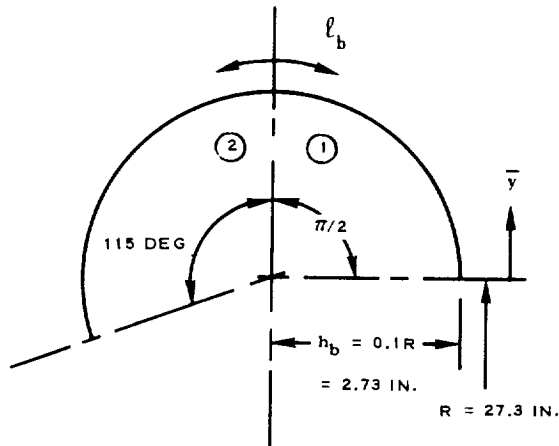
The volume, surface area, and meridian length of the canopy (without burble fence and neglecting lobing) having the origin shown in Figure 6 are

$$V_B = 2.018 R^3 = (2.018)(27.3)^3 = 41,200 \text{ cu in.} = 23.9 \text{ cu ft}$$

$$A_s = 9.439 R^2 = (9.439)(27.3)^2 = 7050 \text{ sq in.} = 49.0 \text{ sq ft}$$

$$\ell_m = 2.654 R = (2.654)(27.3) = 72.5 \text{ in.} = 6.04 \text{ ft}$$

The meridian length, surface area, and volume of the burble fence are estimated for the torus sector of Figure 6 as shown on page 14.



$$\begin{aligned} \ell_b &= 2.73 \left(\frac{115\pi}{180} + \frac{\pi}{2} \right) \\ &= 5.49 + 4.29 = 9.78 \text{ in.} = 0.815 \text{ ft} \end{aligned}$$

The line centroid, \bar{y} (see Sketch 1), is given by

$$\begin{aligned} \bar{y}_1 &= \frac{2h_b}{\pi} = \frac{2(2.73)}{\pi} = 1.735 \text{ in.} \\ \bar{y}_2 &= \frac{2.73 \sin 115 \text{ deg}}{115\pi} (180) = 1.233 \text{ in.} \end{aligned}$$

Therefore, the surface area of the fence can be written as

$$\begin{aligned} A_b &= 2\pi \left[(27.3 + 1.735)(4.29) + (27.3 + 1.233)(5.49) \right] \\ &= 1770 \text{ sq in} = 12.3 \text{ sq ft} \end{aligned}$$

The cross-sectional area (see Sketch 1) is given by

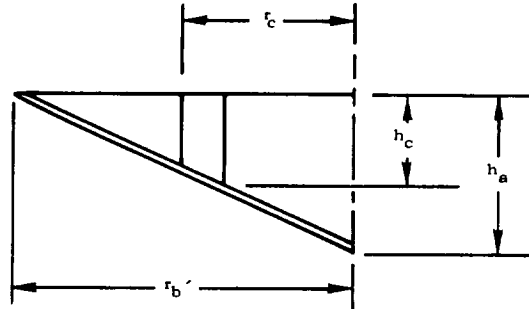
$$\begin{aligned} A_1 &= \frac{\pi}{4} (2.73)^2 = 5.86 \text{ sq in.} \\ A_2 &= \left(\frac{115}{360} \right) (4)(5.86) = 7.5 \text{ sq in.} \end{aligned}$$

The area centroid, $\bar{\bar{y}}$ (see Sketch 1), is given by

$$\begin{aligned} \bar{\bar{y}}_1 &= \frac{2}{3} \bar{y}_1 = \frac{2}{3} (1.735) = 1.157 \text{ in.} \\ \bar{\bar{y}}_2 &= \frac{2}{3} (1.233) = 0.822 \text{ in.} \end{aligned}$$

Therefore the volume of burble fence can be written as

$$\begin{aligned} V_b &= 2\pi \left[(27.3 + 1.157)(5.86) + (27.3 + 0.822)(7.5) \right] \\ &= 2380 \text{ cu in.} = 1.38 \text{ cu ft} \end{aligned}$$



The aeroshell net volume (Sketch 2) is the enclosed volume of the conical aeroshell minus that of the cylindrical sting support. For $r_b' = 10.5$ in., $r_c = 3.25$ in., $h_a = 6.06$ in., and $h_c = 4.18$ in.,

$$V_a = \frac{\pi}{3} r_b^2 h_a - \pi r_c^2 h_c = 702 - 139 = 563 \text{ cu in.} = 0.33 \text{ cu ft}$$

The total surface area, $A = A_s + A_b = 49 + 12 = 61$ sq ft. The total enclosed volume, $V = V_B + V_b + V_a = 23.9 + 1.4 + 0.3 = 25.6$ cu ft.

Detailed shape analysis. - The isotensoid design concept as developed in Reference 3 is based upon equal principal membrane forces in the fabric between meridians (fabric stress, $N_{\phi} = N_{\theta} = f$) that are constant over the entire surface of the decelerator. The tension in each meridian (T_m) also is constant over its entire length. The same stress conditions hold except that the constant stresses and meridian tensions in the front half are higher than those of the rear half due to the introduction of the concentrated burble fence drag load at the equator (see Appendix B). The stresses and meridian tensions are normalized per Reference 3 on the basis of the equatorial radius of the BALLUTE body and the constant gage pressure over the rear half of the BALLUTE. Then,

$$\text{Meridian tension, } T_m = k \frac{p\pi R^2}{n} \quad (4)$$

$$\text{Fabric stress, } f = F \frac{pR}{2} \quad (5)$$



Let the subscripts f and r denote the front and rear halves of the BALLUTE, respectively. The corresponding stress parameters of Equations (4) and (5), as given by the computer program for the conditions of Figure 3, are

$$\begin{aligned} k_f &= 0.5199 & F_f &= 0.1043 \\ k_r &= 0.4421 & F_r &= 0.08866 \end{aligned} \quad (6)$$

The above analysis considers the BALLUTE as a surface of revolution, which would be valid if a meridian spacing on the order of the fabric thread spacing could be achieved. However, even the largest practical number of meridians (n of Equation 4) that can be achieved using current materials and construction methods will not yield a sufficiently small spacing. The resulting surface is not one of revolution but has the scalloped effect observed in parachutes. The fabricated geometry of these lobes is controlled as closely as practical by properly tailoring the gore patterns. The basis of this technique is described below.

First, consider an area on the surface of the theoretical body of revolution in Figure 7. The dashed area of Figure 7 is magnified and is considered as the dashed plane surface in Figure 8. The solid lines of Figure 8 show the lobed fabric where the lob cross section will be considered as a circular arc.

For isotenoid conditions to be valid in Figure 8,

$$N_{\phi} = N_{\theta} = f = F \frac{pR}{2} \quad (5a)$$

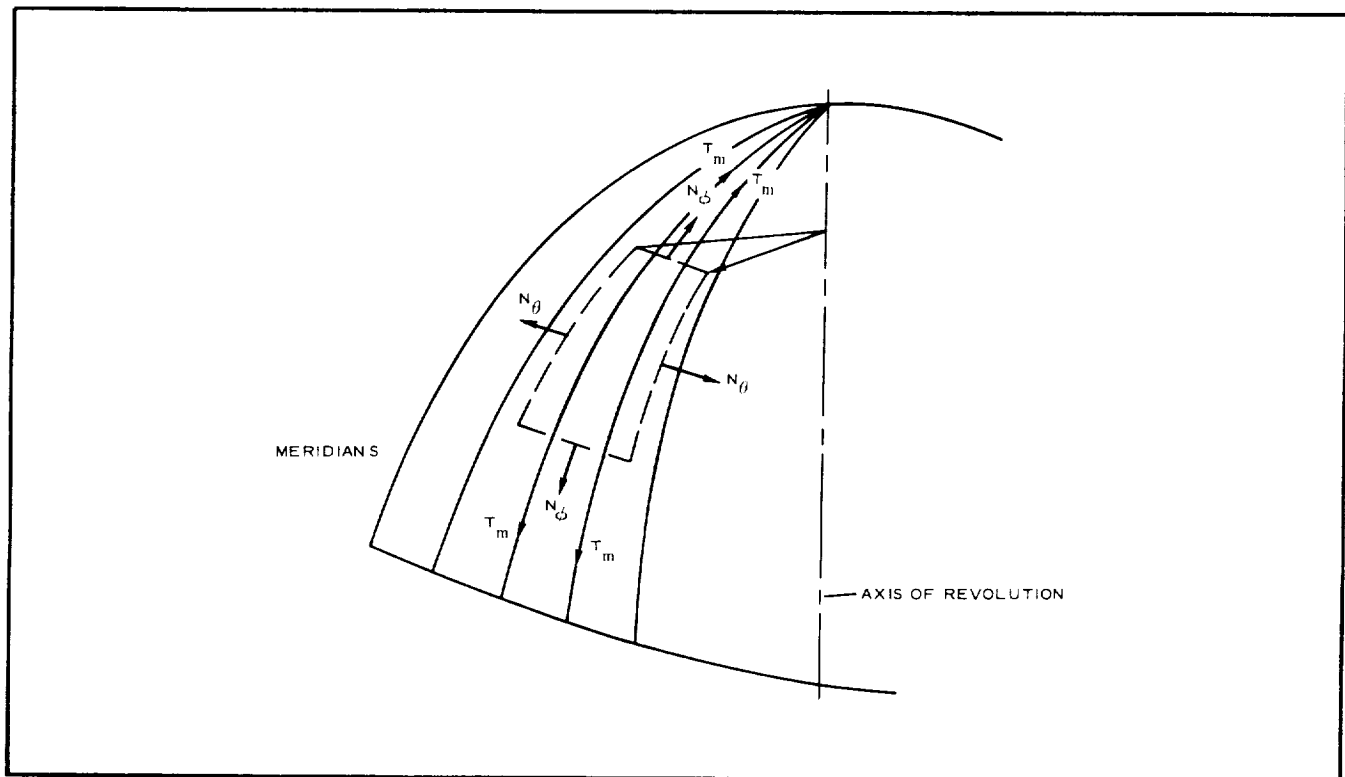


Figure 7 - Surface of Revolution with Meridians



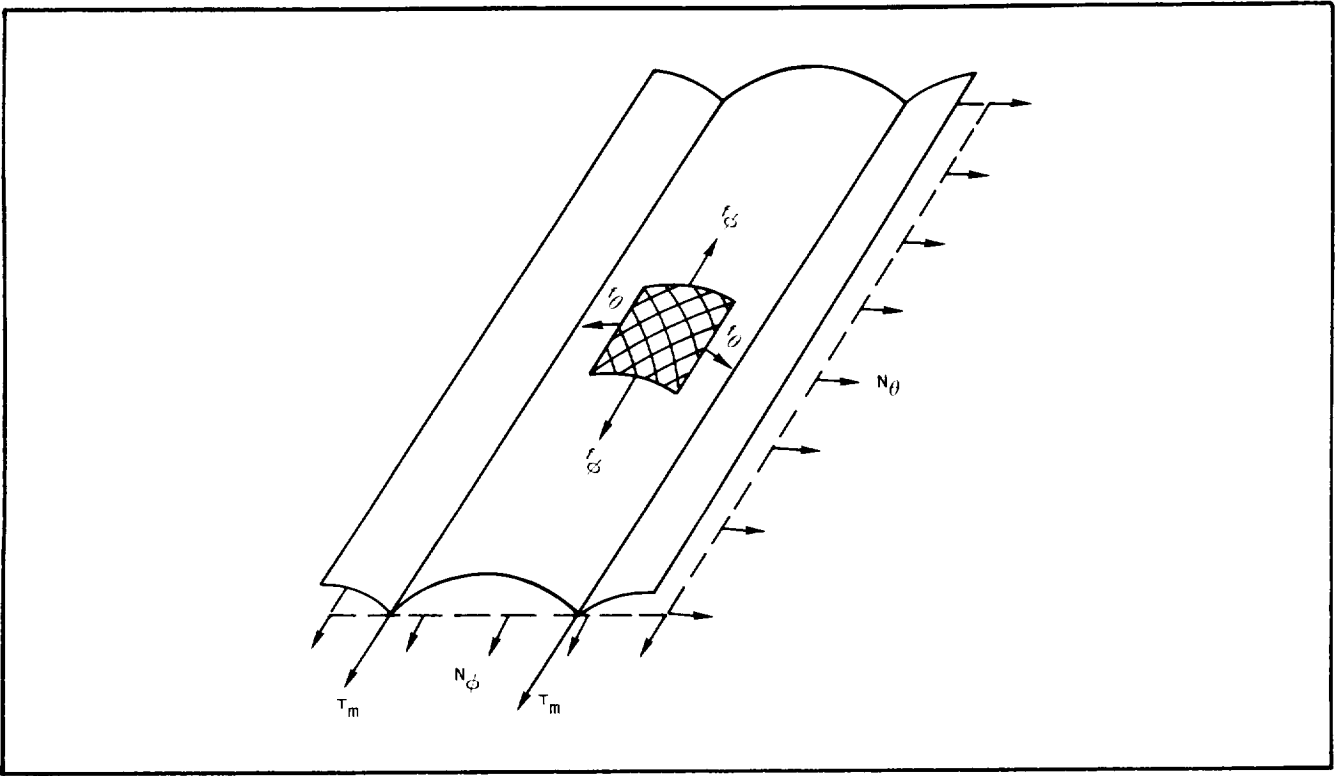


Figure 8 - Surface Element with Lobing

Now, consider the lobe cross section between two meridians and the fabric surface element that is made up of a bias, two-thread set fabric in Figures 9A and 9B, respectively. The required lobe and fabric geometry now can be found from the following equations based on Figures 7, 8 and 9.

Let f_b denote the actual fabric stress in the direction of the bias threads of Figure 9A. By statics in the ϕ and θ directions,

$$2f_b \sin^2 \gamma = f_\phi \quad (7)$$

$$2f_b \cos^2 \gamma = f_\theta \quad (8)$$

Therefore,

$$\frac{f_\phi}{f_\theta} = \tan^2 \gamma \quad (9)$$

By the geometry and statics of Figure 9A,

$$r_g \sin \beta = \pi x/n \quad (10)$$

$$N_\theta = f_\theta \cos \beta \quad (11)$$

$$f_\theta = p r_g \quad (12)$$

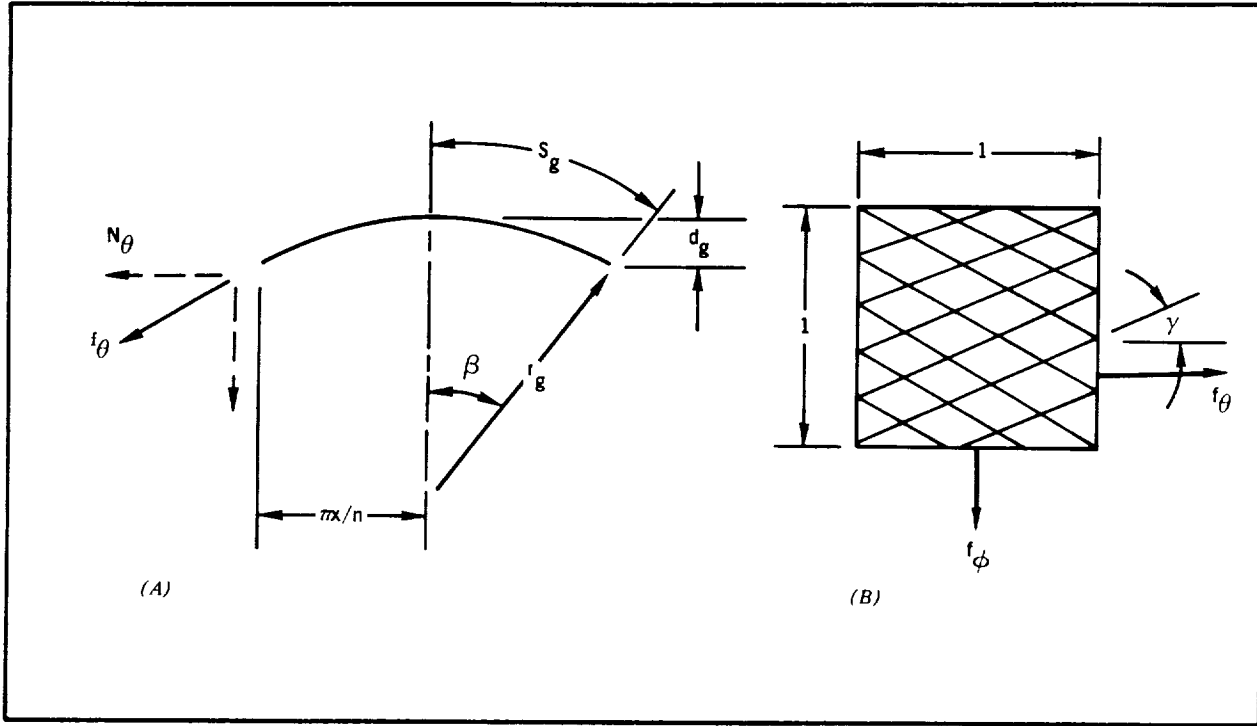


Figure 9 - Lobe Cross Section and Fabric Element

By statics between meridians in the ϕ direction of Figure 8,

$$N_\phi r_g \sin \beta = f_\phi r_g \beta$$

and

$$N_\phi = f_\phi \frac{\beta}{\sin \beta} \quad (13)$$

Equations (5) through (13) represent an 8 by 8 set of equations. By Equations (5), (9), (11), and (13),

$$\tan \gamma = \sqrt{\frac{\sin \beta \cos \beta}{\beta}} \quad (14)$$

By Equations (5), (10), (11), and (12),

$$\tan \beta = \frac{2\pi(x/R)}{nF} \quad (15)$$

From Equation (10),

$$\frac{r_g}{R} = \frac{\pi}{n \sin \beta} (x/R) \quad (16)$$

The half-arc length and the lobe depth are (see Figure 9A)

$$\frac{S_g}{R} = \left(\frac{r_g}{R} \right) \beta \quad (17)$$

$$\frac{d_g}{R} = \left(\frac{r_g}{R} \right) (1 - \cos \beta) \quad (18)$$

The actual fabric stress is given from Equations (5), (7), and (13) as

$$f_b = F \frac{pR}{4} \left(\frac{\sin \beta}{\beta \sin^2 \gamma} \right) \quad (19)$$

Or let

$$F_b = \frac{2f_b}{pR} = \frac{F \sin \beta}{2\beta \sin^2 \gamma} \quad (20)$$

Since Equation (14) states that the bias thread set angle is a function of the central lobe angle, the set angle should vary point by point along the meridian. This is not yet practical from the fabrication viewpoint. Furthermore, the constant 45-deg bias angle construction, as now used, only satisfied Equation (14) for the limit, $\beta \rightarrow 0$, which is compatible with the body of revolution where the meridian spacing approaches the bias thread spacing. The difference of γ values and the 45-deg construction can be considered as an indicator of an upper limit of the deflection of the BALLUTE from the design shape. This upper limit is quite conservative since the threads are not free to rack or pantograph due to the restraints of (1) thread friction, (2) the fabric coating, and (3) boundary conditions.

The nonextensible, meridional, and circumferential strains due to thread racking from 45 deg to the γ angle, respectively, can be given by

$$\epsilon_\phi = \sqrt{2} \sin \gamma - 1 \quad (21)$$

$$\epsilon_\theta = \sqrt{2} \cos \gamma - 1 \quad (22)$$

The corresponding deformed radius is simply

$$x'/R = x/R (1 + \epsilon_\theta) \quad (23)$$

Table IV gives the numerical values based on the preceding equations. Here, the stress coefficient, F , of Equation (5) assumes the values of Equation (6). Also, $n = 48$ is used in Equation (10) to satisfy the criterion that the lobe depth at the equator does not exceed one inch (see Figure 5).

TABLE IV - LOBE GEOMETRY, RADIAL GROWTH, AND
FABRIC STRESSES

x/R	$\frac{\beta}{\text{deg min}}$	d_g/R	r_g/R	S_g/R	$\frac{\gamma}{\text{deg min}}$	ϵ_ϕ (in./in.)	ϵ_θ (in./in.)	x'/R	F_b
0.4100	28 55	0.00743	0.05956	0.03006	42 29	-0.044	0.043	0.460	0.1096
0.5102	32 38	0.00978	0.06193	0.03527					
0.6032	37 8	0.01326	0.06540	0.04239	40 44	-0.077	0.062	0.641	0.1140
0.7148	41 54	0.01791	0.07006	0.05123					
0.8264	46 4	0.02301	0.07515	0.06042	38 6	-0.127	0.113	0.921	0.1229
0.9349	49 34	0.02813	0.08044	0.06959					
0.9607	50 20	0.02956	0.08172	0.07179	36 48	-0.152	0.131	1.090	0.1273
0.9862	51 4	0.03084	0.08299	0.07397					
0.9978	51 24	0.03144	0.08360	0.07500					
1.00	51 27	0.03154	0.08370	0.07516	36 21	-0.163	0.139	1.135	0.1294
1.00	55 53	0.03471	0.07904	0.07709	34 57	-0.190	0.159	1.159	0.1144
0.9933	55 42	0.03433	0.07866	0.07647					
0.9608	54 49	0.03262	0.07696	0.07363	35 4	-0.188	0.158	1.111	0.1145
0.9194	53 37	0.03040	0.07473	0.06993					
0.8389	51 5	0.02624	0.07057	0.06292	36 26	-0.160	0.138	0.954	0.1097
0.7670	48 33	0.02264	0.06697	0.05675					
0.6850	45 19	0.01871	0.06304	0.04986	38 29	-0.119	0.107	0.758	0.1029
0.5885	40 59	0.01439	0.05872	0.04200					
0.4787	35 15	0.00996	0.05430	0.03341	41 11	-0.059	0.064	0.509	0.0958
0.3856	29 39	0.00668	0.05101	0.02640					
0.3000	23 53	0.00415	0.04850	0.02022	43 19	-0.029	0.029	0.309	0.0914
0.2377	19 20	0.00265	0.04698	0.01585					
0.1928	15 53	0.00176	0.04610	0.01278	44 15	-0.012	0.013	0.196	0.0898
0.1730	14 19	0.00142	0.04575	0.01143					
0.1520	12 39	0.00110	0.04544	0.01003	44 31	-0.009	0.008	0.153	0.0894
0.1302	10 53	0.00081	0.04514	0.00857					
0.1263	10 34	0.00077	0.04510	0.00832					
0.1260	10 32	0.00076	0.04508	0.00829	44 39	-0.007	0.005	0.127	0.0893

Decelerator Stress Analysis

Summary. - Table V summarizes the calculated margins of safety and their corresponding design factors. Although wind-tunnel conditions should be considered for the decelerator model analysis, margins and factors also are given for this same model as a flight-test unit. The purpose is to emphasize that (1) the tunnel flow breakdown does not apply to flight considerations and (2) a higher safety factor is used for the wind-tunnel model than for a flight unit (2 versus 1.5). This accounts for reduction in material strength due to creep at elevated temperature over a relatively long time (one-half hour or more) that may occur during testing in a wind tunnel compared with short-time flight loading.

TABLE V - MARGINS OF SAFETY AND DESIGN FACTORS

Item	Wind-tunnel decelerator		Flight-test decelerator	
	Fabric	Meridians	Fabric	Meridians
Margins of safety	1.9	0.80	4.8	2.6
Design factors				
Overload (flow breakdown)	1.5	1.5	1.0	1.0
Dynamic (flag snapping)	1.5	1.5	1.5	1.5
Temperature (350 deg F)	1.38	1.33	1.38	1.33
Seam efficiency	1.25	1.0	1.25	1.0
Racking	1.1	1.0	1.1	1.0
Factor of safety	<u>2.0</u>	<u>2.0</u>	<u>1.5</u>	<u>1.5</u>
Composite design factor (S. F.)	8.55	6.0	4.27	3.0

While minimum gage considerations govern the design, the margins in Table V are necessarily high for the functioning model. Meridian tape rated at 500 lb and coated fabric having a coated weight of 2.36 oz/sq yard and rated at 80 lb/in. were the light gage materials selected.

By a separate analysis, buckling of the pressurized structure was found not to be critical.

Limit loads. - The following analysis serves as the basis for material selection. The maximum fabric stress coefficient from Table IV occurs at the equator and is

$$F_{b_{\max}} = 0.1294 \quad (24)$$

This stress is conservative since the corresponding γ angle is low.



The maximum k_f of Equation (6) along with $F_{b_{\max}}$ of Equation (24) governs the meridian and fabric selections, respectively. The corresponding limit design values then are given by definition as follows.

From the design conditions section and as previously defined,

$$q = 125 \text{ psf}$$

$$M_{\infty} = 3$$

$$T = 350 \text{ deg F}$$

$$R = 27.3 \text{ in.}$$

The reference pressure equals the internal pressure minus the constant external pressure over the rear of the BALLUTE - that is,

$$P = P_i - P_r \quad (25)$$

or in terms of the distributions of Figure 1,

$$\begin{aligned} \frac{p}{P_{\infty}} &= \frac{P_i}{P_{\infty}} - \frac{P_r}{P_{\infty}} \\ &= \frac{P_i}{P_{\infty}} - 0.4 \end{aligned} \quad (26)$$

From the aerodynamic considerations section,

$$C_{P_i} = \frac{P_i - P_{\infty}}{q} = 2 \quad (27)$$

Furthermore, from aerodynamics in this Mach number regime,

$$q = 0.7 M_{\infty}^2 P_{\infty} \quad (28)$$

Then,

$$C_{P_i} = \frac{P_i - P_{\infty}}{0.7 M_{\infty}^2 P_{\infty}}$$

and

$$\frac{P_i}{P_{\infty}} = 0.7 M_{\infty}^2 C_{P_i} + 1 = (0.7)(3)^2 (2) + 1 = 13.6 \quad (29)$$



Substituting Equation (29) into Equation (26),

$$\frac{p}{p_{\infty}} = 13.6 - 0.4 = 13.2 \quad (30)$$

where for $q = 125$ psf (from Equation 28),

$$p_{\infty} = \frac{125}{(0.7)(9)} = 19.84 \text{ psf} = 0.1378 \text{ psi} \quad (31)$$

Therefore,

$$p = (13.2)(0.1378) = 1.82 \text{ psi} \quad (32)$$

Substituting the above values along with $n = 48$ into Equations (4) and (5) gives the following limit loads and stresses:

$$T_m = (0.52) \left[\frac{(1.82) \pi (27.3)^2}{48} \right] = 46.3 \text{ lb} \quad (33)$$

$$f_b = (0.1294) \left[\frac{(1.82)(27.3)}{2} \right] = 3.22 \text{ lb/in.} \quad (34)$$

Design factors. - To convert these limit values to the required room temperature ultimate strengths, design factors are applied that are composed of the following considerations.

Overload factor, (F.S)_O: This factor accounts for an increase in the internal pressure over and above the design pressure. This may occur due to the flow breakdown conditions in the AEDC 16S tunnel. Flow breakdown can be accounted for by adding a pressure of 0.2 p_t to the frontal area. Assuming the internal pressure can increase by the same amount, for M_∞ = 3 and q = 125 psf (Figure 2.4 of Reference 4), p_t = 700 psf and 0.2 p_t = 140 psf.

The design internal pressure by Equations (29) and (31) is

$$p_j = (13.6)(19.8) = 270 \text{ psf}$$

Therefore, the overload factor becomes

$$(F.S)_O = 1 + \frac{140}{270} = 1.5 \quad (35)$$

Dynamic factor, (F.S.)_D: This factor accounts for loads resulting from high dynamic pressures and free-stream velocities acting on relatively large areas of lightweight fabric during inflation. The high-speed cameras on the Aerodynamic Deployable Decelerator Performance Evaluation Program (ADDPEP) vehicle provided considerable data for inspecting this partially inflated condition (Reference 2).



Observed whipping action (referred to as flag snapping) can result in split envelope gores unless a dynamic factor is applied to the steady-state limit loads or unless methods are used to reduce these dynamics loads. The flag snapping ceases as soon as a "ball" of air is in the BALLUTE; therefore, the dynamic effects are diminished by inducing this "ball" of air as rapidly as possible. Since the ram-air process is rather slow, inflation aids such as liquid vaporization at high altitudes have been used for initial inflation.

Experience has indicated that for plain-back trailing BALLUTES, which fully inflate in the neighborhood of one-half second when deployed at supersonic speeds, the following empirical dynamic factor should be used:

$$(F.S)_D = 1.5 \quad (36)$$

Due to lack of further knowledge, this factor will be used although it is suspected to be conservative primarily because the canopy is attached to the aeroshell to alleviate flag snapping.

As a sidelight, an empirical formula was developed to account for the flagging of subsonically deployed trailing BALLUTES that are entirely ram-air inflated:

$$F_{t_u} = \left(\frac{7}{3}\right) q R$$

This ultimate strength criterion accounts for all considerations except for possible elevated temperatures that generally do not occur until after the BALLUTE is fully inflated when flagging has ceased. Although the equation does not apply to $M_\infty = 3$ conditions, the fabric can carry such a load even assuming that the design temperature of 350 deg F occurs during the flagging condition. The margin of safety would be four percent as shown below:

$$F_{t_u} = (F.S.)_T \left(\frac{7}{3}\right) q R$$

Substituting Equation (37) along with the values for q and R from the aerodynamics and design conditions sections, respectively,

$$F_{t_u} = (1.38) \left(\frac{7}{3}\right) \left(\frac{125}{144}\right) (27.3) = 76.4 \text{ lb/in.}$$

The actual ultimate fabric strength given in the materials selection section is 80 lb/in. The margin of safety is, therefore,

$$(M.S)_f = \frac{80}{76.4} - 1 = 0.04$$

Temperature factors $(F.S.)_T$: The design temperature of 350 deg F can be treated as a factor. From Figures 2 and 4 of Reference 5, the strengths of Viton-coated Nomex cloth and of the Nomex webbing at 350 deg F are 72.4 percent and 75 percent of the room temperature strengths, respectively. The corresponding temperature factors are



$$\text{Fabric, (F.S.)}_T = \frac{1}{0.724} = 1.38 \quad (37)$$

$$\text{Meridians, (F.S.)}_T = \frac{1}{0.75} = 1.33 \quad (38)$$

Seam efficiency (F.S.)_S: Seam efficiencies of 80 percent for the fabric and 100 percent for the meridians can be expected based on data obtained from other programs. These efficiencies will be validated by seam tests described under the development tests section. The factors then are

$$\text{Fabric, (F.S.)}_S = \frac{1}{0.8} = 1.25 \quad (39)$$

$$\text{Meridians, (F.S.)}_S = 1 \quad (40)$$

Racking (F.S.)_R: Seam leakage is more peculiar to BALLUTEs than to parachutes. Some cloths rack under loads considerably below the ultimate seam strength. Racking occurs when the cloth yarns running in one direction are pulled locally by the sewing threads into a bunch, thus leaving small local voids in the cloth. Although this does not necessarily degrade the fabric strength, a factor of from 1.0 to 1.2 should be applied to obtain a required porosity. Therefore, the following factor, applied to the fabric only, will be used:

$$(\text{F.S.})_R = 1.1 \quad (41)$$

Basic safety factor, (F.S.): A safety factor of two is used with limit stresses to obtain ultimate stresses in the analysis of the fabric and of the meridians.

Design factors, (S.F.): Table VI gives the composite design factors based on Equations (35) through (41).

TABLE VI - COMPOSITE DESIGN FACTORS

Factors		Fabric	Meridians
Overload	(F.S.) _O	1.5	1.5
Dynamic	(F.S.) _D	1.5	1.5
Temperature	(F.S.) _T	1.38	1.33
Seam efficiency	(F.S.) _S	1.25	1.0
Racking	(F.S.) _R	1.1	1.0
Safety factor	F.S.	<u>2.0</u>	<u>2.0</u>
Design factor	S.F.	8.55	6.0

The required ultimate room temperature strengths are given by applying these design factors to the stresses of Equations (33) and (34),

$$T_{m_u} = (S.F.)_m T_m = (6)(46.3) = 278 \text{ lb}$$

$$F_{t_u} = (S.F.)_f f_b = (8.55)(3.22) = 27.6 \text{ lb/in.}$$

The actual ultimate strengths given in the materials selection section are 500 lb and 80 lb/in. for the meridians and fabric, respectively. Therefore, the margins of safety are

$$(M.S.)_m = \frac{500}{278} - 1 = 0.80$$

$$(M.S.)_f = \frac{80}{27.6} - 1 = 1.9$$

Buckling. - Even with positive (tensile) stresses existing throughout the inflatable structure, a buckling phenomenon could exist; this has been recognized by investigators of pressurized structures (References 6, 7, and 8). However, this possibility was discounted when an analysis of in the plane of the ring and out of the plane of the ring buckling capacities of the configuration found safety factor values of 10.4 and 6.1, respectively, based on design limit external pressure. The analysis is not detailed in this report.

Hard Structure Stress Analysis

Table VII summarizes the hard structure stress analysis. The values provide a comparison of computed safety factors with the factors specified in AEDC Document QCP-000-21.

The values of Table VII are based on loading condition seven of Table I, which is the governing condition for the stress analysis of the hard structure shown in Figure 10. The analysis is not detailed in this report.

DESIGN DOCUMENTATION

General

Design analysis of the selected configuration culminated in the preparation of drawings for the fabrication of an AID (see Appendix D).

Figure 11 shows the dimensional control of the attachments; Figures 12 through 15 show assembly fabrication stages of the model. The components of the AID model assembly are factory replaceable as parts or as assembly fabrications identified in the following Goodyear Aerospace drawings.

610A000-001-101,	model assembly, AID system
610A000-002-102,	decelerator assembly
610A000-101-1,	aeroshell
610A000-102-101,	support assembly
610A000-103-1,	cutter clamp
610A000-103-3 or 11,	inner clamp
610A000-103-101,	reservoir assembly
610A000-103-103,	model-balance pin
610A000-104-101,	outer clamp assembly
Atlas C176-5,	reservoir cutter
Atlas C106,	daisy chain cutter (2)
CEC Type 4-316,	pressure transducer

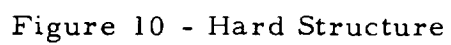
TABLE VII - SAFETY FACTORS FOR HARD STRUCTURE

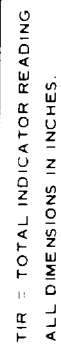
Component and type of load	Steady-state Condition		Flow break- down condition
	Computed safety factor on yield ^a	Computed safety factor on ultimate ^b	Computed safety factor on yield ^c
Aeroshell			
Membrane tension	7.18	13.47	5.54
Support			
Bearing from pin load	3.48	5.81	2.22
Outer clamp			
Shear load on screw	8.33	9.80	6.87
Bearing on clamp	4.25	7.99	3.51
Bearing on aeroshell	3.04	5.70	2.50
Inner clamp			
Shear load on section	5.20	6.10	4.30
Bearing on clamp	5.02	8.36	4.15
Mounting pin			
Shear load on pin	4.55	5.45	2.90

^aSpecified safety factor equals 3.

^bSpecified safety factor equals 4.

^cSpecified safety factor equals 2.





29

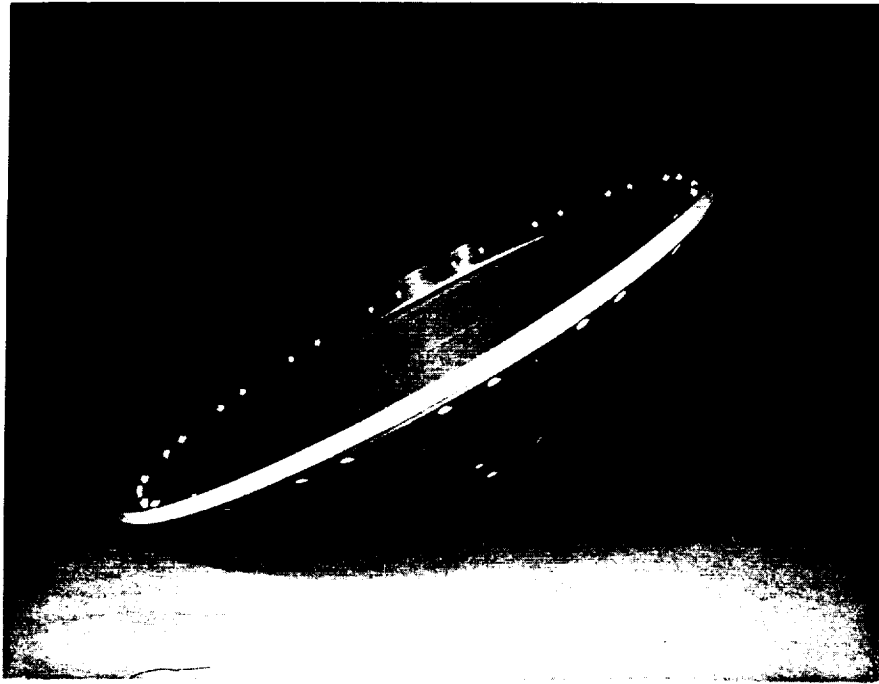


Figure 12 - Aeroshell Cone and Outer Clamp

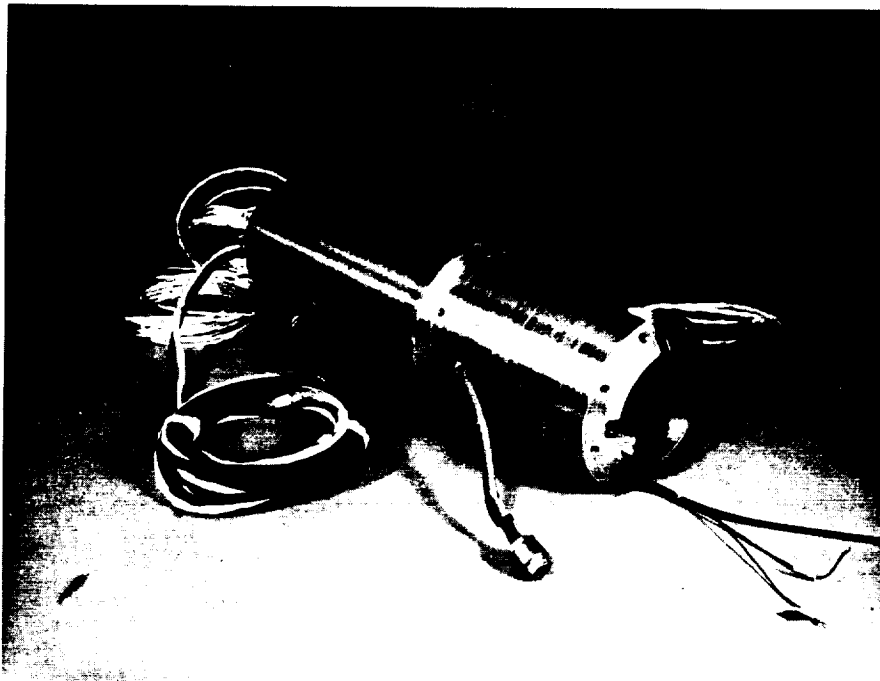


Figure 13 - Support Sleeve and Installed Cable

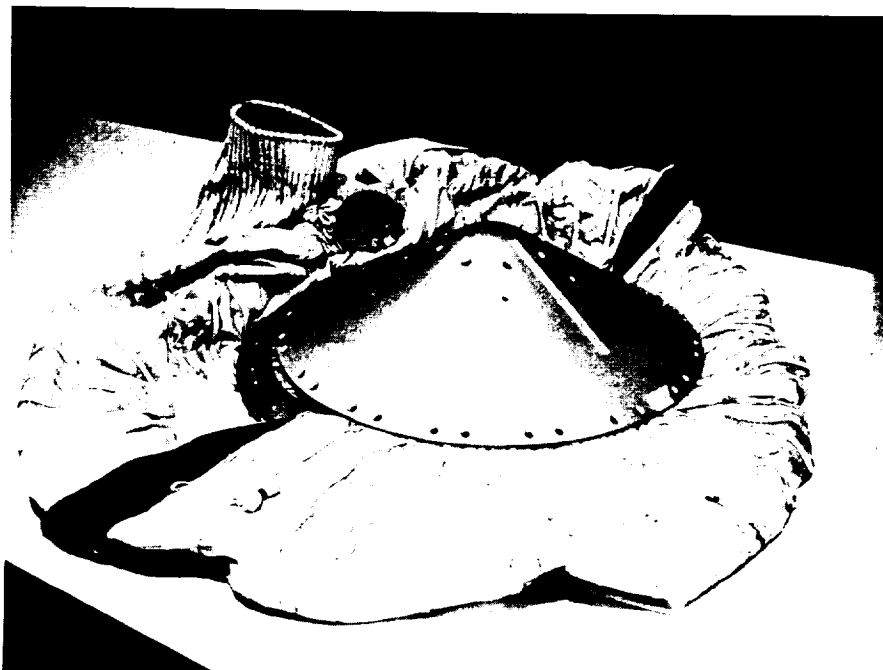


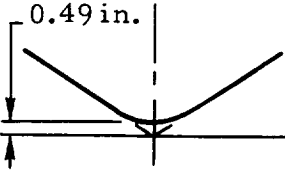
Figure 14 - Decelerator Afterbody, Cone, and Clamp



Figure 15 - Sensors and Operating Components

Tables VIII and IX give the actual weights and calculated centers of gravity for the packaged and deployed configurations of two assembled models.

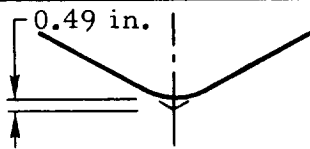
TABLE VIII - ACTUAL WEIGHT AND CENTER OF GRAVITY,
AID NO. 1

 0.49 in. Ref datum apex of aeroshell	Weight (lb)	Center of gravity ^a (in.)	
		Deployed	Packaged
Hard structure	(91.02)	(9.93)	(9.87)
Tube support	71.01	11.03	11.03
Aeroshell	12.78	4.70	4.70
Inner clamp	1.50	9.24	9.24
Outer clamp	3.80	6.96	6.96
Pressure transducer and clamp	0.03	3.80	3.80
Reservoir	0.47	2.70	2.70
Vaporizing fluid	0.38	18.92	2.70
Daisy chain cutter (2)	0.06	11.35	11.35
Reservoir cutter	0.47	4.60	4.60
Cabling	0.36	13.13	13.13
Tubing	0.16	12.30	12.30
Inflatable afterbody	(4.18)	(18.87)	(6.44)
Inlet assembly (4)	0.57	16.90	6.44
Canopyless fence	3.38	18.92	
Burbles fence	0.23	23.00	
Total	95.20	10.31	9.72

^aIn packaged to deployed configuration for AID No. 1, center of gravity shifted 0.59 in. (10.31 - 9.72) with hard structure and 12.43 in. (18.87 - 6.44) without hard structure.

TABLE IX - ACTUAL WEIGHT AND CENTER OF GRAVITY,

AID NO. 2

 Ref datum apex of aeroshell	Weight (lb)	Center of gravity ^a (in.)	
		Deployed	Packaged
Hard structure	(88.82)	(9.94)	(9.81)
Tube support	68.44	11.03	11.03
Aeroshell	12.78	4.70	4.70
Inner clamp	1.50	9.24	9.24
Outer clamp	3.80	6.96	6.96
Pressure transducer and clamp	0.03	3.80	3.80
Reservoir	0.47	2.70	2.70
Vaporizing fluid	0.75	18.92	2.70
Daisy chain cutter (2)	0.06	11.35	11.35
Reservoir cutter	0.47	4.60	4.60
Cabling	0.36	13.13	13.13
Tubing	0.16	12.30	12.30
Inflatable afterbody	(4.18)	(18.87)	(6.44)
Inlet assembly (4)	0.57	16.90	6.44
Canopyless fence	3.38	18.92	
Burbles fence	0.23	23.00	
Total	93.00	10.33	9.66

^aIn packaged to deployed configuration for AID No. 2, center of gravity shifted 0.67 in. (10.33 - 9.66) with hard structure and 12.43 in. (18.87 - 6.44) without hard structure.

Control of Attachment Points

Design and fabrication of a small-scale inflatable decelerator model with features similar to one of actual size is relatively difficult. The hard structure design purposely is made simple, with a small number of parts and

machining operations minimizing the buildup of tolerances. Dimensional control by a judicious assignment of tolerances compatible with shop methods holds the relationship of the outer attachment to the inner attachment to within 0.06 in. This variance, resulting from practical machining tolerances and after-assembly adjustment, is shown in the following analysis.

For the separation of attachment points in the shape profile, where S_x and S_y represent the distance of separation in the two directions,

$$\frac{S_x}{R} = (x/R)_o - (x/R)_i$$

$$\begin{aligned} S_x &= 27.3 (0.440 - 0.126) \\ &= 8.56 \text{ in.} \end{aligned}$$

$$\frac{S_y}{R} = (y/R)_o - (y/R)_i = \frac{r_b}{4}$$

$$\begin{aligned} S_y &= 27.3 (0.137 - 0.027) = \frac{12}{4} \\ &= 3.00 \text{ in.} \end{aligned}$$

By referring to the drawing dimensions and tolerances, letter-coded in Figure 11, the allowable variance from separation of the attachment points was computed from the tolerances given in Table X.

Axial adjustment of the inner clamp prior to match drilling eliminates values for E and F resulting in a corrected variance of 0.06 in. maximum for S_y .

TABLE X - POSSIBLE VARIANCE FROM ESTABLISHED
RELATIONSHIP OF ATTACHMENTS

S_x variance		S_y variance	
Coded tolerance ^a	Value (in.)	Coded tolerance ^a	Value (in.)
A	0.005	C	0.010
A'	0.030	C'	0.005
B	0.005	D	0.01
B'	0.005	D'	0.005
Total	0.045	E	(0.07)
		E'	0.030
		F	(0.02)
		F'	Negligible
		Total	0.15
		Corrected total	0.06

^aTolerances denoted by the prime superscript (') are for surface eccentricity of the revolving shape.

MATERIALS SELECTION

Hard Structure

The completed aeroshell drawing (see Appendix D) calls for aluminum alloy sheet to be spun-form to final shape after an intermediate stabilizing heat treatment. A rigid, close-fitting, low-carbon steel tube serves as the transitional support between the sting-mounted internal balance and the aeroshell. A hardened steel mounting pin is the load-carrying element between the support and AEDC balance.

The decelerator is secured to the hard structure by clamping the canopy end bands. Outer attachment to the aeroshell is achieved by a 6061-T6 aluminum alloy clamping ring; inner attachment to the tube support is achieved by steel clamping sectors.

Approved locking devices selected for retaining machine screw fasteners are Elastic Stop lock spline nuts in the outer clamping ring for attaching to the aeroshell cone; Helicoil lock inserts in the support tube for fastening the aeroshell, inner clamp sectors, daisy chain cutters, and pressure transducer; and regular Elastic Stop nuts for mounting the reservoir tube and reservoir cutter to the aeroshell.

Decelerator

The low material strengths required for designing and fabricating a small-scale decelerator model are difficult to obtain in optimum sizes as off-the-shelf items; however, every consideration was given to scale components within practical reason.

The selection of Nomex cloth coated with Viton provides a minimum-thickness, high-strength material representative of the fabric system to be chosen for free-flight conditions at 350 deg F. Since the basic cloth has an airflow porosity rate of 19 ft/min when subjected to a conventional 0.5-in. water pressure, the leakage rate was reduced by calendering the cloth and applying 0.5 oz/sq yd of Viton elastomer. This lightweight coating does not restrict the cloth lobing capability nor does it lock in the yarns, which would result in lower seam efficiency. After coating, the porosity flow rate was only 0.02 ft/min.

The meridians are MIL-T-5038 Type V tape but are specially woven of Nomex instead of nylon. To simulate the relative meridian size better, the 500-lb tape was folded to 1/4-in. wide for attachment to the fabric. The gore panel seam is a simple one-inch wide lap seam and uses two rows of Federal Specification 751 Type 301 lockstitching and one row of single-throw Type 304 zig-zag stitching. The zig-zag stitch was used to secure the edge of the fabric that is exposed to the airstream. The main gore seam used to attach adjacent gores also is a simple lap seam, is 5/8-in. wide, and uses three rows of single-throw Type 304 zig-zag stitching. Burble fence seams are all Type 304 zig-zag to allow for lobing. To reinforce the gore around the inlet, a Good-year Aerospace-developed 300-lb braided Nomex cord was sewn in place.

The inlet seam is similar to the main gore seam. An expected seam of 80 per cent was validated by seam tests reported under the development tests section.

The physical characteristics of coated Goodyear Aerospace fabric GX601-V0302, with values of warp/fill differentiation, are given in Table XI.

TABLE XI - PHYSICAL CHARACTERISTICS OF
GOODYEAR AEROSPACE-COATED FABRIC

Characteristic	Value
Tensile strength, lb/in. (rated at 80)	96/83
Tear strength (lb/in.)	9.0/6.8
Elongation (%)	27.9/29.0
Thickness (in.)	0.0037
Weight (oz/sq yd)	2.36
Thread count per inch	80/77
Porosity limit (cu ft/sq ft-min)	0.02 at 0.5 inch of water

DEVELOPMENT TESTS

Reservoir Acceptance Pressure Test

For acceptance testing, each reservoir was subjected to better than the expected wind-tunnel test conditions of static pressure, stagnation temperature, and span time. Acceptable units held the measured amount of water without loss.

Deliverable, filled reservoirs of final design were fabricated of soft butyl tubing, were pressure constrained by nylon fabric sleeves, and were exposed for 2-1/4 hr to a bell jar vacuum pressure of 1.3 to 2.9 psfa at 178 to 180 deg F. Vaporizing fluid consisted of equal weights of water and methyl alcohol. The test is validated by the weight data in Table XII. The minute weight loss was from evaporation of outside moisture from the nylon sleeve.

TABLE XII - RESERVOIR WEIGHT DATA

AID number	Reservoir fluid weight		Reservoir weight (grams)	Filled reservoir weight before test (grams)	Filled reservoir weight after test (grams)
	Ounces	Grams			
1	6	170.1	217.5	387.6	386.8
2	12	340.2	205.3	545.5	544.3

Tensile Tests of Nomex Fabrications

The following Nomex material fabrications comprising the decelerator canopy were tensile tested to validate their structural integrity. Unit fabric and seam tests were performed by the raveled strip method on an Instron machine in accordance with Federal Specification CCC-T-191. Break test values of all test specimens are given for each material fabrication; their average is compared with the rated value assured by the manufacturer.

1. Canopy fabric, GAC GX601V0302:

<u>Specimen (warp direction)</u>	<u>Ultimate load (lb/in.)</u>
1	96.0
2	96.5
3	96.0
4	96.0
5	95.5
Average	96.0
Rated	80

<u>Specimen (fill direction)</u>	<u>Ultimate load (lb/in.)</u>
1	92.0
2	80.0
3	83.0
4	81.0
5	80.0
Average	83.0
Rated	80

2. Main gore seam

<u>Specimen (warp direction)</u>	<u>Ultimate load (lb/in.)</u>
1	77.7
2	76.2
3	73.3
4	73.2
5	78.6
Average	75.8
Rated (80% of 80)	64

3. Rear burble fence seam

<u>Specimen (warp direction)</u>	<u>Ultimate load (lb/in.)</u>
1	81.2
2	80.0

<u>Specimen</u> <u>(warp direction)</u>	<u>Ultimate load</u> <u>(lb/in.)</u>
3	84.0
4	82.0
5	81.5
Average	81.7
Rated	64

4. Forward burble fence seam

<u>Specimen</u> <u>(warp direction)</u>	<u>Ultimate load</u> <u>(lb/in.)</u>
1	83.0
2	84.0
3	81.9
4	80.0
5	81.1
Average	82.0
Rated	64

5. Inlet seam

<u>Specimen</u> <u>(warp direction)</u>	<u>Ultimate load</u> <u>(lb/in.)</u>
1	79.1
2	75.0
3	77.0
4	70.1
5	72.3
Average	74.8
Rated	64

6. Meridian tape, MIL-T-5038 Type V of Nomex

<u>Specimen</u>	<u>Ultimate load</u> <u>(lb)</u>
1	560.0
2	555.0
3	552.0
Average	555.6
Rated	500

7. Inlet erection cord, GAC braided weave

<u>Specimen</u>	<u>Ultimate load</u> <u>(lb)</u>
1	325
2	302

<u>Specimen</u>	<u>Ultimate load (lb)</u>
3	357
Average	<u>326</u>
Rated	300

8. Sewing thread, Size E

<u>Specimen</u>	<u>Ultimate load (lb)</u>
1	7.6
2	7.6
3	7.7
4	7.5
5	<u>7.9</u>
Average	<u>7.6</u>
Rated	7

9. Sewing thread, Size F

<u>Specimen</u>	<u>Ultimate load (lb)</u>
1	10.0
2	9.5
3	10.1
4	9.7
5	<u>9.5</u>
Average	<u>9.76</u>
Rated	9

10. Sewing thread, Size FF

<u>Specimen</u>	<u>Ultimate load (lb)</u>
1	11.9
2	12.5
3	13.0
4	12.9
5	<u>12.0</u>
Average	<u>12.5</u>
Rated	11.5

Fabric Permeability Test

Random samples of the canopy fabric first were retroflexed to 1000 cycles and then were tested at room temperature with a flowrater to determine if the porosity exceeded an arbitrary limit of 0.02 cu ft/sq ft-min at a pressure of 0.5 in. of water. Flow values were as follows.

<u>Specimen</u>	<u>Flow</u> <u>(cu ft/sq ft-min)</u>
1	0.01
2	0.05
3	0.01
Average	0.02

Decelerator Packaging Demonstration

Introduction. - The inflatable decelerator must be packaged in a series of concise, discrete steps to ensure that it will deploy in a systematic and repeatable manner.

The envelope fabric must be prevented from rubbing excessively against itself during unfolding in order to eliminate frictional heating, which possibly could decrease fabric strength. In addition, it is desirable to provide for erection of the ram-air inlets into the airstream for immediate transfer from pressurization by self-inflation to ram-air pressurization. The solution to both these requirements basically is a common one.

Approach. - To expose the inlets quickly, portions of surface area upon which they are built must be deployed first, which locates these portions on or near the top of the packaged configuration. In addition, an aspect of the tucked-back canopy that tends to restrict its packaging (compared with a conventional plain-back configuration) is the relatively small core radius of the tucked portion. Thus, the portion of envelope fabric adjacent to the inner attachment circle must be packed in cylindrical-type folds along the mounting cylinder. This material was folded first to allow its logical deployment last.

Figure 16 shows the basic gore longitudinal folds. The requirements were satisfied by first folding the tucked gore vertically and by progressing to horizontal folds from the rear surface toward the front attachment. In a minor modification for benefiting egress, the initial tucked surface was folded over the attachment point shoulder. In addition, pleats were made in the gore width since fabric from a larger diameter was packaged at a smaller diameter, thus resulting in excess material that must be systematically arranged.

Restraint system. - The final restraint, to retain the uninflated decelerator in its packaged configuration, was made with a series of loops assembled together to form a daisy chain hoop around the sleeve support. Figure 17 shows a planform view of the completed assembly. When an electrical initiation signal is given, the redundant cutters activate to sever the chain retaining cord. Once severed, it pulls out of loops No. 1, No. 2, and No. 16; loop No. 2 pulls out of No. 3; and No. 16 out of No. 15. This order continues until loops No. 8 and No. 10 pull out of loop No. 9. Thus, the chain restraint is completely released. The loops pull through one another when forced by the internal pressure from the self-inflation system.

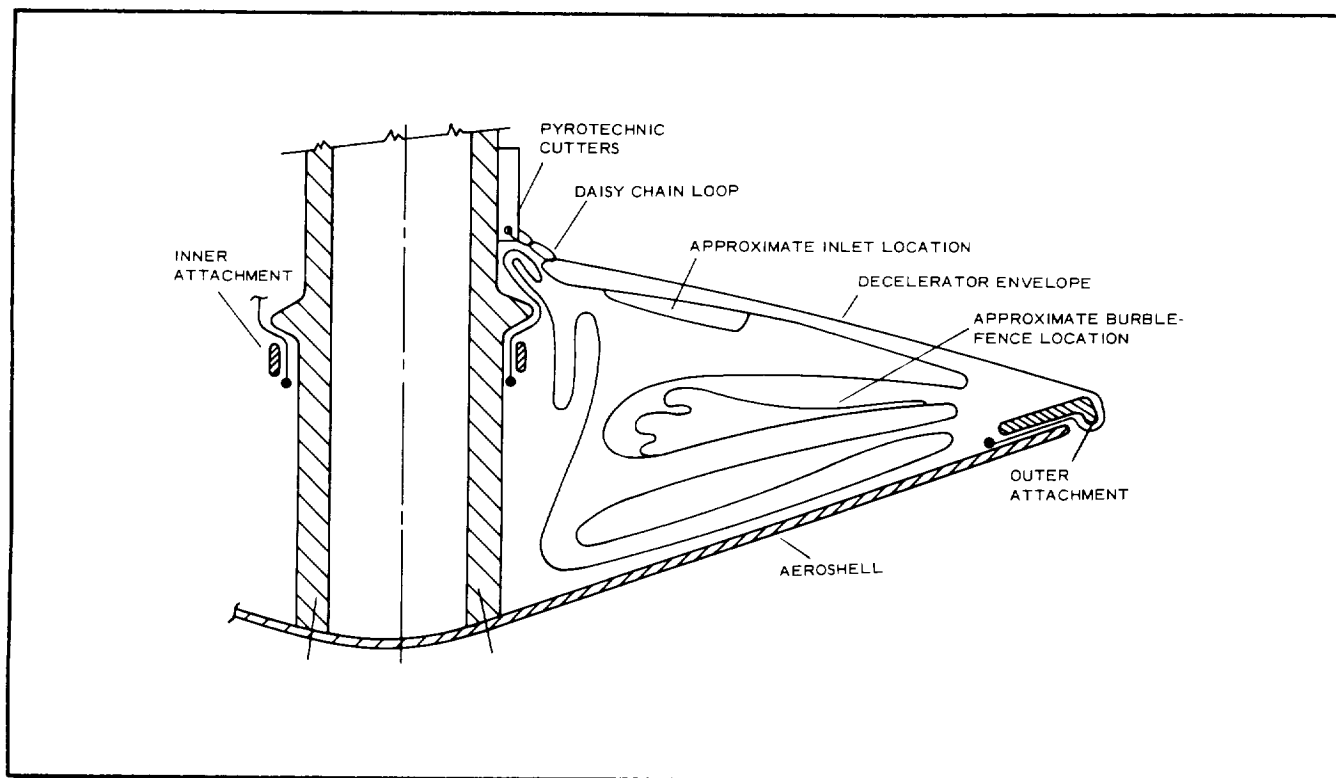


Figure 16 - Basic Envelope Folds

The loops that form the chain are equally spaced on meridians at 16 places around the envelope circumference. They are properly positioned on the meridians so that, when the meridians are slightly tensioned from the aeroshell attachment by drawing up the daisy chain hoop, the fabric envelope serves as its own packing cover. When the envelope is fully inflated, the loops are tight against the surface and cause only minor local disturbance in the flow.

Validation. - Decelerator packaging was straightforward, and the method was proved by successful package release in 0.018 sec during every test for inflation-deployment. The internal pressure peaks developed during package release were not deleterious to the fabric envelope.

Inflated Shape Inspection

Introduction. - To validate the designed and tailored shape, the inflated shape was inspected by measuring the free rear surface of the decelerator, inflated to steady-state pressure ($C_{p_i} = 2$), while the forward surface was held to the required contour.

Preparation and inspection. - Major equipment required to perform the inspection was a combination fixture used for both front contour restriction and rear contour inspection. By sweeping the surface of revolution with the isotenoid profile in wetted sand, the front contour was relatively simple to duplicate. The isotenoid shape defined by coordinates in Appendix B, or

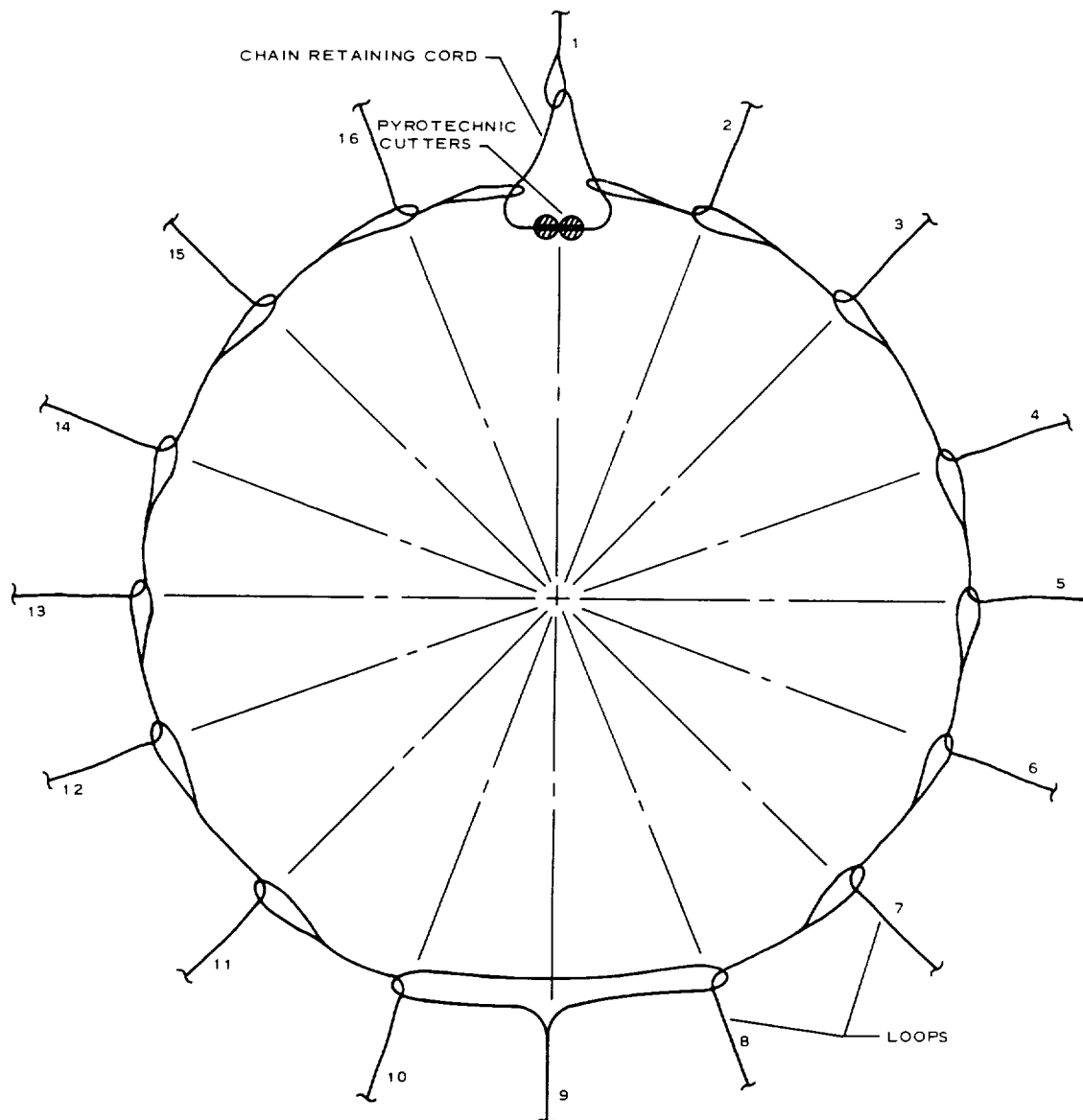


Figure 17 - Daisy Chain Hoop

more specifically the arbitrary station coordinates of Figure 18, was retained long enough for inspection by using hardened foundry sand in a ruggedly constructed box (see Figure 19).

Both the test model and rear contour inspection template were mounted on the axis of revolution, with the template offset one inch axially as the basis for comparative measurements of gage extensions to determine profile variances of the rear surface (see Figure 20).

With two of the four inlets plugged, inflation was achieved from factory air lines through the outer two inlets by manual valve control of one line to maintain the steady-state pressure ($p_i - p_{\infty}$) at approximately 1.8 psig. The envelope pressure was monitored on an oscillograph that was set up and calibrated to the model-mounted differential pressure transducer.

Inspection documentation. - With the inflation pressure ($p_i - p_{\infty}$) regulated between 1.8 and 1.9 psig, profile measurements of eight extension gages at the x locations in the template were taken separately on four representative meridians. Variances from the theoretical y value were recorded as shown in Figure 21. The maximum variance of 0.2 in. occurred at only seven of the 32 measurements. The lobing height approximated one inch.

Common variances of +1.5 in. were measured during a shape inflation of only 0.2 psig; the applied inspection pressure of 1.8 psig reduced the variances to the minimums of Figure 21.

Conclusion. - Some validity of the isotenoid theory was demonstrated successfully by the close conformance of the inflated shape to the theoretical shape. To achieve this, the established profile for the predicted consistent differential pressure over the entire rear surface during free flight was closely duplicated by inflation under static conditions in combination with the simulated positioning of the front surface.

Good accuracy in fabricating 16 gores and 48 meridians to the tailored shape was indicated from the measured profile variances. The resulting accuracy of producing an operating size to the design size also was unprecedented; the actual length of profile periphery closely matched the design profile as evidenced by both +0.2 in. and -0.2 in. maximum variances from theoretical.

Deployment and Inflation Tests

Introduction. - The AID unit was successively inflation-deployed in the environmental chamber at 20 psfa static pressure and at approximately 170 deg F, which was measured on the model by thermocouples. As heat is required for inflation by fluid vaporization, the test temperature of 170 deg F was assumed for the chamber tests as being realistic of the fluid temperature to be attained in the wind tunnel.

A series of four development tests were required to attain a desired level of internal pressure. Appendix C served as background for the tests.



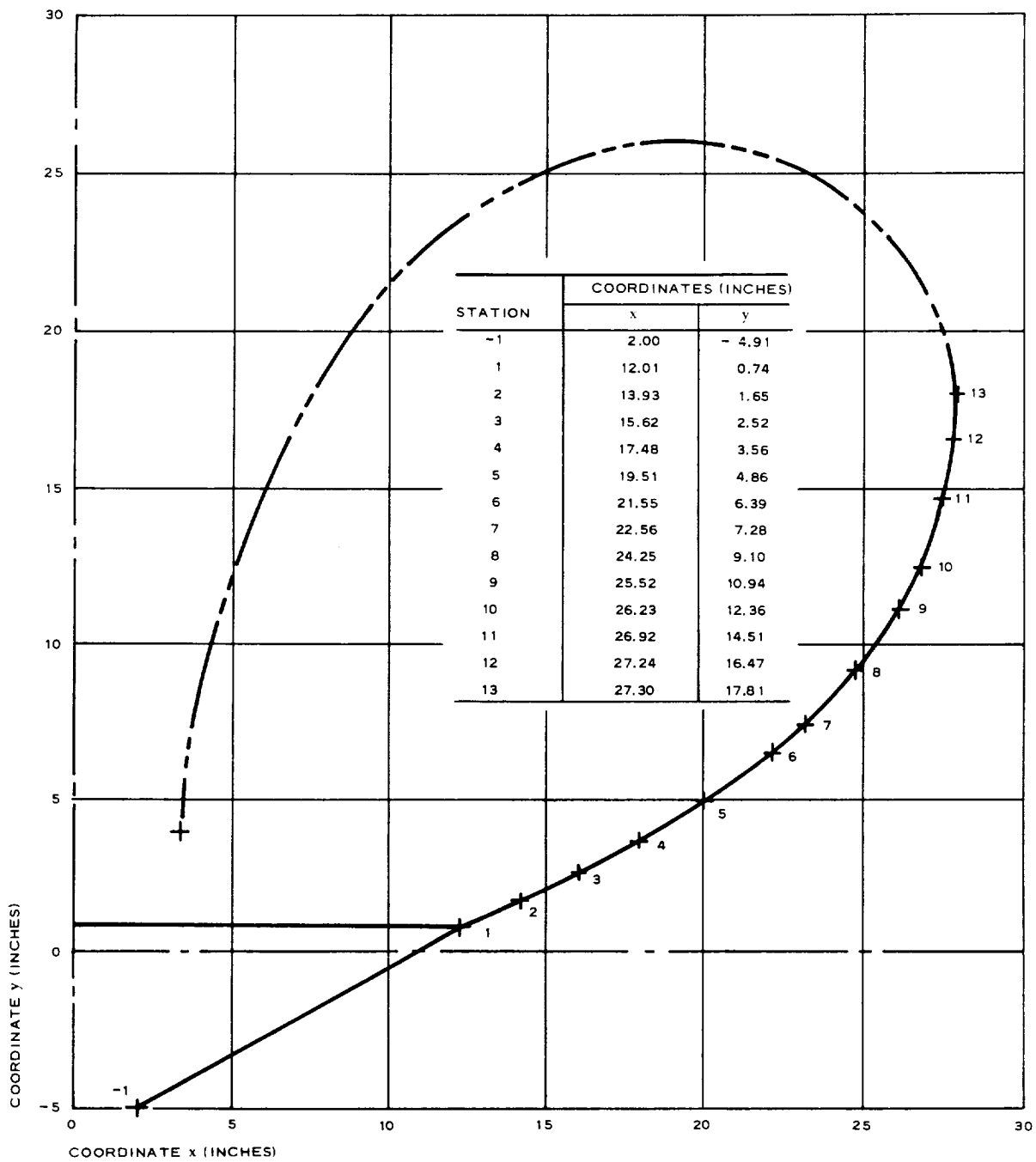


Figure 18 - Front Contour Profile

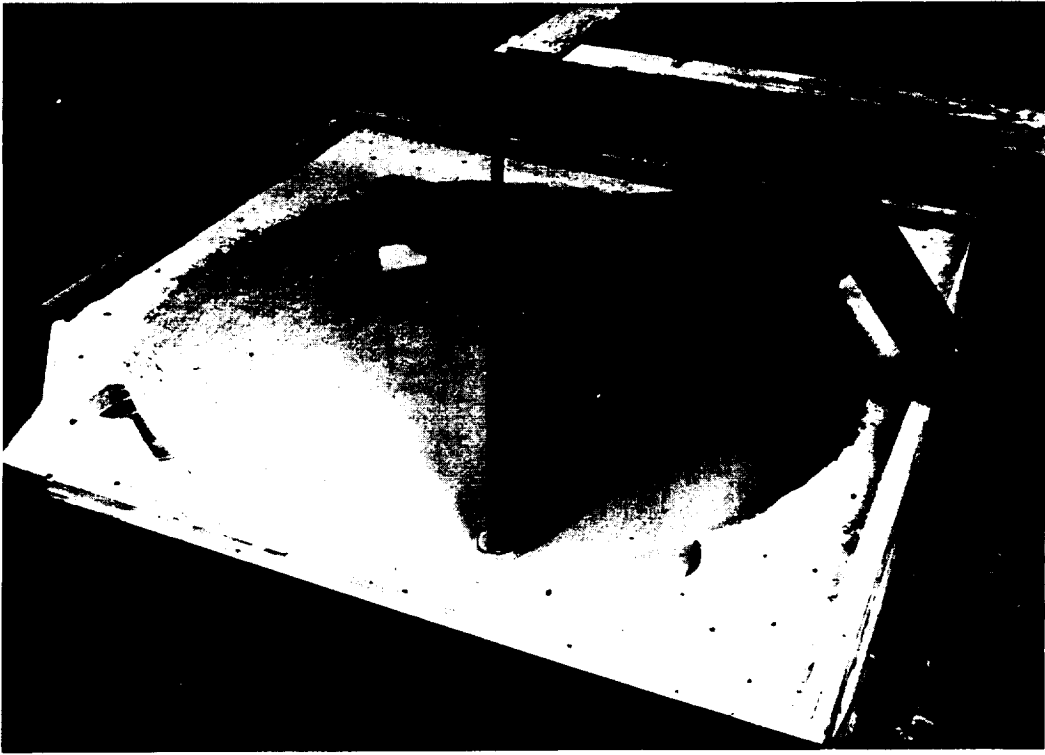


Figure 19 - AID Inspection Fixture, Front Contour



Figure 20 - AID Contour Inspection

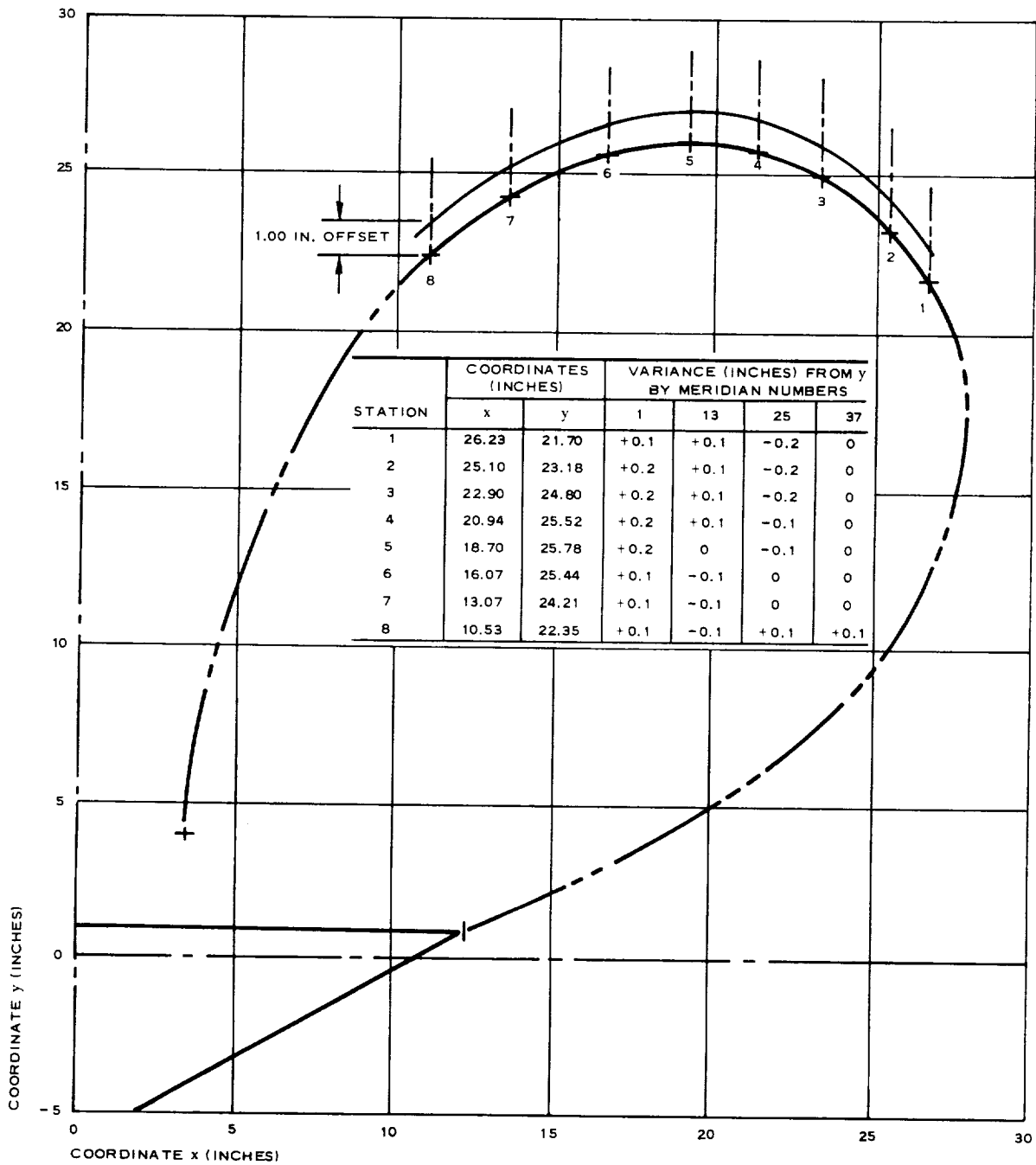


Figure 21 - Rear Contour Profile and Variances

Test documentation. - Data for each deployment was obtained from motion pictures and from oscillographic traces of firing current, inflation pressure, and temperatures. As time correlation was provided by firing the flash bulb simultaneously with the reservoir cutter ($t = 0$), comparison with the high-speed pictures and data reduction of the traces from the developed calibration rates were completed in the generated plots of temperature and pressure in Figures 22 and 23.

Test No. 1 was the first of four tests in which the principal variable from test to test was the amount of vaporizing fluid, which was used in increasing amounts to raise the level of inflation pressure progressively. Selection of 2.2 oz of water was based on ideal heat conversion to a C_{p_i} limit of 2 (see Appendix C); however, a C_{p_i} of only 0.3 was attained after full inflation as evidenced by the inflation pressure ($p_i - p_{\infty}$) of 0.23 psi (see Figure 22).

The 3.3 oz of water-alcohol mixture for Test No. 2 also was based on ideal heat conversion to a C_{p_i} of 2. A C_{p_i} of 0.7 was attained, which was a somewhat greater efficiency than with using plain water. This pressure coefficient corresponds to the inflation pressure ($p_i - p_{\infty}$) of 0.6 psi (see Figure 22). Figures 24 and 25 are typical of the decelerator setup of free deployment and of the deployed decelerator at close to the maximum inflation pressure. The distorted appearance in comparison with the design shape was expected from deployment at static conditions.

By an approximate determination from the level of efficiency of Tests No. 1 and 2, 12 oz of water-alcohol in a larger constrained tube reservoir were selected for Test No. 3. This mixture resulted in fabric rupture of the decelerator on straining beyond its isotenoid shape as it tended toward a torus in the static environment. Data plots are shown in Figure 22.

For Test No. 4, the same fluid weight and the same size reservoir were used except that the tube was compartmented in an attempt to limit the rate of vaporization and peak pressure during package release. The principal change, however, was for guiding and maintaining the deployed decelerator in the approximate isotenoid shape by a modification to the A frame support and by minor additions to the decelerator. The decelerator was modified by adding a reinforcing sleeve at the tuckback and by adding four radial-restricting circumferential hoop tapes along the tuckback as shown in Figure 26. The shape-controlling guide shown in Figure 27 consisted of two frame-supported tubular hoops for contacting the tailored decelerator at selected Stations 4 and 9 (Figure 18) on the front profile contour. All 12 stringers also made contact at Station 7.

The excellent inflation shown in Figure 28 attained a C_{p_i} of 1.3. This value corresponded to the inflation pressure ($p_i - p_{\infty}$) of 1.08 indicated in the data reduction of Figure 23, which was generated from the oscillographic traces.

CONDITIONS (ALL TESTS)

$$p_{\infty} = 20 \text{ PSF}$$

INLET SLEEVES CLOSED

FREE DEPLOYMENT

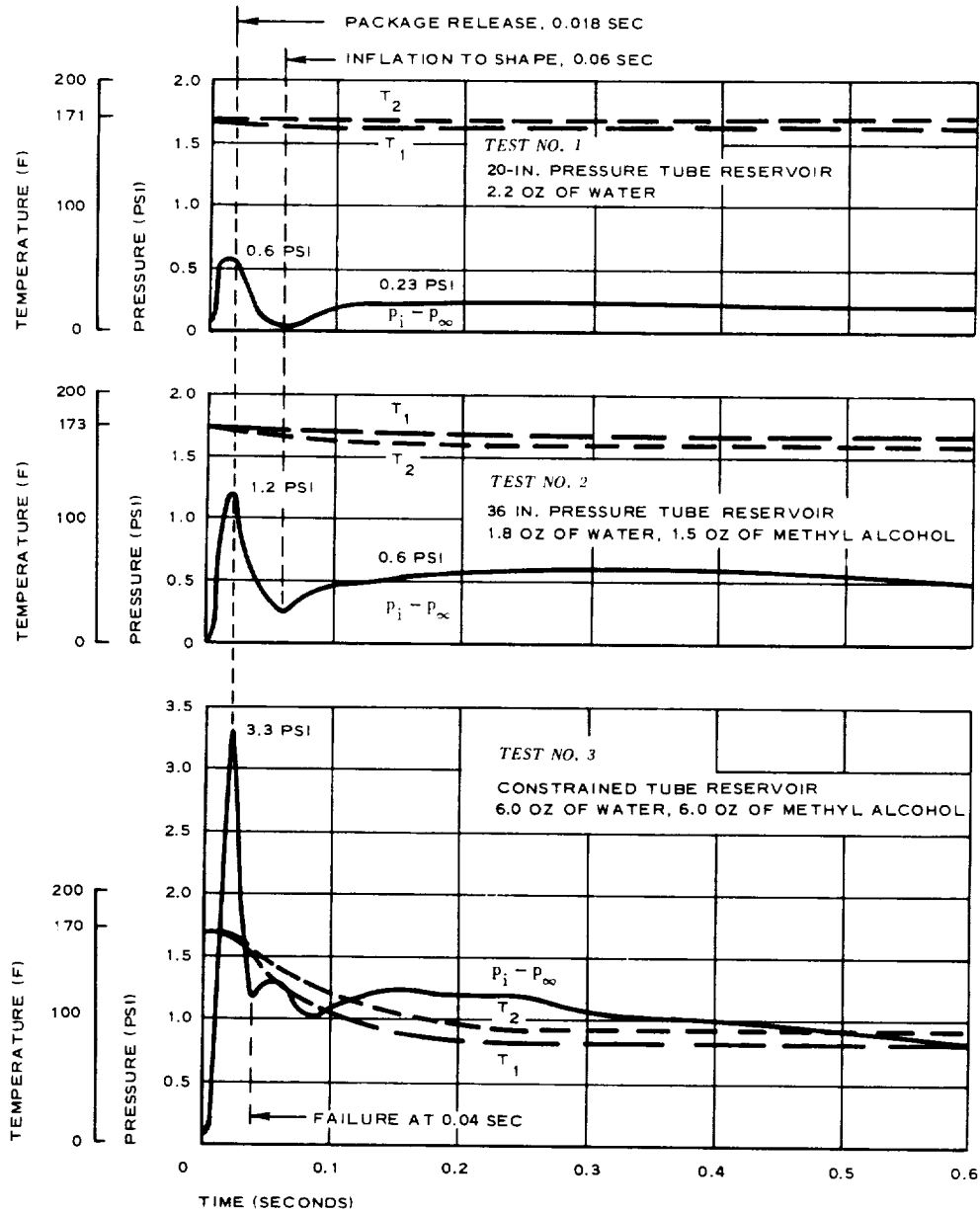


Figure 22 - Pressure and Temperature at AID Deployments

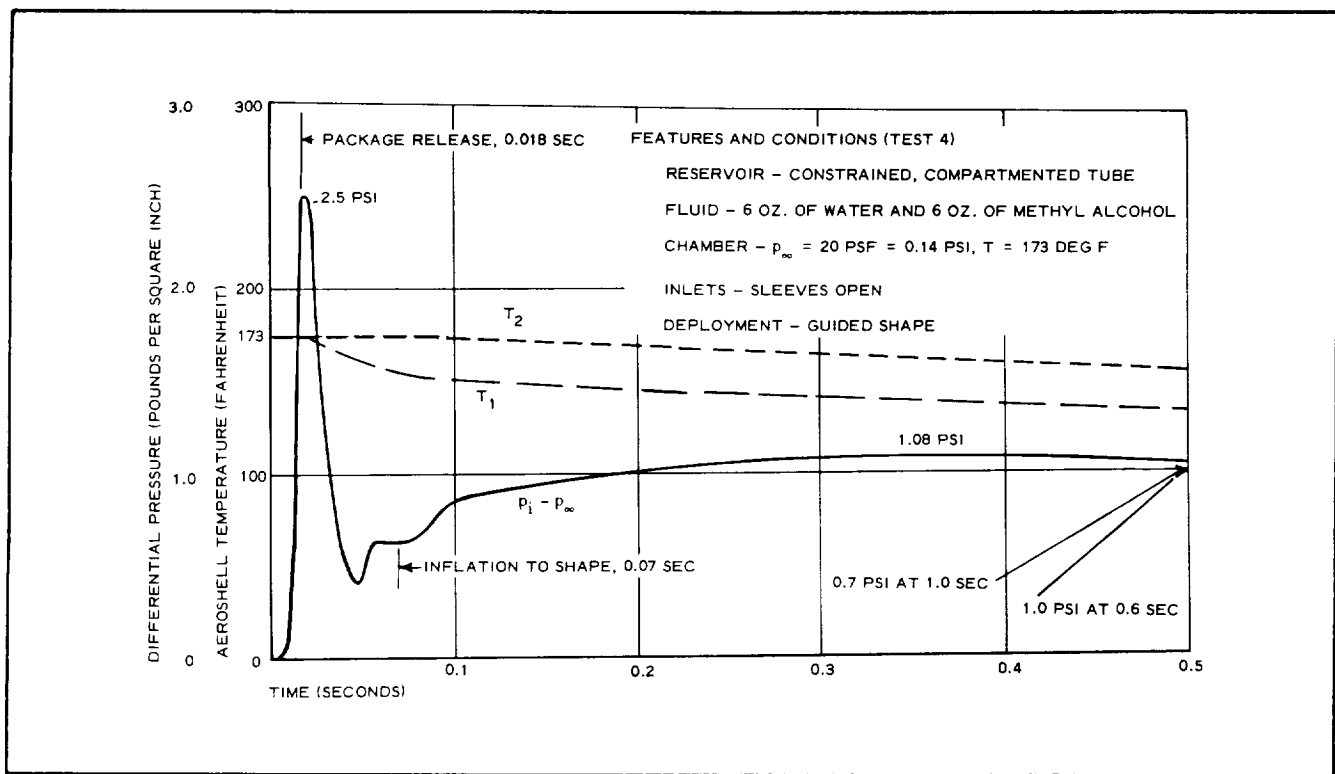


Figure 23 - Pressure and Temperature at AID Deployment (Test No. 4)

Conclusion. - An examination of the temperature plots for T_1 and T_2 in Figures 22 and 23 finds no consistency in temperature changes among tests or between thermocouples from which meaningful conclusions can be drawn, except that thermocouples are needed at additional locations and more tests are required for analysis.

The pressure plots of successful tests show consistency in package release at 0.018 sec, inflation to shape at 0.06 to 0.07 sec, and maximum inflation pressure at approximately 0.35 sec. A relatively high level of pressure also is evident for at least one second before dissipation of the inflating vapor.

From a review of the picture documentation and post-test examination of the unit, no deleterious leakage was apparent, and integrity of the envelope was ensured within the limits of test simulations.

From past experience, a C_{p_i} of 1 was sufficient for free-flight operation of 80-deg included-angle BALLUTES. A plot of vaporizing fluid weight versus internal pressure for the tests indicated the recommended requirement of eight ounces of water-alcohol to attain the inflation-deployment C_{p_i} of 1 (see Figure 29).

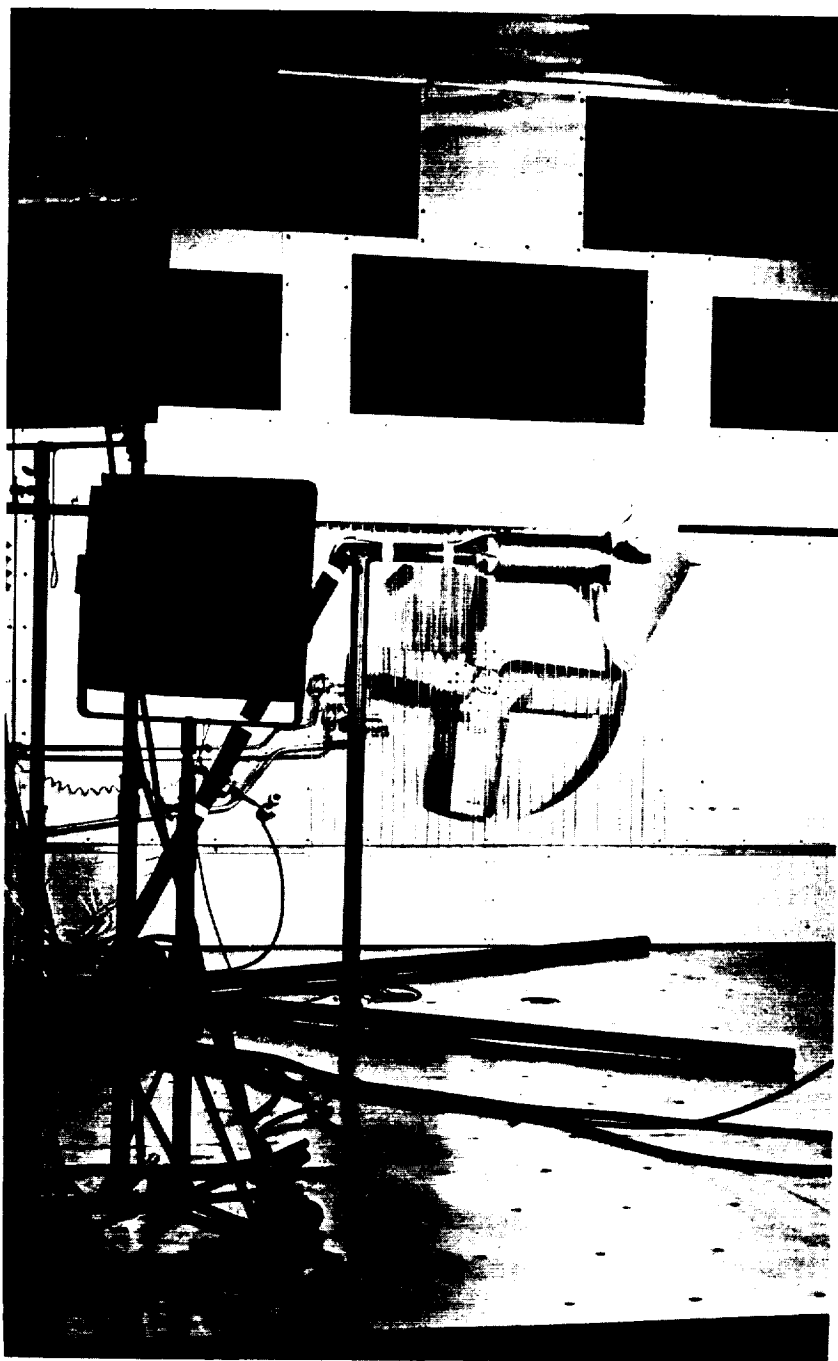


Figure 24 - Regular Deployment Setup



Figure 25 - Test No. 2 Deployment

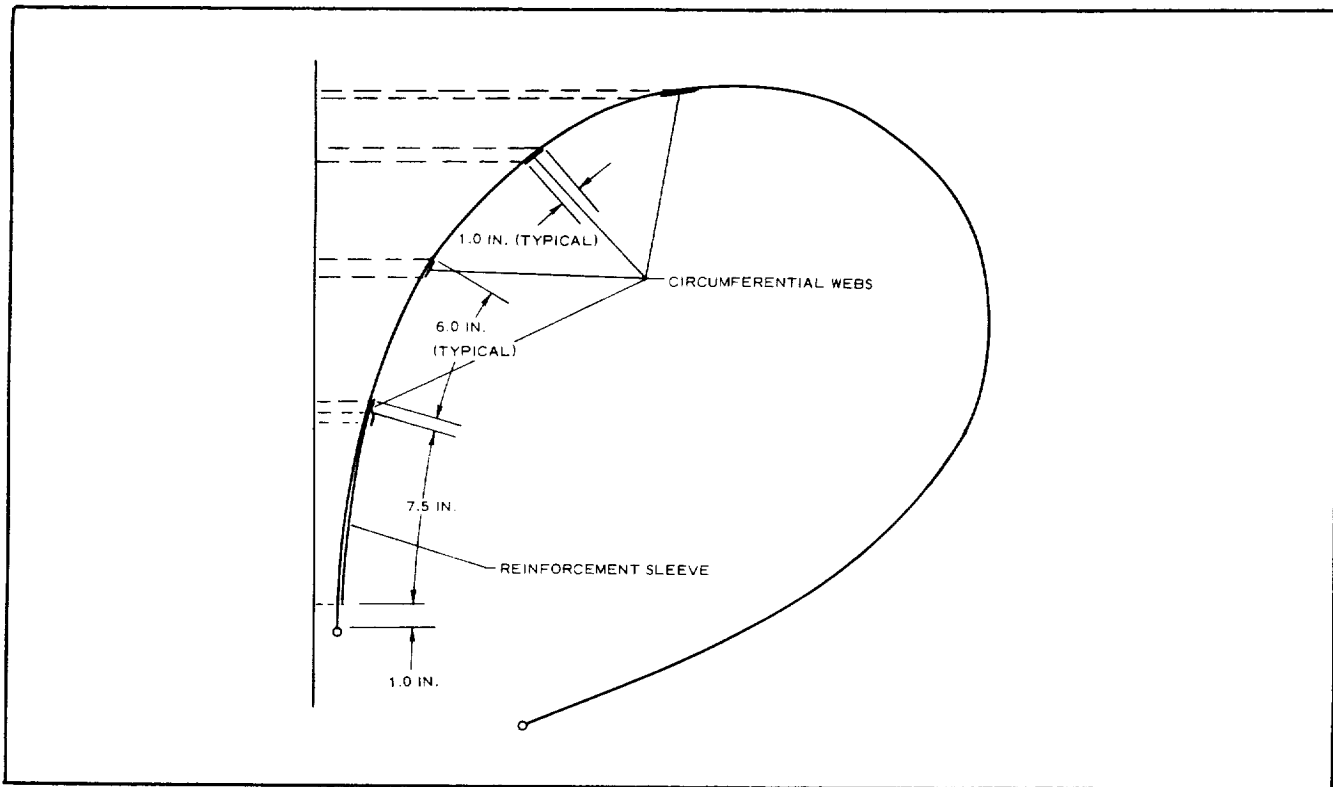


Figure 26 - Structural Additions

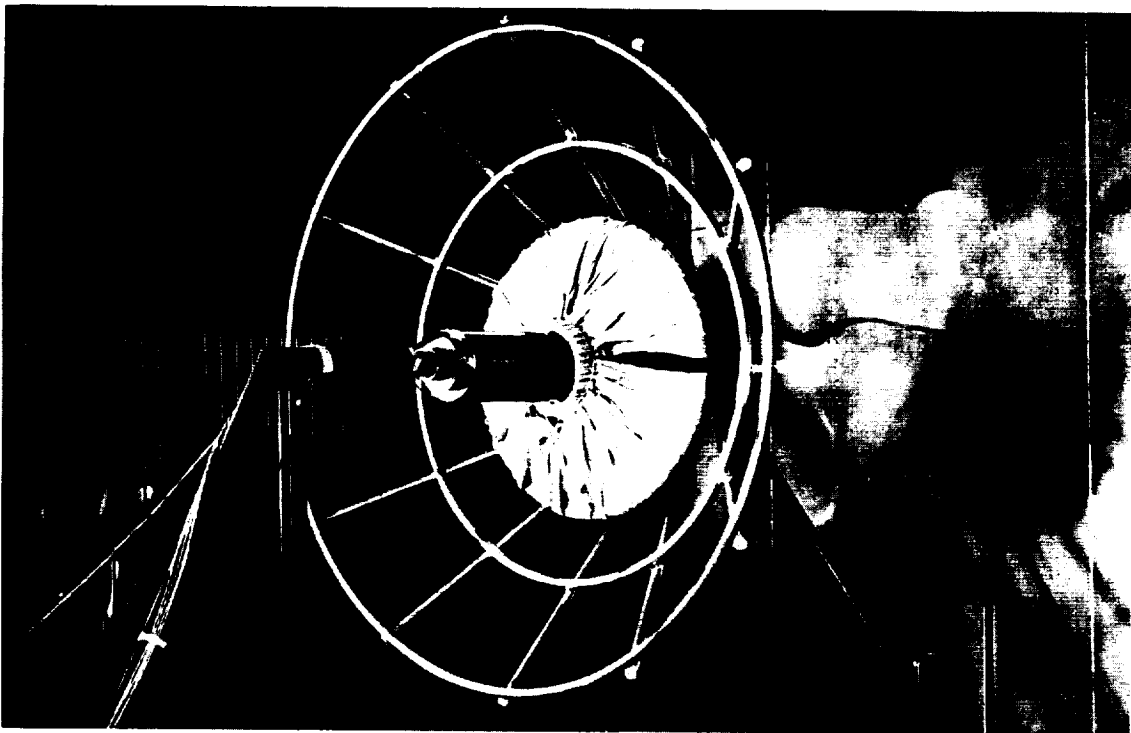


Figure 27 - Guided-Shape Deployment Setup

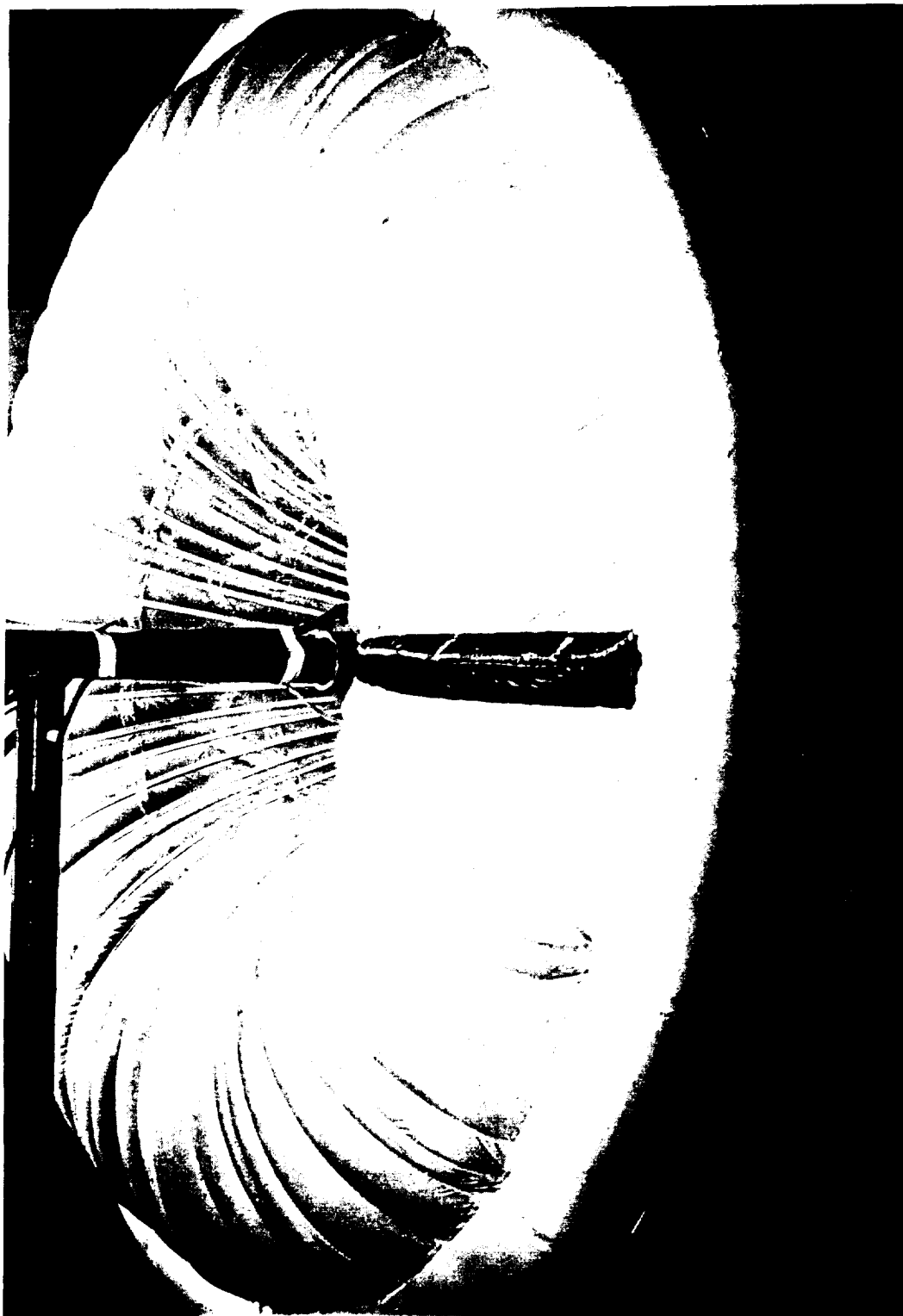


Figure 28 - Test No. 4 Guided Deployment

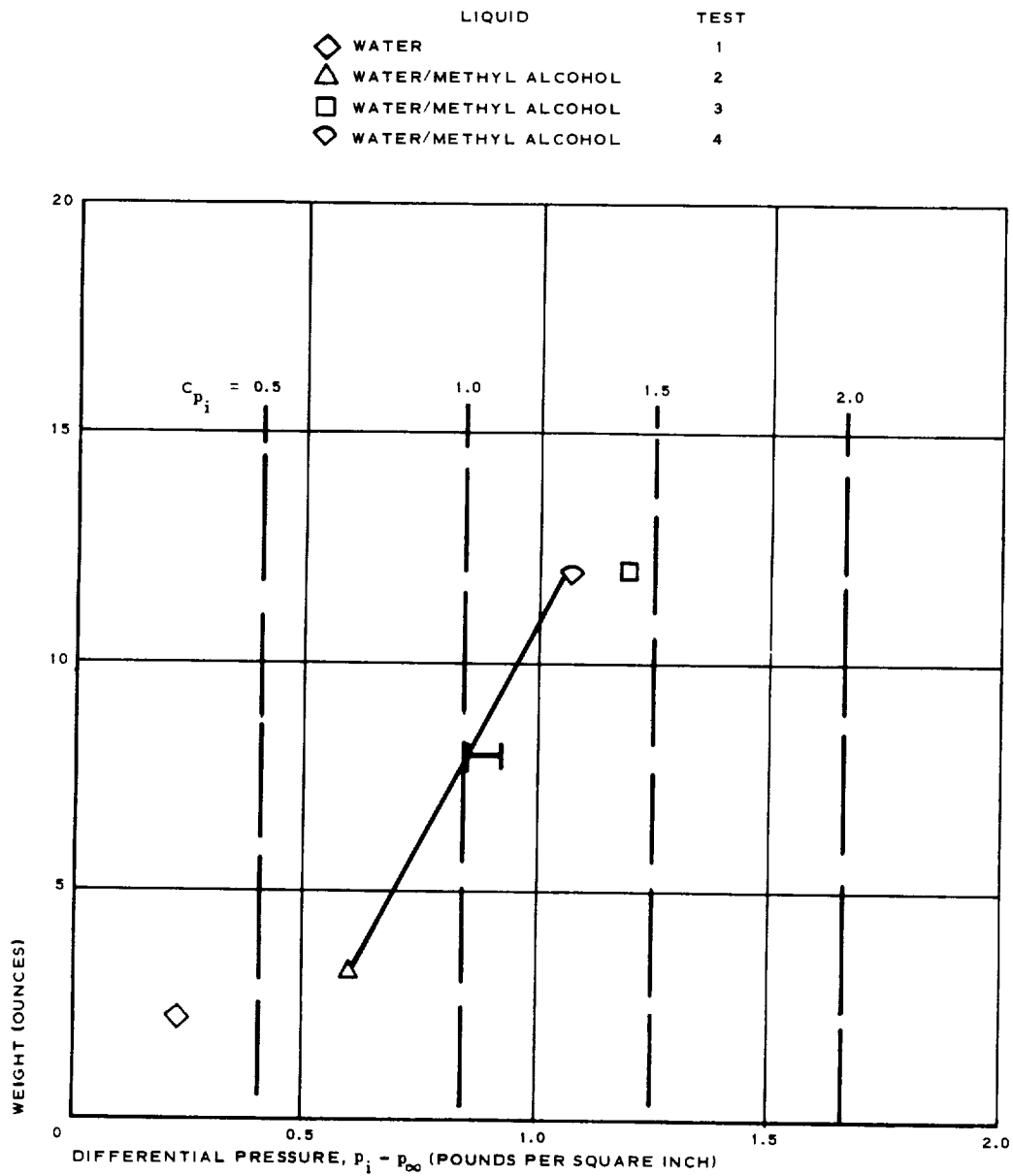


Figure 29 - Fluid Weight versus Inflation Pressure

CONCLUSIONS AND RECOMMENDATIONS

Introduction

Scheduled inspection and test demonstrations of the model were used to evaluate system design and fabrication of the AID concept for Mars entry. Detailed conclusions, determined principally from the performed demonstrations, and followon recommendations suggested for approach toward an ultimate real-flight design are given below.

Conclusions

An attached inflatable decelerator was produced compatible with the isotenoid theory. An isotenoid shape was computer-developed from the expected pressure distribution and in satisfaction of fixed boundary constraints to suit the aeroshell hard-structure configuration. The resulting shape approached the design optimum of least weight. By using a contoured fixture for front shape constraint, the tailored shape was validated statically, with internal pressure providing the design pressure differential over the rearward half.

The hardbody aeroshell was accurately constructed to support the decelerator on the wind-tunnel loading-measuring balance and was equipped to serve as the operating vehicle for wind-tunnel test. Hard-structure clamp attachments for the decelerator provided a degree of accuracy compatible with the defined shape. Dependable operating components were installed in the aeroshell structure for effecting deployment. Proved sensors also were incorporated in the aeroshell for measuring the operating pressure and temperature.

A highly responsive vapor inflation system for positive inlet deployment was demonstrated in the Goodyear Aerospace vacuum chamber. The envelope structure withstood a deployment inflating pressure equivalent to a C_{pi} of 1.3 when restricted to the design shape. Time constants of inflation-deployments during the several chamber tests were 0.018 sec for package release, 0.07 sec for shape inflation, and 0.35 sec for maximum internal pressure.

The demonstrations of decelerator shape validation, envelope packaging and release, and inflation-deployment operation served to qualify the two units in preparation for the intended wind-tunnel testing to prove workability of the AID concept.

Recommendations

Definitive studies of inlet sizing and location and of mechanical versus vapor inflation deployments are required in the continuing development of attached inflatable decelerators. Immediate followon efforts in the approach to an optimum inflatable decelerator should include study and test to advance inlet technology and efficiency.

For any candidate system considered in these studies, an analytical approach to the dynamics of inlet and envelope deployment might be applied that will incorporate the elements of opening force and deployment restrictions. A packaging and deployment method compatible with an inlet design should be developed with sufficient response to deploy positively into the flow for ensuring full ram-air inflation of the decelerator volume.

Further refinements will be needed in the analysis and test of vapor inflations to optimize deployment designs by this method; better initial temperature control and more measurable temperature data during test are required for validations.

The shape and design of attached decelerators for large flight models must be optimized with governing considerations of structural stability, low weight over drag, and inflation techniques for positive, uniform erection of the envelope.

APPENDIX A

DECELERATOR PARAMETERS AS FUNCTIONS OF THE OUTER ATTACHMENT ANGLE

This appendix discusses some of the background work conducted to facilitate selection of the design profile shape. Figures 30 and 31 are based on the results of the isotenoid computer solutions for attachment angles of $\phi = 19.5$, 23.6, and 30 deg, which correspond to the respective profile shapes of Figures 3, 4, and 32. Figure 30 shows the drag coefficient and the weight parameter, which includes the fabric weight along with the meridian weight, versus the attachment angle. The drag coefficient is a rather constant value of $C_D = 1.1$. Although the weight decreases with decreasing attachment angles, the required number of lobes (n) and the theoretically required bias angle (γ) of the fabric as determined at the critical equatorial location become prohibitive for angles less than about 20 deg.

These considerations were secondary in selecting the design shape since the overriding requirement of meeting an agreed inner attachment constraint of $(x/R)_i = 0.13$ could be satisfied only by the profile shape corresponding to the attachment angle of $\phi = 23.6$ deg.

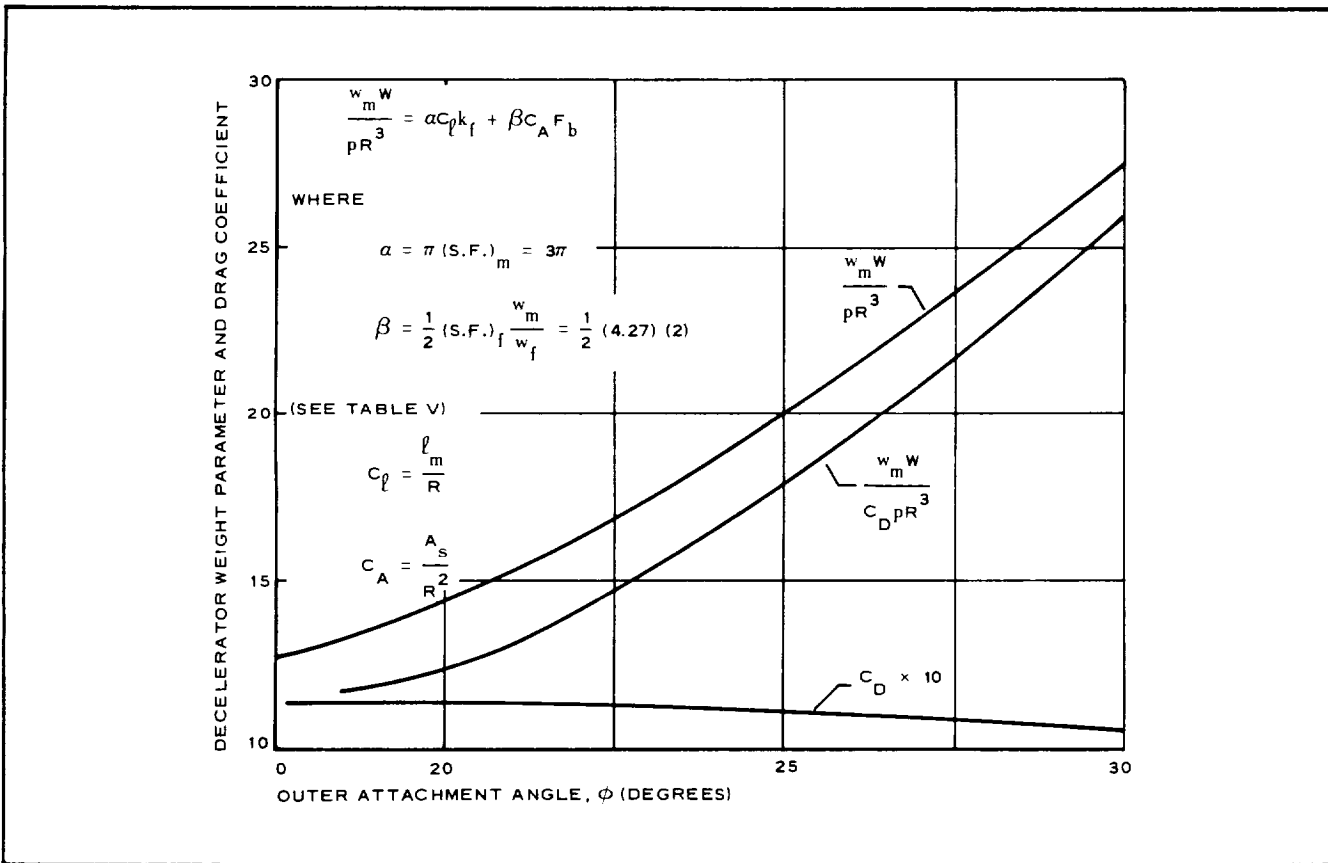
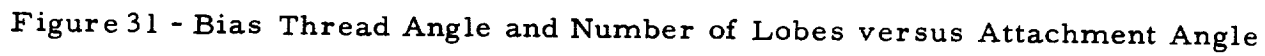


Figure 30 - Decelerator Weight Parameter and Drag Coefficient versus Attachment Angle



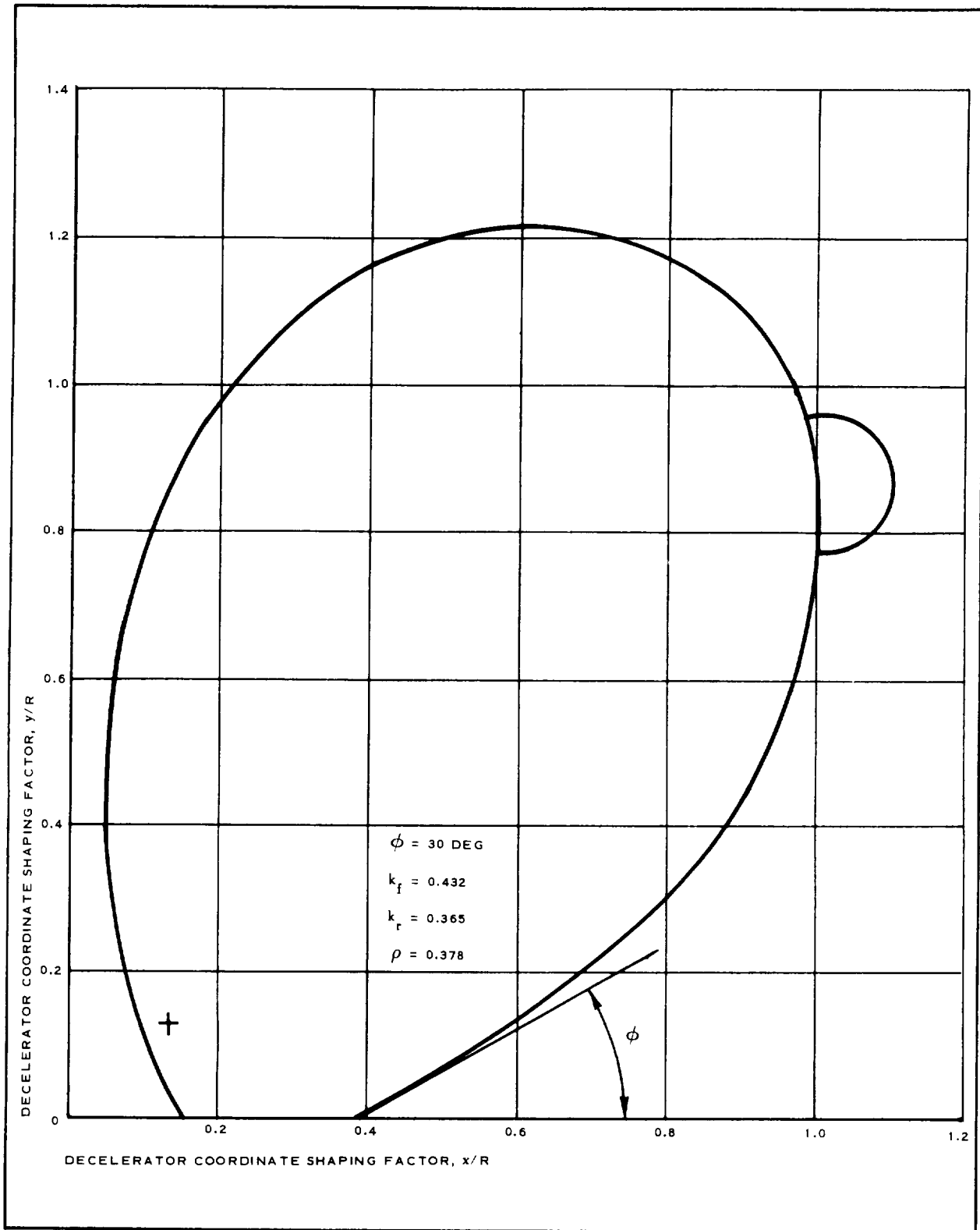


Figure 32 - Shape Profile for 30-Deg Attachment Angle

(The reverse is blank.)

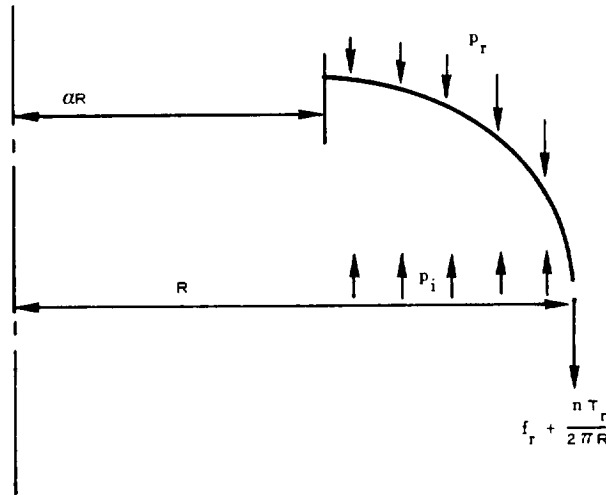
APPENDIX B

SHAPE DEVELOPMENT

EQUILIBRIUM EQUATIONS

For the isotenoid shape, it is assumed that fabric stresses and meridian cable tensions are constant. With the burble fence attached at the equator, there will be a discontinuity in stresses between the front and the back. The relation between fabric stresses and meridian cable tensions can be obtained by cutting the shape at the equator. Figure 33 shows the loading diagram.

At a point on the equator just behind the burble fence, the following equilibrium equations are obtained.



$$2\pi R f_r + nT_r = p\pi R^2(1 - a^2) \quad (p = p_i - p_r)$$

Let

$$F_r = \frac{2f_r}{pR}$$

$$k_r = \frac{nT_r}{p\pi R^2}$$

$$F_r + k_r = 1 - a^2 \quad (42)$$

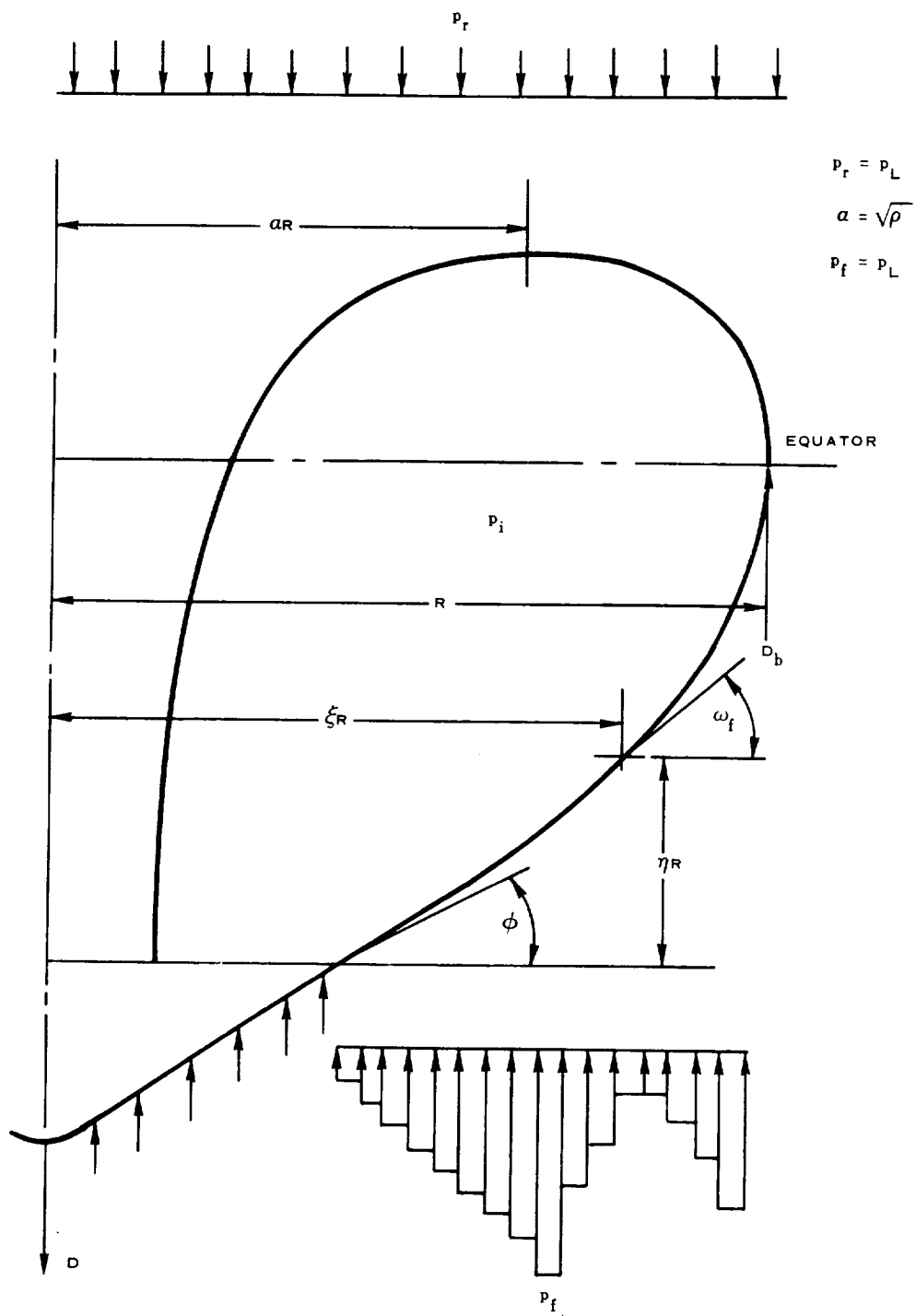
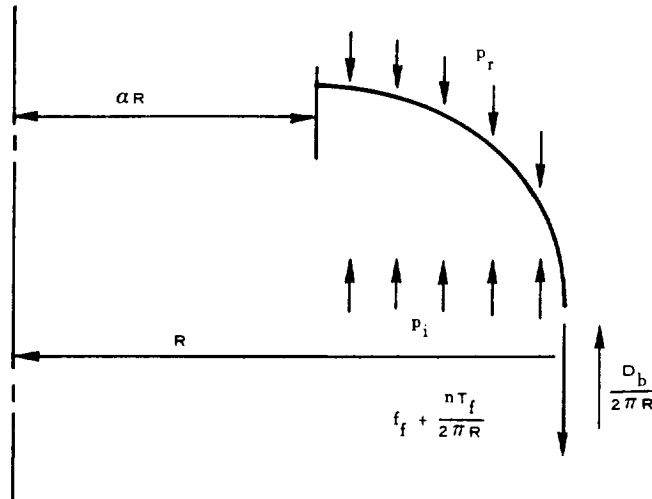


Figure 33 - Loading Diagram

At a point just in front of the burble fence, the force due to the burble fence enters.



$$2\pi R f_f + nT_f = p\pi R^2(1 - \alpha^2) + D_b$$

Let

$$F_f = \frac{2f_f}{pR}$$

$$k_f = \frac{nT_f}{p\pi R^2}$$

$$\beta = \frac{D_b}{p\pi R^2}$$

$$F_f + k_f = 1 - \alpha^2 + \beta \quad (43)$$

$$F_f + k_f = \gamma(F_r + k_r) \quad (44)$$

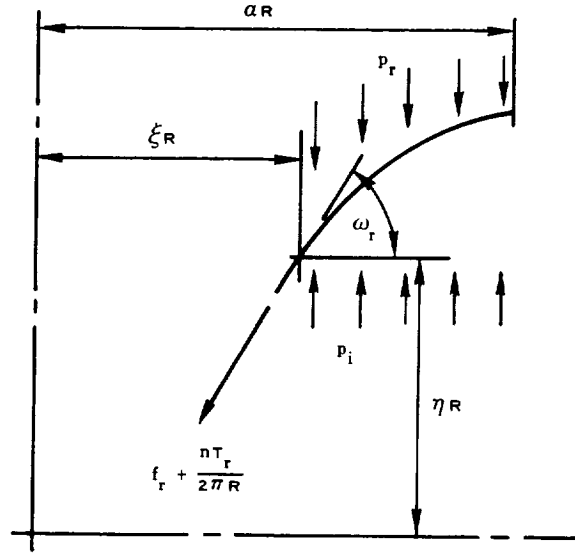
where

$$\gamma = \frac{1 - \alpha^2 + \beta}{1 - \alpha^2} = 1 + \frac{\beta}{1 - \alpha^2}$$

It is assumed that the burble fence is attached so that

$$F_f = \gamma F_r, \quad k_f = \gamma k_r \quad (45)$$

GOVERNING EQUATION FOR REAR HALF



$$\left[\xi (1 - a^2 - k_r) + k_r \right] \sin \omega_r = a^2 - \xi^2 \quad (46)$$

now

$$\frac{d\eta}{d\xi} = \tan \omega_r$$

or

$$d\eta = \tan \omega_r d\xi \quad (47)$$

This equation can be integrated numerically by solving Equation (46) for $\tan \omega_r$. When $\tan \omega_r$ becomes large, Equation (46) can be solved for ξ in terms of ω_r as follows:

$$\xi = g(\omega_r)$$

$$d\xi = g'(\omega_r) d\omega_r$$

Therefore,

$$d\eta = \tan \omega_r g'(\omega_r) d\omega_r$$

With this equation, the integration can be carried out with respect to ω_r .

GOVERNING EQUATION FOR FRONT HALF

The front half is divided into N intervals of constant pressure. The equation in the i^{th} interval is then:

$$\left[\xi(1 - \alpha^2 - k_f + \beta) + k_f \right] \sin \omega_f + (\alpha^2 - \xi^2) - H_i + p'_{fi} \xi^2 - p_{fi} \xi^2 + p'_r(1 - \xi^2) - \beta = 0 \quad (48)$$

where

p_{fi} = front pressure over i^{th} increment

$$p'_{fi} = \frac{p_{fi}}{p}$$

$$p'_r = \frac{p_r}{p}$$

$$H_i = \sum_{j=i}^N p'_{fj} (\xi_{j+i}^2 - \xi_j^2)$$

Again,

$$\frac{d\eta}{d\xi} = \tan \omega_f \quad (49)$$

or

$$d\eta = \tan \omega_f d\xi$$

This equation can be integrated by solving Equation (48) for $\tan \omega_f$, or Equation (48) can be solved for ξ in terms of ω_f and the integration carried out with respect to ω_f .

COMPUTER PROGRAM

The computer program first reads in the front pressure distribution for ϕ , which corresponds to ω_f at the edge of the aeroshell. It then prescribes a value of α and using Equation (48) for the first increment calculates k_f . If k_f is negative, it takes the next value of α and so on until a positive k_f is obtained. It then calculates F_f from Equation (43). If F_f is negative, it takes the next value of k and so on until positive values for both k_f and F_f are obtained. Equation (49) then is integrated numerically (using the trapezoidal rule). For



three-fourths of the distance from ξ to 1, the integration is carried out with respect to ξ . From that point, the integration is carried out with respect to ω_f . This integration gives the front shape. k_r and F_r then are calculated from Equation (45), and Equation (47) is integrated to obtain the back shape. For the back shape, the integration is carried out with respect to ω_r over the entire range.

Computer outputs in dimensionless values, printed out as corresponding to the developed isotenoid shape for the attachment angle (ϕ), are as follows:

k_f	meridian tension coefficient, front
F_f	circumferential membrane stress coefficient, front
k_r	meridian tension coefficient, rear
F_r	circumferential membrane stress coefficient, rear
$(y/R)_e$	coordinate at the equator, $(x/R)_{\max}$
$(y/R)_{\max}$	maximum coordinate y/R
$\sqrt{\rho} = \alpha$	coordinate x/R at $(y/R)_{\max}$
$(x/R)_{\min}$	minimum coordinate x/R
C_D	drag coefficient for the system based on $x/R = 1.1$
ℓ_m/R	meridian length coefficient
A_s/R^2	surface area of revolution coefficient

A profile shape can be machine plotted or its defining points printed out. An example of a computer printout is the 344 points of cartesian coordinates representing the isotenoid plot for $\phi = 23.6$ deg in Table XIII.



TABLE XIII - ISOTENSOID COORDINATES, 344 POINTS

 $(\phi = 23.6 \text{ DEG})$

x/R	y/R	x/R	y/R
3.8000-01	0.0	6.4040-01	1.3047-01
3.8620-01 ^a	2.7126-03 ^a	6.4660-01	1.3417-01
3.9240-01	5.4388-03	6.5280-01	1.3791-01
3.9860-01	8.1788-03	6.5900-01	1.4170-01
4.0480-01	1.0933-02	6.6520-01	1.4552-01
4.1100-01	1.3702-02	6.7140-01	1.4939-01
4.1720-01	1.6486-02	6.7760-01	1.5331-01
4.2340-01	1.9284-02	6.8380-01	1.5727-01
4.2960-01	2.2099-02	6.9000-01	1.6129-01
4.3580-01	2.4929-02	6.9620-01	1.6535-01
4.4200-01	2.7776-02	7.0240-01	1.6947-01
4.4820-01	3.0639-02	7.0860-01	1.7364-01
4.5440-01	3.3519-02	7.1480-01	1.7787-01
4.6060-01	3.6417-02	7.2100-01	1.8216-01
4.6680-01	3.9333-02	7.2720-01	1.8651-01
4.7300-01	4.2266-02	7.3340-01	1.9092-01
4.7920-01	4.5219-02	7.3960-01	1.9539-01
4.8540-01	4.8191-02	7.4580-01	1.9994-01
4.9160-01	5.1182-02	7.5200-01	2.0455-01
4.9780-01	5.4194-02	7.5820-01	2.0924-01
5.0400-01	5.7226-02	7.6440-01	2.1401-01
5.1020-01	6.0280-02	7.7060-01	2.1886-01
5.1640-01	6.3356-02	7.7680-01	2.2379-01
5.2260-01	6.6453-02	7.8300-01	2.2881-01
5.2880-01	6.9574-02	7.8920-01	2.3392-01
5.3500-01	7.2718-02	7.9540-01	2.3912-01
5.4120-01	7.5887-02	8.0160-01	2.4443-01
5.4740-01	7.9080-02	8.0780-01	2.4984-01
5.5360-01	8.2298-02	8.1400-01	2.5536-01
5.5980-01	8.5542-02	8.2020-01	2.6100-01
5.6600-01	8.8814-02	8.2640-01	2.6676-01
5.7220-01	9.2112-02	8.3260-01	2.7265-01
5.7840-01	9.5440-02	8.3880-01	2.7868-01
5.8460-01	9.8796-02	8.4500-01	2.8486-01
5.9080-01	1.0218-01	8.5120-01	2.9120-01
5.9700-01	1.0560-01	8.5740-01	2.9770-01
6.0320-01	1.0905-01	8.6360-01	3.0439-01
6.0940-01	1.1253-01	8.6980-01	3.1120-01
6.1560-01	1.1605-01	8.7600-01	3.1835-01
6.2180-01	1.1960-01	8.8220-01	3.2566-01
6.2800-01	1.2318-01	8.8840-01	3.3321-01
6.3420-01	1.2681-01	8.9460-01	3.4092-01
		8.9152-01	3.3711-01

^aExamples are coordinate values 0.38620 and 0.00271.

TABLE XIII - ISOTENSOID COORDINATES, 344 POINTS

 $(\phi = 23.6 \text{ DEG})(\text{Continued})$

x/R	y/R	x/R	y/R
8.9460-01	3.4103-01	9.9777-01	6.0335-01
8.9772-01	3.4507-01	9.9845-01	6.1149-01
9.0080-01	3.4913-01	9.9901-01	6.1963-01
9.0392-01	3.5334-01	9.9944-01	6.2777-01
9.0700-01	3.5756-01	9.9975-01	6.3592-01
9.1013-01	3.6194-01	9.9994-01	6.4407-01
9.1320-01	3.6634-01	1.0000-00	6.5223-01
9.1633-01	3.7092-01	9.9997-01	6.5659-01
9.1940-01	3.7552-01	9.9986-01	6.6095-01
9.2253-01	3.8033-01	9.9969-01	6.6531-01
9.2560-01	3.8515-01	9.9945-01	6.6966-01
9.2873-01	3.9021-01	9.9914-01	6.7402-01
9.3180-01	3.9530-01	9.9877-01	6.7837-01
9.3494-01	4.0065-01	9.9832-01	6.8271-01
9.3800-01	4.0604-01	9.9781-01	6.8705-01
9.4114-01	4.1174-01	9.9723-01	6.9138-01
9.4420-01	4.1748-01	9.9658-01	6.9570-01
9.4735-01	4.2360-01	9.9586-01	7.0002-01
9.5040-01	4.2975-01	9.9507-01	7.0432-01
9.5252-01	4.3417-01	9.9422-01	7.0861-01
9.5458-01	4.3860-01	9.9330-01	7.1290-01
9.5660-01	4.4304-01	9.9231-01	7.1717-01
9.5872-01	4.4787-01	9.9125-01	7.2143-01
9.6079-01	4.5271-01	9.9012-01	7.2567-01
9.6280-01	4.5757-01	9.8893-01	7.2990-01
9.6493-01	4.6290-01	9.8767-01	7.3412-01
9.6700-01	4.6826-01	9.8634-01	7.3831-01
9.6900-01	4.7363-01	9.8495-01	7.4249-01
9.7115-01	4.7963-01	9.8349-01	7.4666-01
9.7322-01	4.8565-01	9.8196-01	7.5080-01
9.7520-01	4.9169-01	9.8036-01	7.5492-01
9.7737-01	4.9862-01	9.7870-01	7.5903-01
9.7944-01	5.0557-01	9.7697-01	7.6311-01
9.8140-01	5.1253-01	9.7518-01	7.6717-01
9.8307-01	5.1879-01	9.7332-01	7.7120-01
9.8466-01	5.2506-01	9.7139-01	7.7521-01
9.8617-01	5.3135-01	9.6940-01	7.7920-01
9.8760-01	5.3764-01	9.6734-01	7.8316-01
9.8901-01	5.4427-01	9.6522-01	7.8710-01
9.9034-01	5.5091-01	9.6303-01	7.9100-01
9.9158-01	5.5756-01	9.6078-01	7.9488-01
9.9273-01	5.6422-01	9.5846-01	7.9873-01
9.9380-01	5.7089-01	9.5608-01	8.0255-01
9.9498-01	5.7899-01	9.5363-01	8.0634-01
9.9696-01	5.9522-01	9.5112-01	8.1009-01

TABLE XIII - ISOTENSOID COORDINATES, 344 POINTS

 $(\phi = 23.6 \text{ DEG})(\text{Continued})$

x/R	y/R	x/R	y/R
9.4855-01	8.1381-01	7.7214-01	9.3341-01
9.4591-01	8.1750-01	7.6701-01	9.3469-01
9.4321-01	8.2116-01	7.6184-01	9.3589-01
9.4045-01	8.2478-01	7.5663-01	9.3701-01
9.3763-01	8.2863-01	7.5137-01	9.3806-01
9.3474-01	8.3191-01	7.4606-01	9.3902-01
9.3179-01	8.3542-01	7.4072-01	9.3991-01
9.2878-01	8.3889-01	7.3533-01	9.4072-01
9.2571-01	8.4232-01	7.2990-01	9.4145-01
9.2257-01	8.4571-01	7.2442-01	9.4210-01
9.1938-01	8.4905-01	7.1891-01	9.4267-01
9.1612-01	8.5236-01	7.1335-01	9.4315-01
9.1281-01	8.5562-01	7.0776-01	9.4354-01
9.0943-01	8.5884-01	7.0213-01	9.4385-01
9.0600-01	8.6202-01	6.9646-01	9.4407-01
9.0251-01	8.6515-01	6.9075-01	9.4421-01
8.9895-01	8.6823-01	6.8500-01	9.4425-01
8.9534-01	8.7126-01	6.7922-01	9.4421-01
8.9167-01	8.7425-01	6.7340-01	9.4407-01
8.8795-01	8.7719-01	6.6754-01	9.4384-01
8.8416-01	8.8008-01	6.6165-01	9.4352-01
8.8032-01	8.8291-01	6.5573-01	9.4310-01
8.7643-01	8.8570-01	6.4977-01	9.4258-01
8.7247-01	8.8843-01	6.4378-01	9.4197-01
8.6846-01	8.9111-01	6.3775-01	9.4125-01
8.6440-01	8.9373-01	6.3170-01	9.4044-01
8.6028-01	8.9630-01	6.2561-01	9.3952-01
8.5611-01	8.9881-01	6.1949-01	9.3851-01
8.5188-01	9.0127-01	6.1334-01	9.3738-01
8.4760-01	9.0367-01	6.0717-01	9.3615-01
8.4326-01	9.0601-01	6.0096-01	9.3482-01
8.3887-01	9.0829-01	5.9473-01	9.3337-01
8.3443-01	9.1950-01	5.8847-01	9.3182-01
8.2994-01	9.1266-01	5.8219-01	9.3015-01
8.2539-01	9.1476-01	5.7588-01	9.2837-01
8.2080-01	9.1679-01	5.6954-01	9.2648-01
8.1615-01	9.1876-01	5.6318-01	9.2447-01
8.1146-01	9.2066-01	5.5680-01	9.2234-01
8.0671-01	9.2249-01	5.5039-01	9.2009-01
8.0192-01	9.2426-01	5.4397-01	9.1772-01
7.9707-01	9.2596-01	5.3752-01	9.1522-01
7.9218-01	9.2760-01	5.3105-01	9.1260-01
7.8724-01	9.2916-01	5.2457-01	9.0985-01
7.8225-01	9.3065-01	5.1806-01	9.0698-01
7.7722-01	9.3207-01	5.1154-01	9.0397-01

TABLE XIII - ISOTENSOID COORDINATES, 344 POINTS

($\phi = 23.6$ DEG)(Continued)

x/R	y/R	x/R	y/R
5.0500-01	9.0083-01	2.4978-01	6.4318-01
4.9844-01	8.9755-01	2.4372-01	6.3195-01
4.9187-01	8.9414-01	2.3773-01	6.2042-01
4.8529-01	8.9059-01	2.3181-01	6.0856-01
4.7869-01	8.8689-01	2.2596-01	5.9638-01
4.7208-01	8.8305-01	2.2019-01	5.8387-01
4.6546-01	8.7907-01	2.1451-01	5.7102-01
4.5883-01	8.7493-01	2.0892-01	5.5782-01
4.5220-01	8.7065-01	2.0343-01	5.4426-01
4.4555-01	8.6621-01	1.9805-01	5.3034-01
4.3890-01	8.6161-01	1.9278-01	5.1606-01
4.3224-01	8.5685-01	1.8763-01	5.0140-01
4.2557-01	8.5193-01	1.8261-01	4.8636-01
4.1891-01	8.4684-01	1.7774-01	4.7093-01
4.1224-01	8.4158-01	1.7301-01	4.5512-01
4.0557-01	8.3615-01	1.6844-01	4.3892-01
3.9890-01	8.3055-01	1.6404-01	4.2233-01
3.9224-01	8.2476-01	1.5982-01	4.0536-01
3.8557-01	8.1879-01	1.5580-01	3.8799-01
3.7892-01	8.1264-01	1.5198-01	3.7025-01
3.7226-01	8.0629-01	1.4838-01	3.5213-01
3.6562-01	7.9975-01	1.4500-01	3.3365-01
3.5899-01	7.9301-01	1.4187-01	3.1482-01
3.5237-01	7.8607-01	1.3899-01	2.9566-01
3.4576-01	7.7892-01	1.3637-01	2.7619-01
3.3916-01	7.7156-01	1.3403-01	2.5643-01
3.3259-01	7.6398-01	1.3198-01	2.3640-01
3.2603-01	7.5618-01	1.3023-01	2.1614-01
3.1949-01	7.4815-01	1.2878-01	1.9569-01
3.1298-01	7.3988-01	1.2764-01	1.7507-01
3.0650-01	7.3139-01	1.2683-01	1.5433-01
3.0004-01	7.2264-01	1.2634-01	1.3350-01
2.9361-01	7.1365-01	1.2617-01	1.1263-01
2.8722-01	7.0440-01	1.2634-01	9.1757-02
2.8087-01	6.9489-01	1.2683-01	7.0929-02
2.7455-01	6.8511-01	1.2764-01	5.0185-02
2.6828-01	6.7506-01	1.2878-01	2.9566-02
2.6206-01	6.6472-01	1.3023-01	9.1093-03
2.5589-01	6.5410-01	1.3198-01	-1.1148-02

APPENDIX C

INFLATION ANALYSIS

It was intended to inflate the attached decelerator upon deployment with a liquid that vaporizes upon being exposed to the low static pressure of the tunnel. Once the vapor-induced inflation takes place, the ram-air inlets on the decelerator surface are exposed and fill out the enclosed volume completely with ram air. The purpose of this analysis is to estimate the amount of liquid necessary to inflate the envelope initially to full volume using the vaporization technique of inflation.

The decelerator canopy is packaged on the back side of the aeroshell with the liquid packaged within the fabric envelope. For the intended test, the model is sting-mounted in the AEDC (PWT) 16S tunnel. A two-hour startup time is required to reach test conditions of $M_\infty = 3$ and a dynamic pressure of 120 psf. Figure 34 shows a schematic of this installation. During this period, the model is exposed to a stagnation temperature of 180 deg F. Thus, it is anticipated that the model and onboard accessories also approach this temperature over the two-hour time exposure. The tunnel static pressure during this same time period is reduced to about 20 psf. Therefore, as the time of deployment approaches, the model temperature approaches 180 deg F when the static pressure reaches 20 psf. However, the liquid packaged in a sealed container at normal ambient pressure (14.7 psi), not only is at an

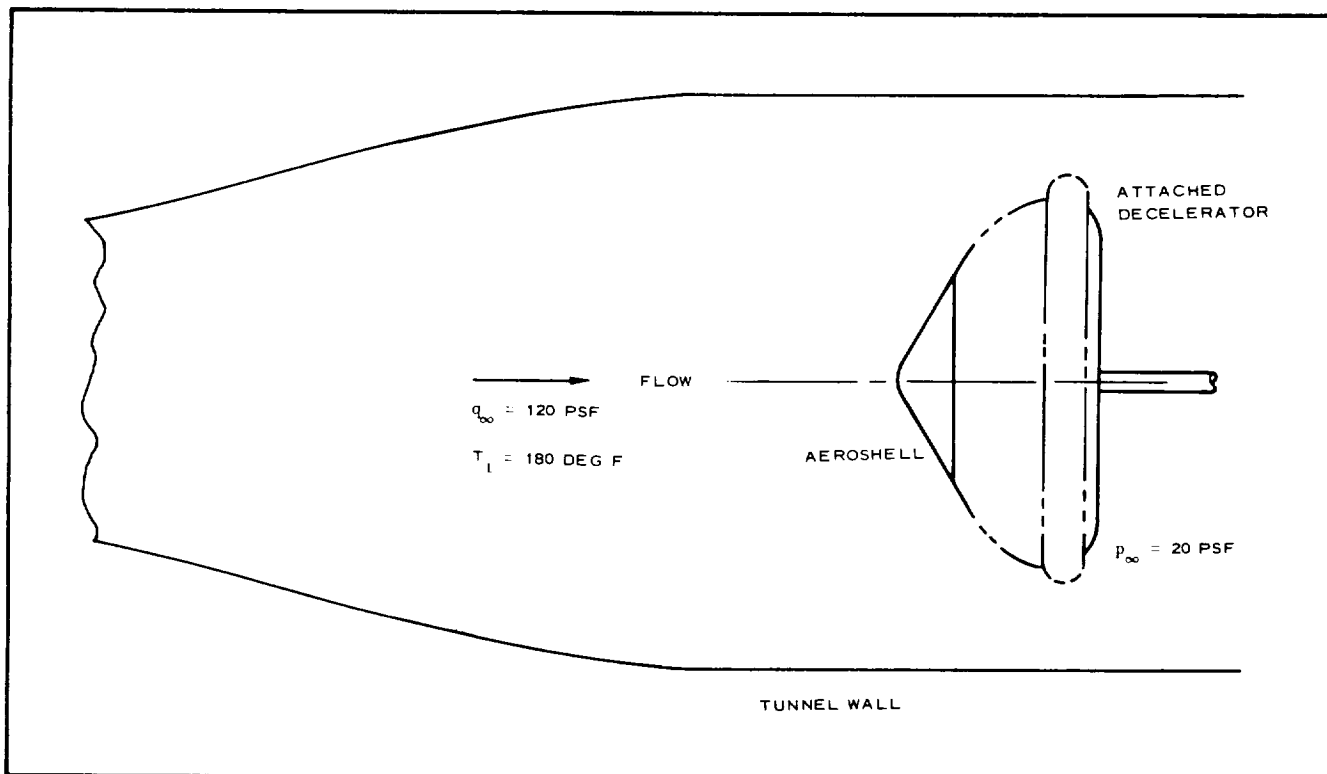


Figure 34 - Wind-Tunnel Setup

elevated temperature at this time but also is at an elevated pressure compared with the tunnel environment. Assuming water is used for inflation, the liquid remains in its normal state, since the pressure is 14.7 psi and the temperature is 180 deg F.

The decelerator volume was evaluated to be 26 cu ft when fully inflated. It was proposed that an internal pressure coefficient of 2 is required for the wind-tunnel test conditions. The internal decelerator pressure was calculated from the pressure coefficient:

$$C_{P_i} = \frac{P_i - P_{\infty}}{q_{\infty}} \quad (50)$$

where

$$q_{\infty} = 120 \text{ psf (dynamic pressure)}$$

$$C_{P_i} = 2 \text{ (internal pressure coefficient)}$$

$$P_{\infty} = 20 \text{ psf (test section static pressure)}$$

Then

$$P_i = C_{P_i} q_{\infty} + P_{\infty} = 260 \text{ psf}$$

The equation of state was now applied to determine the weight of water required, which upon vaporization yields the required internal pressure.

$$P_i = \frac{WRT_i}{V} \quad (51)$$

where

W weight of water required (lb)

R water vapor gas constant (85.81 ft-lb/lb-deg R)

T_i internal equilibrium temperature (deg R)

V decelerator volume (cu ft)

The internal temperature of the water vapor required in Equation (51) is the equilibrium temperature the vapor reaches once all the liquid is vaporized. This statement assumes that ideally complete vaporization can be realized due to the gross amount of heat available in the structural components. This temperature can be obtained from water vapor-pressure data such as shown in Figure 35. The internal pressure of the decelerator was proposed to be 260 psf (0.123 atm). At this pressure, the equilibrium temperature is 120 deg F. Solving Equation (51) for the weight of water required yielded

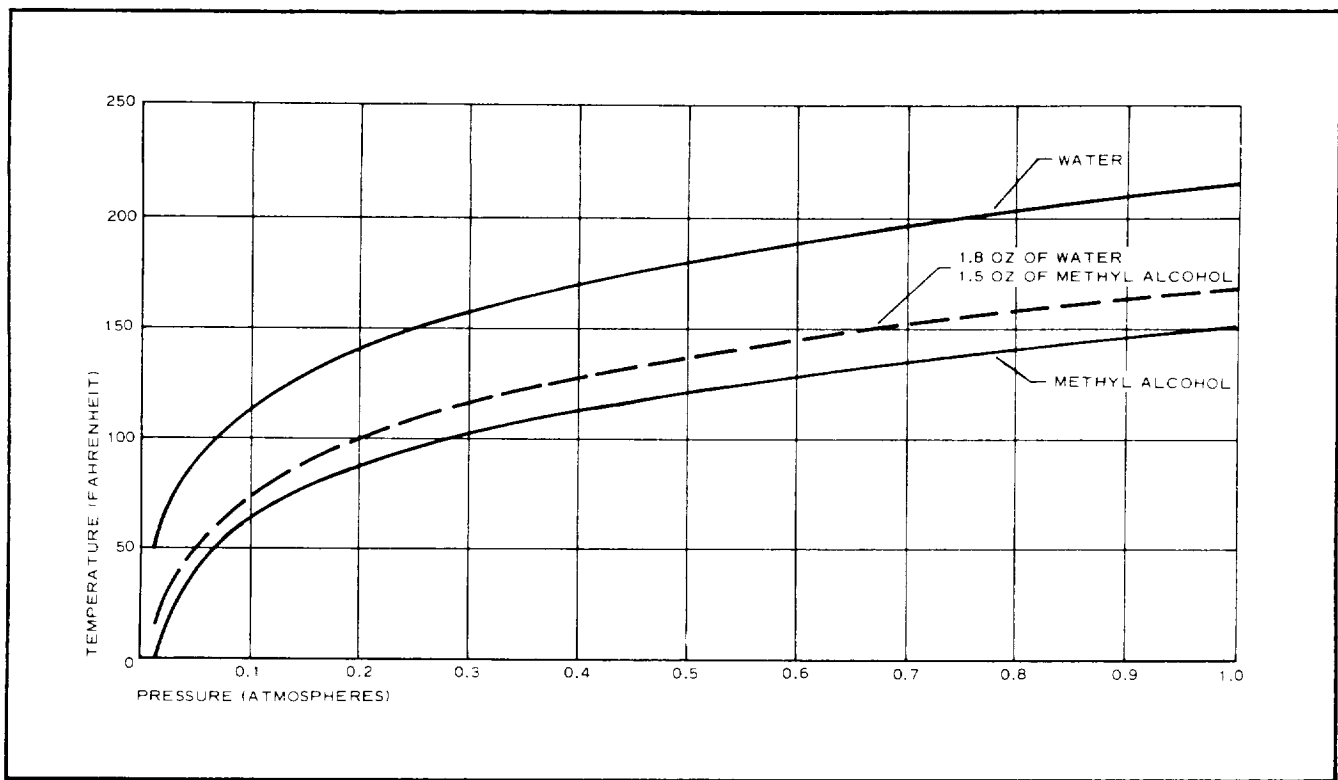


Figure 35 - Vapor Pressure Data

$$\begin{aligned}
 W &= \frac{P_i V}{RT_i} \\
 &= \frac{260(26)}{86(580)} \\
 &= 0.136 \text{ lb}
 \end{aligned}$$

The heat required to vaporize this amount of water is estimated by the following relationship:

$$Q_v = Wh_v \quad (52)$$

where

Q_v heat required for vaporization (Btu)

h_v heat of vaporization (Btu/lb)

The heat of vaporization is obtained from steam tables and at a pressure of 20 psf (0.139 psi) is equal to 1070 Btu/lb. Therefore, the heat required to vaporize the water is

$$Q_v = 0.136(1070) = 145 \text{ Btu}$$

A portion of this heat becomes available from the sensible heat decrease of the liquid as soon as its container is fractured and the fluid is exposed to the static pressure of the tunnel. This amount of heat is calculated from the following relationship:

$$Q_s = WC(T_a - T_b) \quad (53)$$

where

Q_s = sensible heat realized from water (Btu)

C = specific heat of water (1 Btu/lb-deg F)

T_b = 50 deg F vapor pressure temperature at
20 psf

T_a = 180 deg F initial temperature

Therefore,

$$Q_s = (0.136)1(180 - 50) = 18 \text{ Btu}$$

Since this amount of heat is not sufficient to vaporize all the liquid, the remainder of the heat required must be obtained from the sensible heat contained in the fabric and in the aeroshell. The additional heat required is

$$\begin{aligned} Q &= Q_v - Q_s \\ &= 145 - 18 = 127 \text{ Btu} \end{aligned}$$

Assuming the fabric is at a temperature of 180 deg F and the specific heat of Nomex fabric is 0.29 Btu/lb-deg F, then for a fabric weight of four pounds,

$$\begin{aligned} Q &= W_f C_f (T_a - T_b) \\ &= (4)0.29(180 - 120) = 70 \text{ Btu} \end{aligned}$$

Since this amount of energy is insufficient to vaporize the water, the remainder of the energy must be extracted from the sensible heat energy contained in the aeroshell, which is more than sufficient to vaporize the water.

The use of other liquids also was investigated; these results are summarized in Table XIV. The vapor pressure characteristics of these liquids also are shown in Figure 35.

TABLE XIV - LIQUID VAPORIZATION CHARACTERISTICS

Vaporizing fluid	Weight required (oz)	Volume (cu in.)	Heat required (Btu)	Internal pressure (psf)
Water	2.2	3.8	145	260
Methyl alcohol	4.3	9.3	130	260
Mixture	1.8 (water) 1.5 (methyl alcohol)	6.4	165	260

A comparison of these results showed that, while less heat is required to vaporize the methyl alcohol, a larger storage space is required to store it. In addition, the methyl alcohol vaporizes during the tunnel pull-down operation, thus requiring a more impermeable packaging container. A mixture of water and alcohol, which has been used successfully in Goodyear Aerospace decelerator programs, also can be utilized for the vaporization technique, although the largest amount of heat is required to vaporize this liquid. The simplest overall design problems, however, apparently are encountered with water.

It was recommended, therefore, that water be used initially for this test operation, but subsequent testing in this application found a more effective mixture.

APPENDIX D

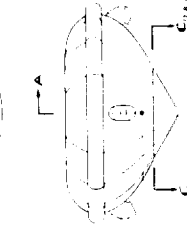
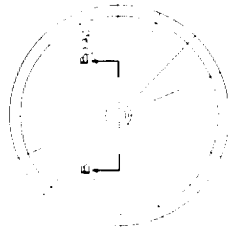
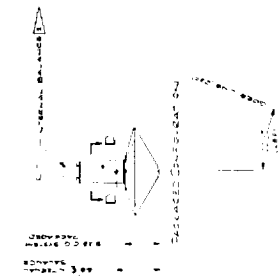
DRAWINGS

The working drawings for the attached inflatable decelerator system were generated by Goodyear Aerospace and are given below (see Figures 36 through 53).

1. Drawing 610A000-001: Model Assembly, 60-Inch D_P , Attached Inflatable Decelerator (four sheets), 18 August 1967.
2. Drawing 610A000-002: Decelerator Assembly, 60-Inch D_P (six sheets), 18 August 1967.
3. Drawing 610A000-101: Aeroshell, Attached Inflatable Decelerator, 18 August 1967.
4. Drawing 610A000-102: Support Assembly, Attached Inflatable Decelerator, 18 August 1967.
5. Drawing 610A000-103: Model Details, Attached Inflatable Decelerator, 18 August 1967.
6. Drawing 610A000-104: Clamp Assembly, Attached Inflatable Decelerator, 18 August 1967.
7. Drawing 610A000-105: Inlet Assembly, 4-Inch Diameter, 18 August 1967.
8. Drawing 610A000-106: Sleeve, Inlet, 4-Inch Diameter, 18 August 1967.
9. Drawing 610A000-107: Base, Inlet, 18 August 1967.
10. Drawing 530A005-110: Ring, Ballute Inlet, 15 April 1966.

PRECEDING PAGE BLANK NOT FILMED.

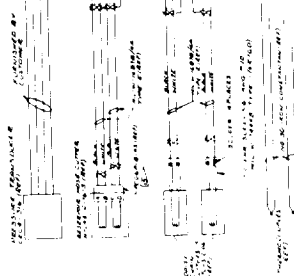
FOLDOUT FRAME



DESIGNED FOR OPERATION

NOTE: ASSEMBLY

FIGURE 36-1



1. THE FOLLOWING INFORMATION IS FOR YOUR INFORMATION ONLY. IT IS NOT TO BE USED AS A BASIS FOR ANY OTHER ACTION.

2. THE FOLLOWING INFORMATION IS FOR YOUR INFORMATION ONLY. IT IS NOT TO BE USED AS A BASIS FOR ANY OTHER ACTION.

3. THE FOLLOWING INFORMATION IS FOR YOUR INFORMATION ONLY. IT IS NOT TO BE USED AS A BASIS FOR ANY OTHER ACTION.

4. THE FOLLOWING INFORMATION IS FOR YOUR INFORMATION ONLY. IT IS NOT TO BE USED AS A BASIS FOR ANY OTHER ACTION.

5. THE FOLLOWING INFORMATION IS FOR YOUR INFORMATION ONLY. IT IS NOT TO BE USED AS A BASIS FOR ANY OTHER ACTION.

6. THE FOLLOWING INFORMATION IS FOR YOUR INFORMATION ONLY. IT IS NOT TO BE USED AS A BASIS FOR ANY OTHER ACTION.

7. THE FOLLOWING INFORMATION IS FOR YOUR INFORMATION ONLY. IT IS NOT TO BE USED AS A BASIS FOR ANY OTHER ACTION.

8. THE FOLLOWING INFORMATION IS FOR YOUR INFORMATION ONLY. IT IS NOT TO BE USED AS A BASIS FOR ANY OTHER ACTION.

9. THE FOLLOWING INFORMATION IS FOR YOUR INFORMATION ONLY. IT IS NOT TO BE USED AS A BASIS FOR ANY OTHER ACTION.

10. THE FOLLOWING INFORMATION IS FOR YOUR INFORMATION ONLY. IT IS NOT TO BE USED AS A BASIS FOR ANY OTHER ACTION.

11. THE FOLLOWING INFORMATION IS FOR YOUR INFORMATION ONLY. IT IS NOT TO BE USED AS A BASIS FOR ANY OTHER ACTION.

12. THE FOLLOWING INFORMATION IS FOR YOUR INFORMATION ONLY. IT IS NOT TO BE USED AS A BASIS FOR ANY OTHER ACTION.

13. THE FOLLOWING INFORMATION IS FOR YOUR INFORMATION ONLY. IT IS NOT TO BE USED AS A BASIS FOR ANY OTHER ACTION.

14. THE FOLLOWING INFORMATION IS FOR YOUR INFORMATION ONLY. IT IS NOT TO BE USED AS A BASIS FOR ANY OTHER ACTION.

15. THE FOLLOWING INFORMATION IS FOR YOUR INFORMATION ONLY. IT IS NOT TO BE USED AS A BASIS FOR ANY OTHER ACTION.

16. THE FOLLOWING INFORMATION IS FOR YOUR INFORMATION ONLY. IT IS NOT TO BE USED AS A BASIS FOR ANY OTHER ACTION.

17. THE FOLLOWING INFORMATION IS FOR YOUR INFORMATION ONLY. IT IS NOT TO BE USED AS A BASIS FOR ANY OTHER ACTION.

18. THE FOLLOWING INFORMATION IS FOR YOUR INFORMATION ONLY. IT IS NOT TO BE USED AS A BASIS FOR ANY OTHER ACTION.

19. THE FOLLOWING INFORMATION IS FOR YOUR INFORMATION ONLY. IT IS NOT TO BE USED AS A BASIS FOR ANY OTHER ACTION.

20. THE FOLLOWING INFORMATION IS FOR YOUR INFORMATION ONLY. IT IS NOT TO BE USED AS A BASIS FOR ANY OTHER ACTION.

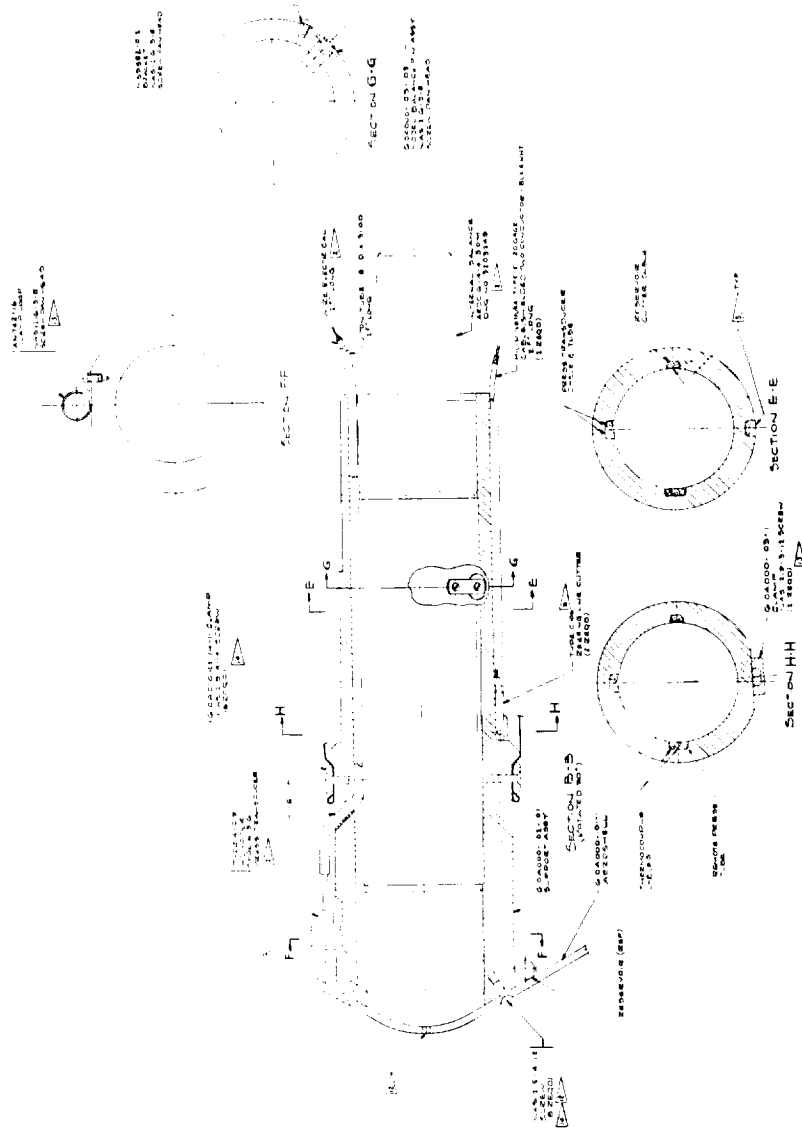
ITEM NO.	DESCRIPTION	QUANTITY	UNIT	REMARKS
1
2
3
4
5
6
7
8
9
10
11
12
13
14
15
16
17
18
19
20
21
22
23
24
25
26
27
28
29
30
31
32
33
34
35
36
37
38
39
40
41
42
43
44
45
46
47
48
49
50
51
52
53
54
55
56
57
58
59
60
61
62
63
64
65
66
67
68
69
70
71
72
73
74
75
76
77
78
79
80
81
82
83
84
85
86
87
88
89
90
91
92
93
94
95
96
97
98
99
100

Figure 36 - Model Assembly with 60-In. Dp (Drawing 610A000-001, Sheet 1)

(The reverse is blank)

TOP SECRET

· ALLOUT FRAME



FOLDOUT PAGE

81

FOLDOUT FRAME

10

PRECEDING PAGE BLANK NOT FILMED.

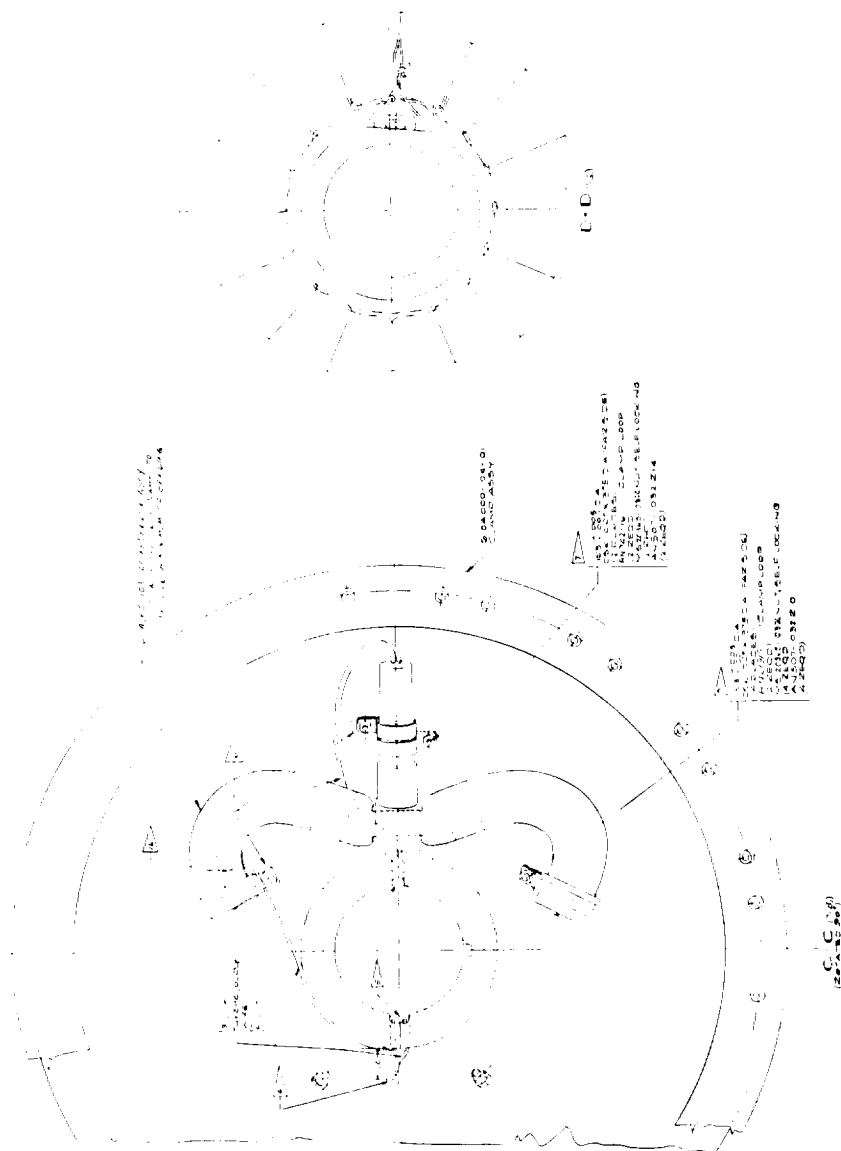
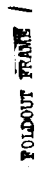


Figure 38 - Model Assembly with 60-In. D_p (Sheet 3)

(The reverse is blank.)

83

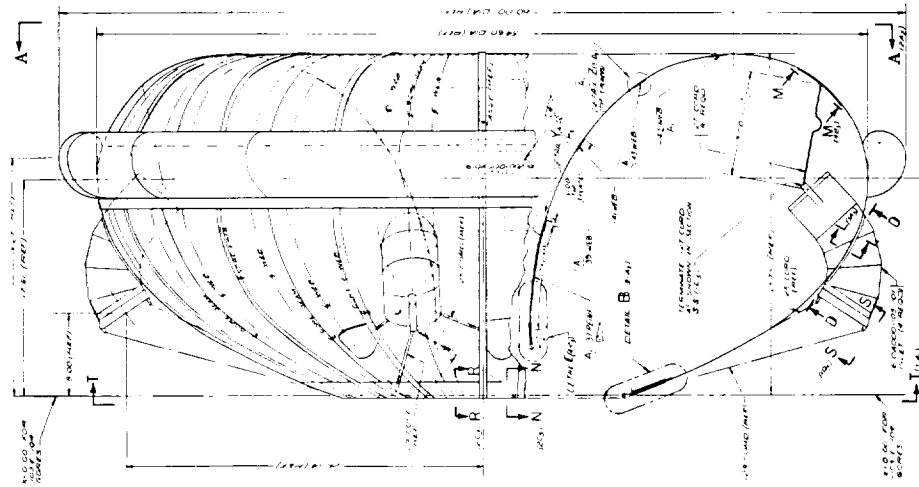
12



२३

58

PRECEDING PAGE BLANK NOT FILMED. FOLDOUT FRAME



NOTES: UNLESS OTHERWISE SPECIFIED
 1. ALL DIMENSIONS ARE IN INCHES, FRACTIONS OF INCHES SHALL BE TO NEAREST 1/16 INCH.
 2. ALL DIMENSIONS ARE TO CENTER UNLESS OTHERWISE SPECIFIED.
 3. ALL DIMENSIONS ARE TO CENTER UNLESS OTHERWISE SPECIFIED.
 4. ALL DIMENSIONS ARE TO CENTER UNLESS OTHERWISE SPECIFIED.
 5. ALL DIMENSIONS ARE TO CENTER UNLESS OTHERWISE SPECIFIED.
 6. ALL DIMENSIONS ARE TO CENTER UNLESS OTHERWISE SPECIFIED.
 7. ALL DIMENSIONS ARE TO CENTER UNLESS OTHERWISE SPECIFIED.
 8. ALL DIMENSIONS ARE TO CENTER UNLESS OTHERWISE SPECIFIED.
 9. ALL DIMENSIONS ARE TO CENTER UNLESS OTHERWISE SPECIFIED.
 10. ALL DIMENSIONS ARE TO CENTER UNLESS OTHERWISE SPECIFIED.
 11. ALL DIMENSIONS ARE TO CENTER UNLESS OTHERWISE SPECIFIED.
 12. ALL DIMENSIONS ARE TO CENTER UNLESS OTHERWISE SPECIFIED.
 13. ALL DIMENSIONS ARE TO CENTER UNLESS OTHERWISE SPECIFIED.
 14. ALL DIMENSIONS ARE TO CENTER UNLESS OTHERWISE SPECIFIED.
 15. ALL DIMENSIONS ARE TO CENTER UNLESS OTHERWISE SPECIFIED.
 16. ALL DIMENSIONS ARE TO CENTER UNLESS OTHERWISE SPECIFIED.
 17. ALL DIMENSIONS ARE TO CENTER UNLESS OTHERWISE SPECIFIED.
 18. ALL DIMENSIONS ARE TO CENTER UNLESS OTHERWISE SPECIFIED.
 19. ALL DIMENSIONS ARE TO CENTER UNLESS OTHERWISE SPECIFIED.
 20. ALL DIMENSIONS ARE TO CENTER UNLESS OTHERWISE SPECIFIED.
 21. ALL DIMENSIONS ARE TO CENTER UNLESS OTHERWISE SPECIFIED.
 22. ALL DIMENSIONS ARE TO CENTER UNLESS OTHERWISE SPECIFIED.
 23. ALL DIMENSIONS ARE TO CENTER UNLESS OTHERWISE SPECIFIED.
 24. ALL DIMENSIONS ARE TO CENTER UNLESS OTHERWISE SPECIFIED.
 25. ALL DIMENSIONS ARE TO CENTER UNLESS OTHERWISE SPECIFIED.
 26. ALL DIMENSIONS ARE TO CENTER UNLESS OTHERWISE SPECIFIED.
 27. ALL DIMENSIONS ARE TO CENTER UNLESS OTHERWISE SPECIFIED.
 28. ALL DIMENSIONS ARE TO CENTER UNLESS OTHERWISE SPECIFIED.
 29. ALL DIMENSIONS ARE TO CENTER UNLESS OTHERWISE SPECIFIED.
 30. ALL DIMENSIONS ARE TO CENTER UNLESS OTHERWISE SPECIFIED.
 31. ALL DIMENSIONS ARE TO CENTER UNLESS OTHERWISE SPECIFIED.
 32. ALL DIMENSIONS ARE TO CENTER UNLESS OTHERWISE SPECIFIED.
 33. ALL DIMENSIONS ARE TO CENTER UNLESS OTHERWISE SPECIFIED.
 34. ALL DIMENSIONS ARE TO CENTER UNLESS OTHERWISE SPECIFIED.
 35. ALL DIMENSIONS ARE TO CENTER UNLESS OTHERWISE SPECIFIED.
 36. ALL DIMENSIONS ARE TO CENTER UNLESS OTHERWISE SPECIFIED.
 37. ALL DIMENSIONS ARE TO CENTER UNLESS OTHERWISE SPECIFIED.
 38. ALL DIMENSIONS ARE TO CENTER UNLESS OTHERWISE SPECIFIED.
 39. ALL DIMENSIONS ARE TO CENTER UNLESS OTHERWISE SPECIFIED.
 40. ALL DIMENSIONS ARE TO CENTER UNLESS OTHERWISE SPECIFIED.
 41. ALL DIMENSIONS ARE TO CENTER UNLESS OTHERWISE SPECIFIED.
 42. ALL DIMENSIONS ARE TO CENTER UNLESS OTHERWISE SPECIFIED.
 43. ALL DIMENSIONS ARE TO CENTER UNLESS OTHERWISE SPECIFIED.
 44. ALL DIMENSIONS ARE TO CENTER UNLESS OTHERWISE SPECIFIED.
 45. ALL DIMENSIONS ARE TO CENTER UNLESS OTHERWISE SPECIFIED.
 46. ALL DIMENSIONS ARE TO CENTER UNLESS OTHERWISE SPECIFIED.
 47. ALL DIMENSIONS ARE TO CENTER UNLESS OTHERWISE SPECIFIED.
 48. ALL DIMENSIONS ARE TO CENTER UNLESS OTHERWISE SPECIFIED.
 49. ALL DIMENSIONS ARE TO CENTER UNLESS OTHERWISE SPECIFIED.
 50. ALL DIMENSIONS ARE TO CENTER UNLESS OTHERWISE SPECIFIED.
 51. ALL DIMENSIONS ARE TO CENTER UNLESS OTHERWISE SPECIFIED.
 52. ALL DIMENSIONS ARE TO CENTER UNLESS OTHERWISE SPECIFIED.
 53. ALL DIMENSIONS ARE TO CENTER UNLESS OTHERWISE SPECIFIED.
 54. ALL DIMENSIONS ARE TO CENTER UNLESS OTHERWISE SPECIFIED.
 55. ALL DIMENSIONS ARE TO CENTER UNLESS OTHERWISE SPECIFIED.
 56. ALL DIMENSIONS ARE TO CENTER UNLESS OTHERWISE SPECIFIED.
 57. ALL DIMENSIONS ARE TO CENTER UNLESS OTHERWISE SPECIFIED.
 58. ALL DIMENSIONS ARE TO CENTER UNLESS OTHERWISE SPECIFIED.
 59. ALL DIMENSIONS ARE TO CENTER UNLESS OTHERWISE SPECIFIED.
 60. ALL DIMENSIONS ARE TO CENTER UNLESS OTHERWISE SPECIFIED.
 61. ALL DIMENSIONS ARE TO CENTER UNLESS OTHERWISE SPECIFIED.
 62. ALL DIMENSIONS ARE TO CENTER UNLESS OTHERWISE SPECIFIED.
 63. ALL DIMENSIONS ARE TO CENTER UNLESS OTHERWISE SPECIFIED.
 64. ALL DIMENSIONS ARE TO CENTER UNLESS OTHERWISE SPECIFIED.
 65. ALL DIMENSIONS ARE TO CENTER UNLESS OTHERWISE SPECIFIED.
 66. ALL DIMENSIONS ARE TO CENTER UNLESS OTHERWISE SPECIFIED.
 67. ALL DIMENSIONS ARE TO CENTER UNLESS OTHERWISE SPECIFIED.
 68. ALL DIMENSIONS ARE TO CENTER UNLESS OTHERWISE SPECIFIED.
 69. ALL DIMENSIONS ARE TO CENTER UNLESS OTHERWISE SPECIFIED.
 70. ALL DIMENSIONS ARE TO CENTER UNLESS OTHERWISE SPECIFIED.
 71. ALL DIMENSIONS ARE TO CENTER UNLESS OTHERWISE SPECIFIED.
 72. ALL DIMENSIONS ARE TO CENTER UNLESS OTHERWISE SPECIFIED.
 73. ALL DIMENSIONS ARE TO CENTER UNLESS OTHERWISE SPECIFIED.
 74. ALL DIMENSIONS ARE TO CENTER UNLESS OTHERWISE SPECIFIED.
 75. ALL DIMENSIONS ARE TO CENTER UNLESS OTHERWISE SPECIFIED.
 76. ALL DIMENSIONS ARE TO CENTER UNLESS OTHERWISE SPECIFIED.
 77. ALL DIMENSIONS ARE TO CENTER UNLESS OTHERWISE SPECIFIED.
 78. ALL DIMENSIONS ARE TO CENTER UNLESS OTHERWISE SPECIFIED.
 79. ALL DIMENSIONS ARE TO CENTER UNLESS OTHERWISE SPECIFIED.
 80. ALL DIMENSIONS ARE TO CENTER UNLESS OTHERWISE SPECIFIED.
 81. ALL DIMENSIONS ARE TO CENTER UNLESS OTHERWISE SPECIFIED.
 82. ALL DIMENSIONS ARE TO CENTER UNLESS OTHERWISE SPECIFIED.
 83. ALL DIMENSIONS ARE TO CENTER UNLESS OTHERWISE SPECIFIED.
 84. ALL DIMENSIONS ARE TO CENTER UNLESS OTHERWISE SPECIFIED.
 85. ALL DIMENSIONS ARE TO CENTER UNLESS OTHERWISE SPECIFIED.
 86. ALL DIMENSIONS ARE TO CENTER UNLESS OTHERWISE SPECIFIED.
 87. ALL DIMENSIONS ARE TO CENTER UNLESS OTHERWISE SPECIFIED.
 88. ALL DIMENSIONS ARE TO CENTER UNLESS OTHERWISE SPECIFIED.
 89. ALL DIMENSIONS ARE TO CENTER UNLESS OTHERWISE SPECIFIED.
 90. ALL DIMENSIONS ARE TO CENTER UNLESS OTHERWISE SPECIFIED.
 91. ALL DIMENSIONS ARE TO CENTER UNLESS OTHERWISE SPECIFIED.
 92. ALL DIMENSIONS ARE TO CENTER UNLESS OTHERWISE SPECIFIED.
 93. ALL DIMENSIONS ARE TO CENTER UNLESS OTHERWISE SPECIFIED.
 94. ALL DIMENSIONS ARE TO CENTER UNLESS OTHERWISE SPECIFIED.
 95. ALL DIMENSIONS ARE TO CENTER UNLESS OTHERWISE SPECIFIED.
 96. ALL DIMENSIONS ARE TO CENTER UNLESS OTHERWISE SPECIFIED.
 97. ALL DIMENSIONS ARE TO CENTER UNLESS OTHERWISE SPECIFIED.
 98. ALL DIMENSIONS ARE TO CENTER UNLESS OTHERWISE SPECIFIED.
 99. ALL DIMENSIONS ARE TO CENTER UNLESS OTHERWISE SPECIFIED.
 100. ALL DIMENSIONS ARE TO CENTER UNLESS OTHERWISE SPECIFIED.

ITEM NO.	DESCRIPTION	QTY	UNIT	REMARKS
1
2
3
4
5
6
7
8
9
10
11
12
13
14
15
16
17
18
19
20
21
22
23
24
25
26
27
28
29
30
31
32
33
34
35
36
37
38
39
40
41
42
43
44
45
46
47
48
49
50
51
52
53
54
55
56
57
58
59
60
61
62
63
64
65
66
67
68
69
70
71
72
73
74
75
76
77
78
79
80
81
82
83
84
85
86
87
88
89
90
91
92
93
94
95
96
97
98
99
100

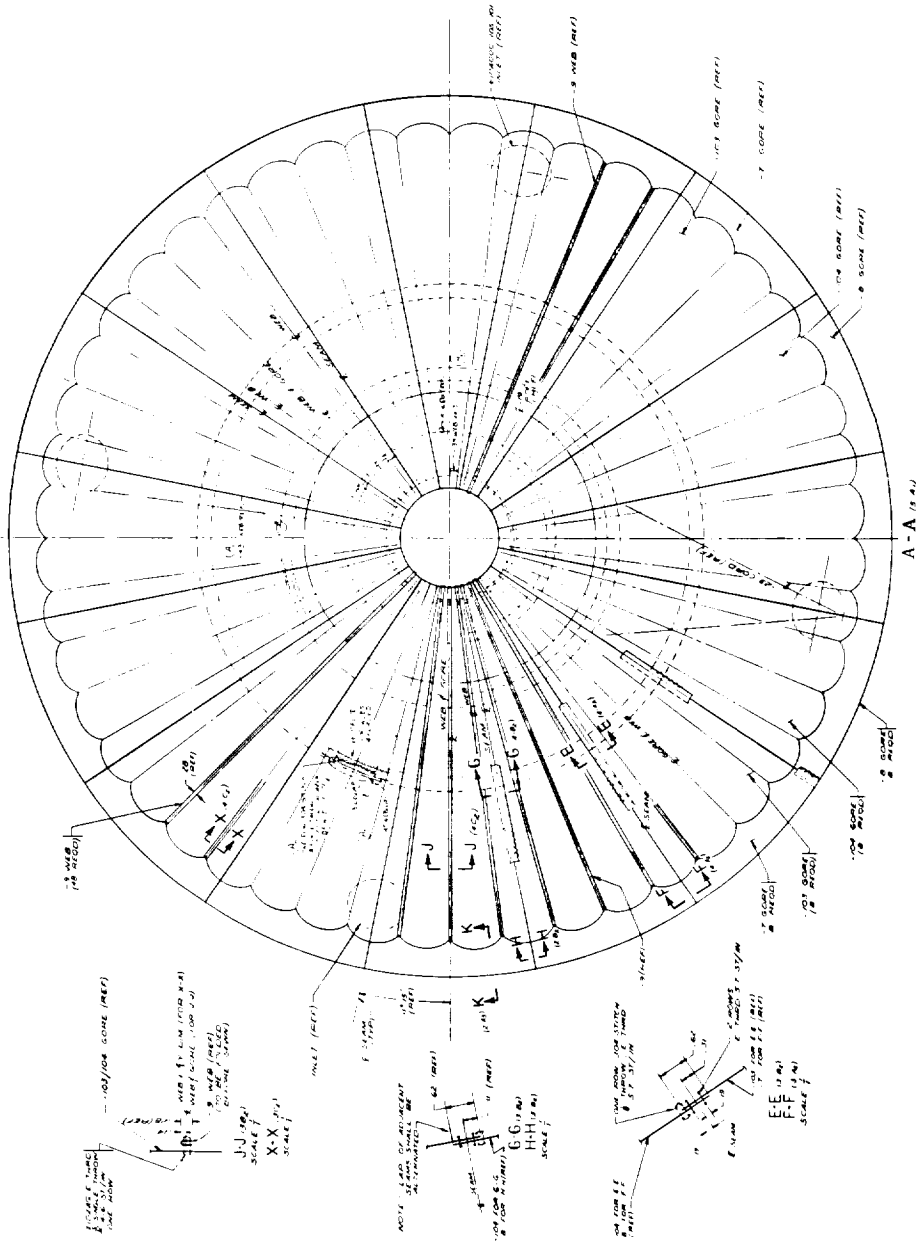
Figure 40 - Decelerator Assembly with 60-In. Dp
 (Drawing 610A000-002, Sheet 1)

FOLDOUT FRAME /

FOLDOUT FRAME

PRECEDING PAGE BLANK NOT FILMED.

PRECEDING PAGE BLANK NOT FILMED.



FOLDOUT FRAME

Figure 41 - Decelerator Assembly with 60-In. D_p (Sheet 2)

FOLDOUT FRAME

(The reverse is blank)

POULPOUT FRAME

...IT FRAMES

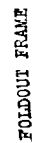


Figure 42 - Decelerator Assembly with 60-In. D_P (Sheet 3)

(The reverse is blank.)

FOLDOUT FRAME

[illegible]

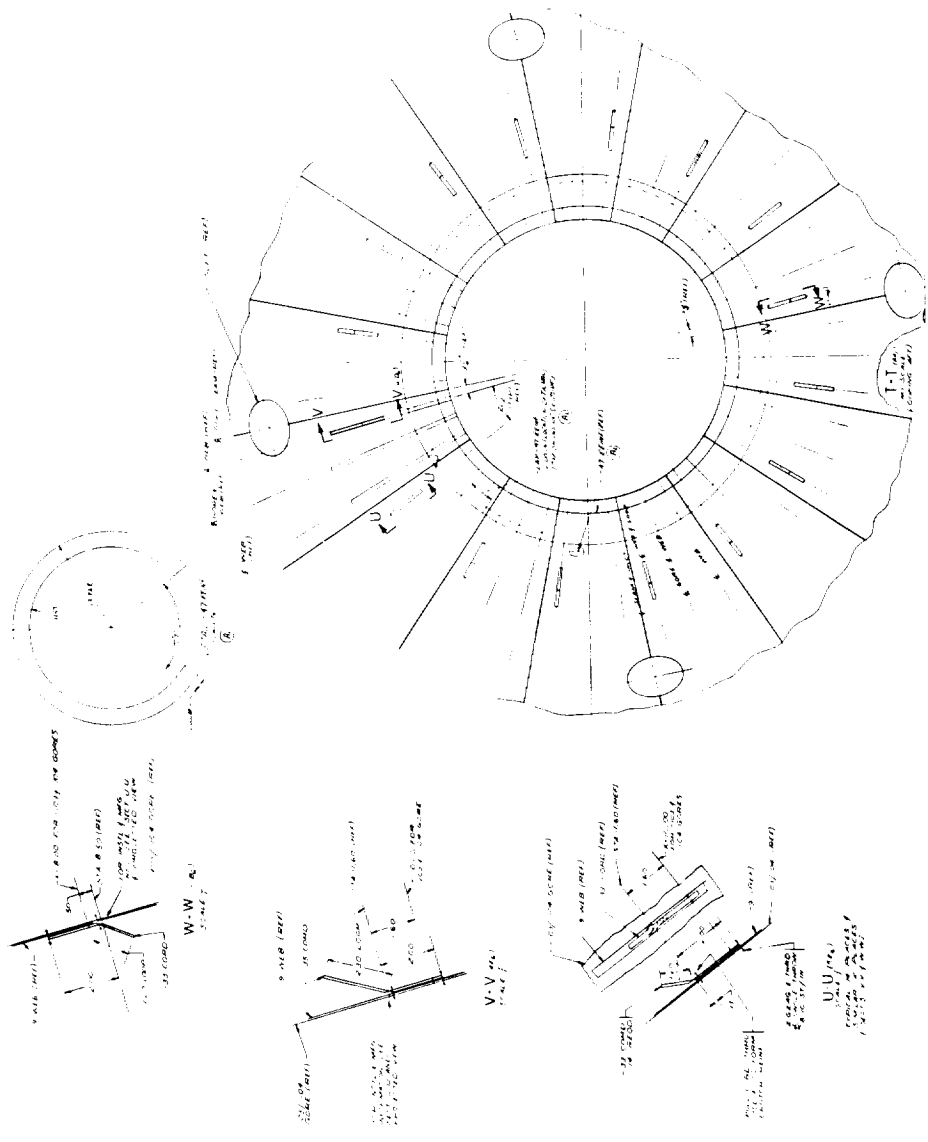
Figure 44 - Decelerator Assembly with 60-In. D_p (Sheet 5)

95

FOLDOUT FRAME

FIGURE 45

PRECEDING PAGE BLANK NOT FILMED.



FOLDOUT FRAME

Figure 45 - Decelerator Assembly with 60-In. Dp (Sheet 6)

FOLDOUT FRAME (The reverse is blank.)

FOLGOUT NAME

PRECEDING PAGE BLANK NOT FILMED.

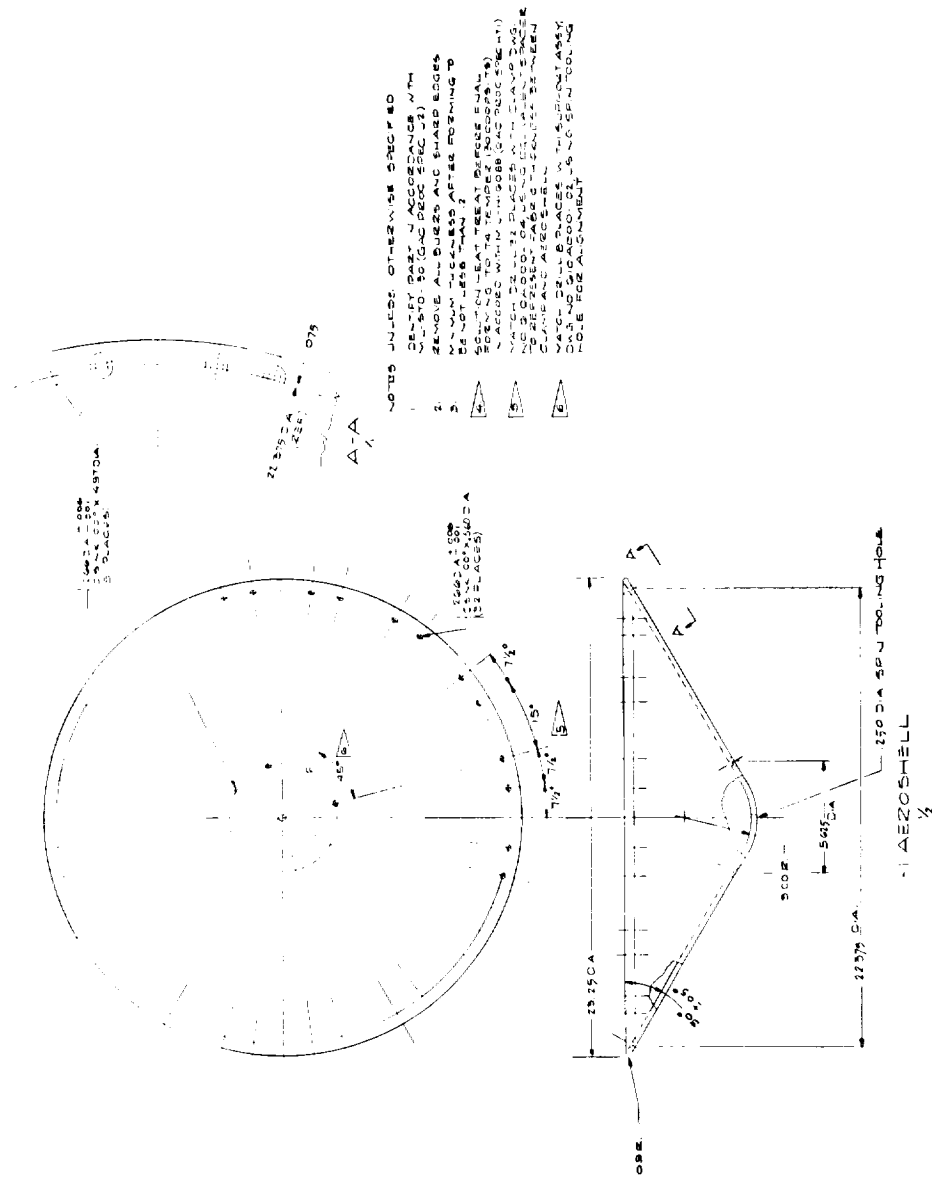


Figure 46 - Aeroshell (Drawing 610A000-101)

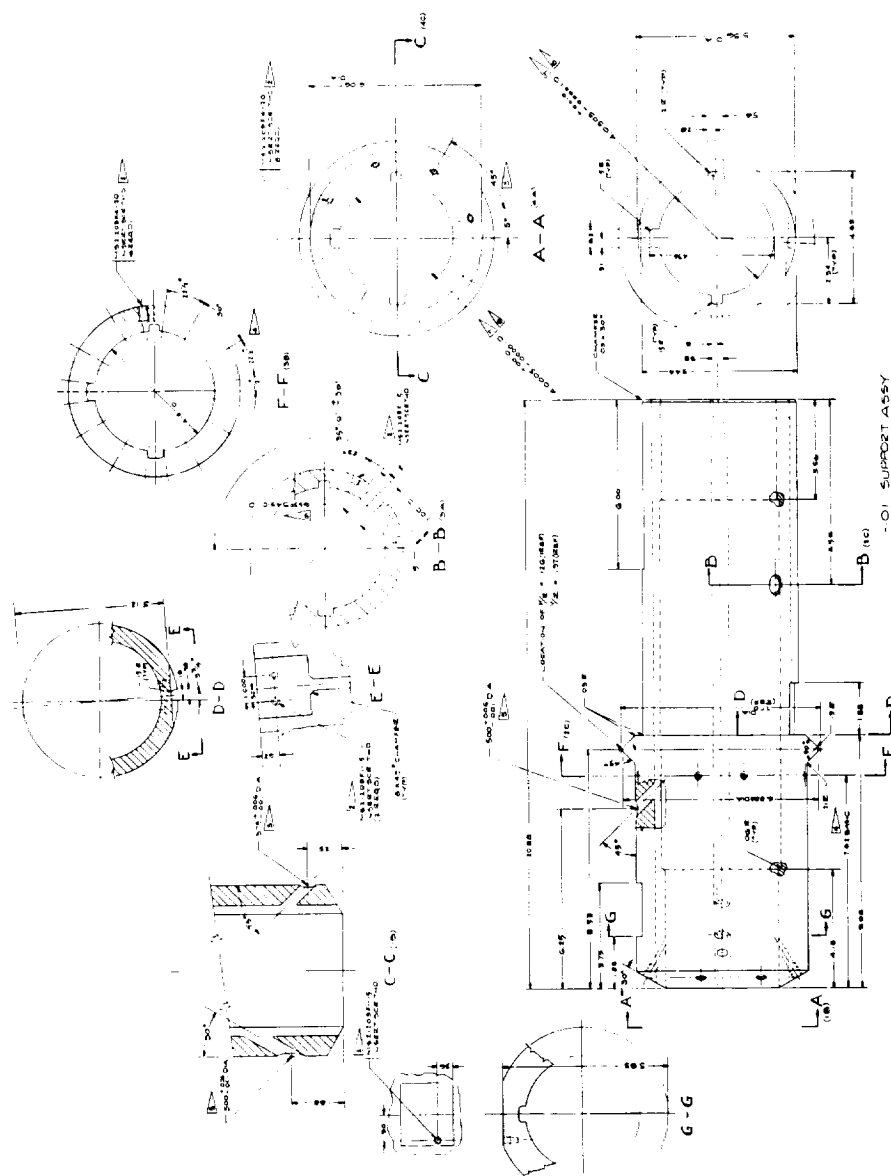
1944

(The reverse is blank.)

PRECEDING PAGE BLANK NOT FILMED.

FOLDOUT FRAME

FOLDOUT FRAME



NOTES

1. THIS DRAWING IS A FOLDOUT FRAME. IT IS NOT TO BE USED FOR DIMENSIONS. DIMENSIONS ARE TO BE TAKEN FROM THE MAIN DRAWING.

2. ALL DIMENSIONS ARE IN INCHES UNLESS OTHERWISE SPECIFIED.

3. ALL DIMENSIONS ARE TO BE TAKEN FROM THE MAIN DRAWING.

4. ALL DIMENSIONS ARE TO BE TAKEN FROM THE MAIN DRAWING.

5. ALL DIMENSIONS ARE TO BE TAKEN FROM THE MAIN DRAWING.

6. ALL DIMENSIONS ARE TO BE TAKEN FROM THE MAIN DRAWING.

7. ALL DIMENSIONS ARE TO BE TAKEN FROM THE MAIN DRAWING.

8. ALL DIMENSIONS ARE TO BE TAKEN FROM THE MAIN DRAWING.

9. ALL DIMENSIONS ARE TO BE TAKEN FROM THE MAIN DRAWING.

10. ALL DIMENSIONS ARE TO BE TAKEN FROM THE MAIN DRAWING.

NO.	DESCRIPTION	DATE	BY	CHKD.	APP'D.
1	DESIGN	10/1/58	J. H. HARRIS		
2	ENGINEERING	10/1/58	J. H. HARRIS		
3	MANUFACTURING	10/1/58	J. H. HARRIS		
4	INSPECTION	10/1/58	J. H. HARRIS		
5	REVISION	10/1/58	J. H. HARRIS		
6	REVISION	10/1/58	J. H. HARRIS		
7	REVISION	10/1/58	J. H. HARRIS		
8	REVISION	10/1/58	J. H. HARRIS		
9	REVISION	10/1/58	J. H. HARRIS		
10	REVISION	10/1/58	J. H. HARRIS		

Figure 47 - Support Assembly (Drawing 610A000-102)

FOLDOUT FRAME /

(The reverse is blank.)

PRECEDING PAGE BLANK NOT FILMED:

PRECEDING PAGE BLANK NOT FILMED:

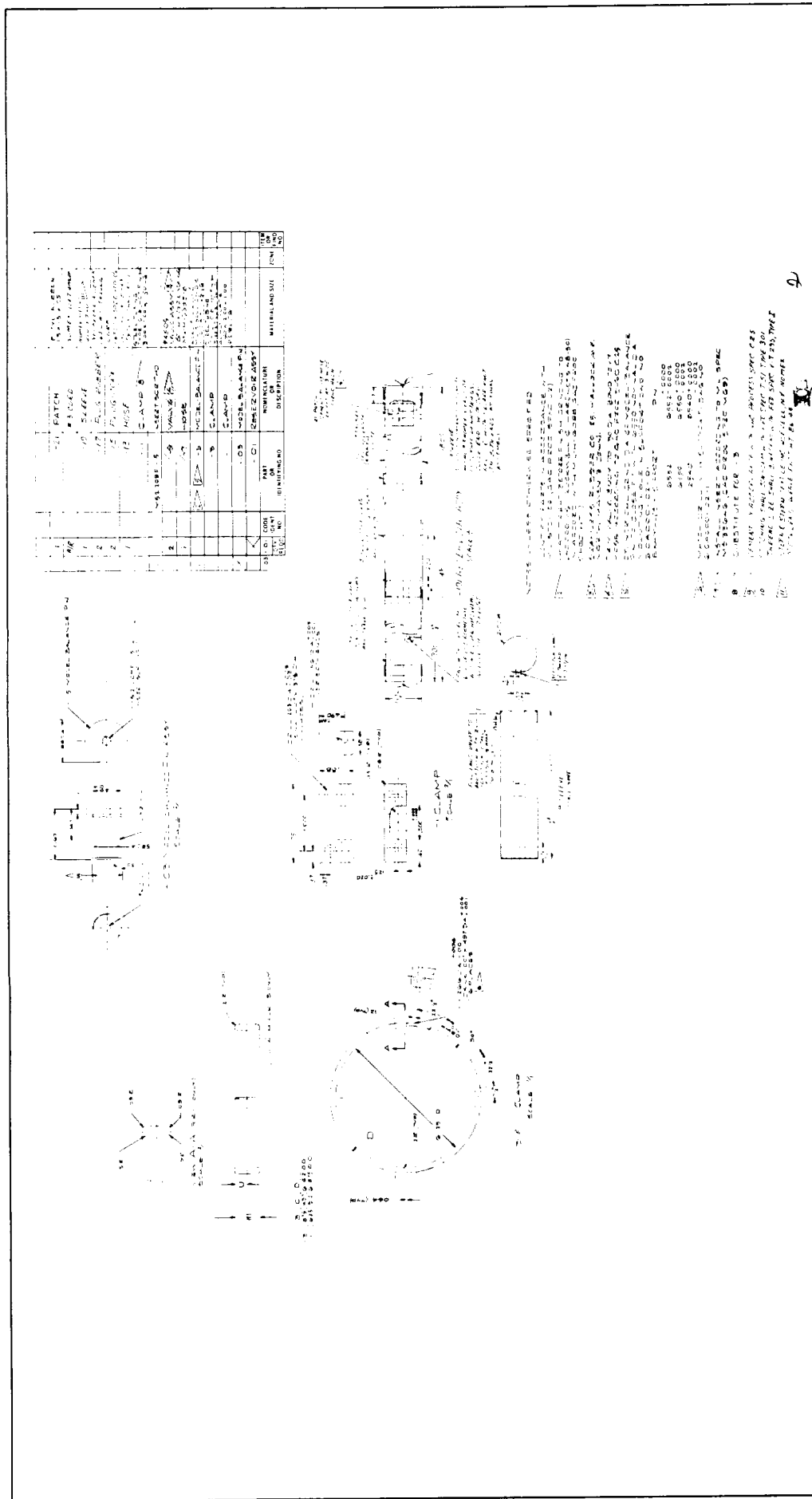


Figure 48 - Model Details (Drawing 610A000-103)

(The reverse is blank.)

PRECEDING PAGE BLANK NOT FILMED.

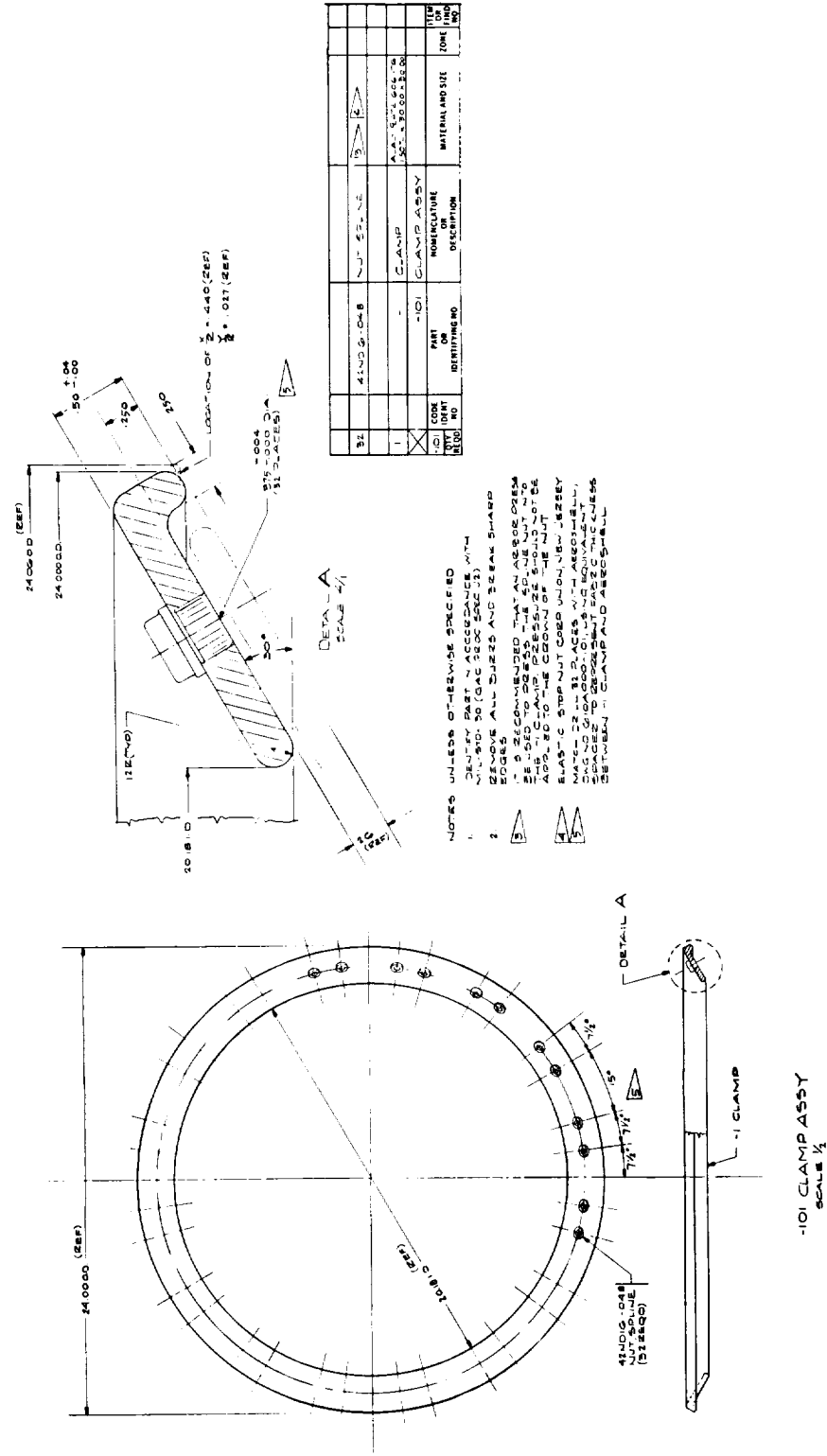


Figure 49 - Clamp Assembly (Drawing 610A000-104)

...TIDOUT FRAME

OUTOUT FRAME

PRECEDING PAGE BLANK NOT FILMED.

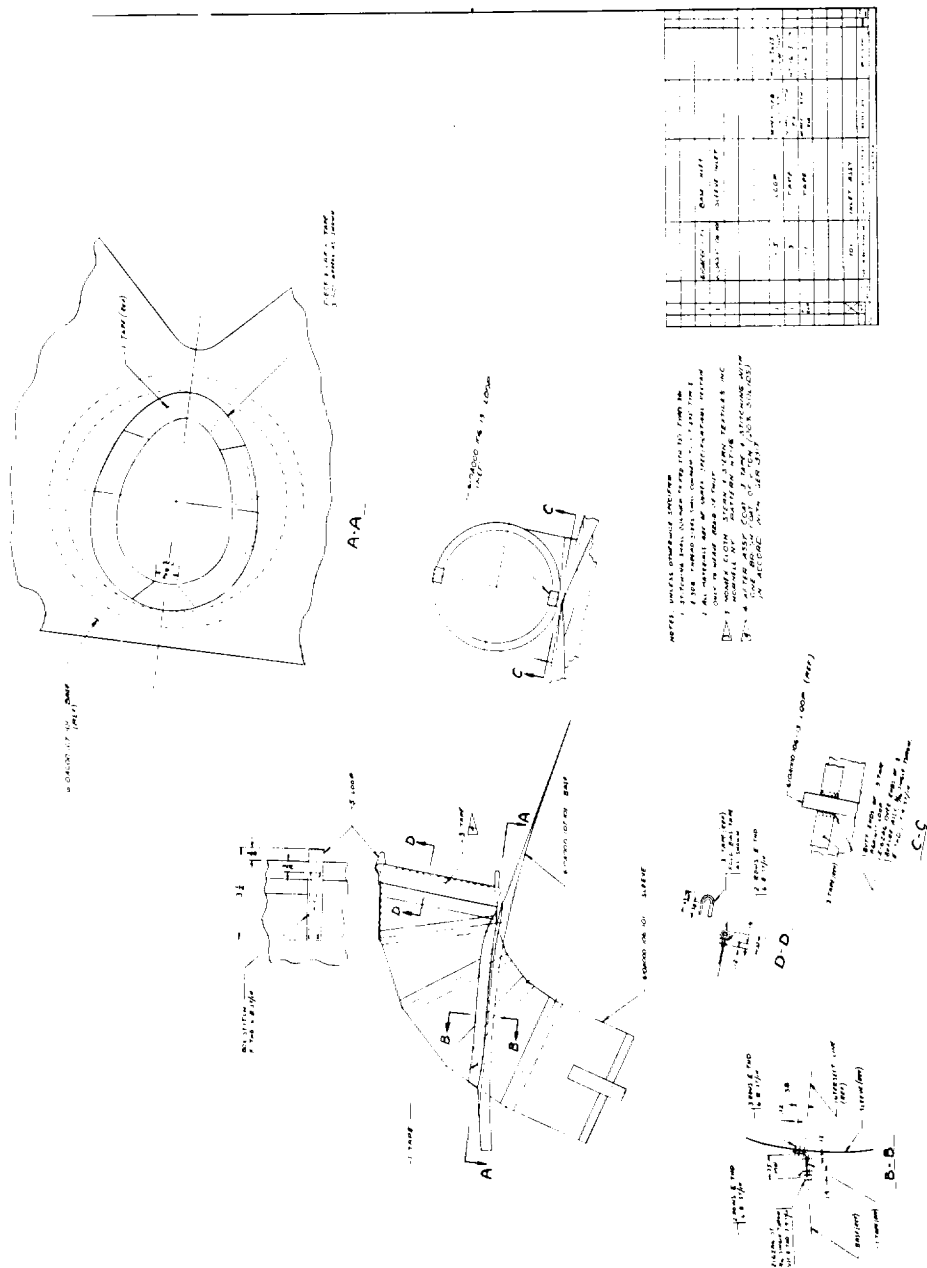


Figure 50 - Inlet Assembly, 4-In. Diameter
(Drawing 610A000-105)
(The reverse is blank)

FOLDOUT FRAME

FOLDOUT FRAME

PRECEDING PAGE BLANK NOT FILMED.

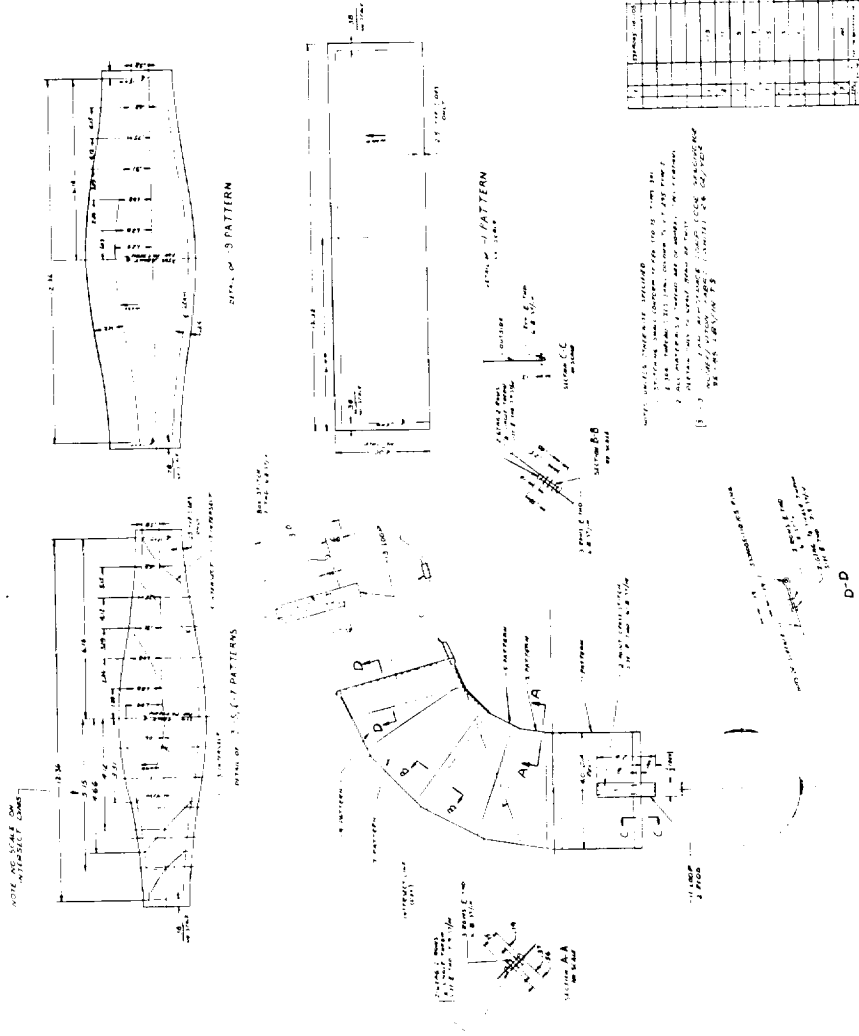
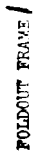


Figure 51 - Inlet Sleeve, 4-In. Diameter
(Drawing 610A000-106)
(The reverse is blank.)

FOLDOUT FRAME

የህዝብ ጥያቄ



(The reverse is blank.)

PRECEDING PAGE BLANK NOT FILMED.

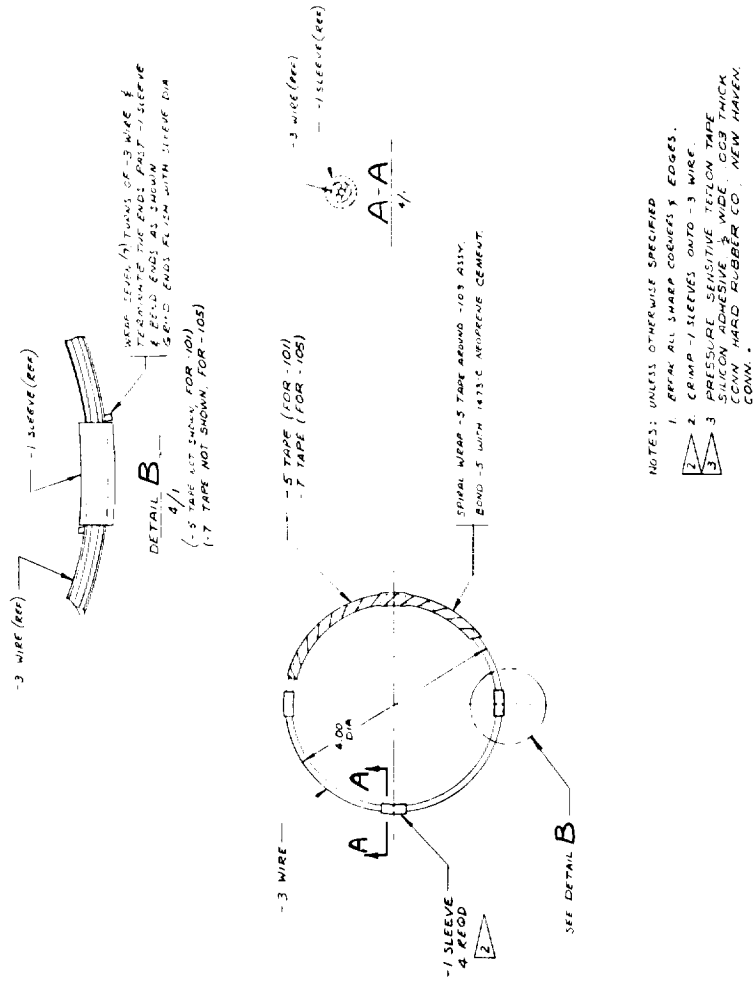


Figure 53 - BALLUTE Inlet Ring (Drawing 530A005-110)
FOLDOUT FRAME

LIST OF REFERENCES

1. Jaremenko, I. M.: "Aerodynamic Characteristics of the Ballute in the 0.1 to 10 Mach Number Speed Regime," AIAA Paper No. 67-228. Fifth Annual AIAA Meeting, New York, 23 through 26 January 1967.
2. Bloetscher, F.: Aerodynamic Deployable Decelerator Performance-Evaluation Program, Phase II, Technical Report AFFDL-TR-67-25. Akron, Ohio, Goodyear Aerospace Corporation, April 1967.
3. Houtz, N.: "Optimization of Inflatable Drag Devices by Isotensoid Design," AIAA Paper No. 64-437. First Annual AIAA Meeting, Washington, D. C., 29 June through 2 July 1964.
4. Test Facilities Handbook, Sixth Edition. Arnold Engineering Development Center, Arnold Air Force Station, Tenn., November 1966.
5. Nissel, R. E.: "Strength to Weight Values for Nomex Cloth and Webbing at Ambient and Elevated Temperatures," ARD 10, 574. Akron, Ohio, Goodyear Aerospace Corporation, 24 April 1967.
6. Topping, A. D.: "Shear Deflections and Buckling Characteristics of Inflated Members." Journal of Aircraft, Vol 1, No. 5, pp 289-292.
7. Flugge, W.: Stresses in Shells. Springer Verlag, Berlin, 1960.
8. Houmard, J. E., and Marketos, J. D.: Approximate Analyses of the Structural Stability of the C-Annulus Space Station Models, GER-10755. Akron, Ohio, Goodyear Aerospace Corporation, 18 September 1962.
9. Drawing No. 3203249: Internal Balance Mounting. Arnold Engineering Development Center, Arnold Air Force Station, Tenn., 11 August 1967.

NASA CR-66613
National Aeronautics and Space Administration
DEVELOPMENT OF ATTACHED INFLATABLE
DECELERATORS FOR SUPERSONIC APPLICATION.
Barton, R. Reed, 22 May 1968, 115 pp. Contract No.
NAS1-7359, contractor report number GER-13680

I. Barton, R. Reed
II. NASA CR-66613

An attached inflatable decelerator is considered for augmenting needed drag of a capsule during Mars entry. The inflatable afterbody, configured as a variation from a tucked-back Ballute, is packaged within a 120-deg conical aeroshell for deployment at Mach 3.0 and at a dynamic pressure of 125 psf. Outer attachment of the expandable afterbody is made to the hard-body aeroshell profile, and inner attachment is made to a tubular support for wind-tunnel mounting.

The model was designed, fabricated, and development tested and is recommended for wind-tunnel testing to prove workability of the concept.

NASA

